Astron. Astrophys. 275, 101–152 (1993)

ASTRONOMY AND ASTROPHYSICS

The chemical evolution of the galactic disk ⋆,⋆⋆

I. Analysis and results

B. Edvardsson[1], J. Andersen[2], B. Gustafsson[1], D. L. Lambert[3], P. E. Nissen[4], and J. Tomkin[3]

[1] Astronomical Observatory, Box 515, S–751 20 Uppsala, Sweden
[2] Copenhagen University Observatory, Brorfeldevej 23, DK–4340 Tølløse, Denmark
[3] Department of Astronomy, University of Texas, Austin, TX 78712–1083, USA
[4] Institute of Physics and Astronomy, University of Aarhus, DK–8000 Aarhus C, Denmark

Received February 24, accepted April 5, 1993

Abstract. With the aim to provide observational constraints on the evolution of the galactic disk, we have derived abundances of O, Na, Mg, Al, Si, Ca, Ti, Fe, Ni, Y, Zr, Ba and Nd, as well as individual photometric ages, for 189 nearby field F and G disk dwarfs. The galactic orbital properties of all stars have been derived from accurate kinematic data, enabling estimates to be made of the distances from the galactic center of the stars' birthplaces.

Our extensive high resolution, high S/N, spectroscopic observations of carefully selected northern and southern stars provide accurate equivalent widths of up to 86 unblended absorption lines per star between 5000 and 9000 Å. The abundance analysis was made with greatly improved theoretical LTE model atmospheres. Through the inclusion of a great number of iron-peak element absorption lines the model fluxes reproduce the observed UV and visual fluxes with good accuracy. A new theoretical calibration of $T_{\rm eff}$ as a function of Strömgren $b-y$ for solar-type dwarfs has been established. The new models and $T_{\rm eff}$ scale are shown to yield good agreement between photometric and spectroscopic measurements of effective temperatures and surface gravities, but the photometrically derived very high overall metallicities for the most metal rich stars are not supported by the spectroscopic analysis of weak spectral lines.

Individual ages were derived from fits in the $T_{\rm eff}$ – log g plane of these somewhat evolved dwarfs to isochrones by VandenBerg (1985). We expect the uncertainties in the relative ages to be about 25%, although the absolute errors may be larger.

Distances, proper motions and radial velocities were translated to galactic U, V and W velocity components which in turn were independently used by M. Grenon and J. Sommer-Larsen to calculate stellar orbital parameters, which agree within 5%. Following Grenon, the mean galactocentric distances were used as estimates of stellar birth places to investigate abundance gradients in the disk at different epochs.

The relative iron abundances [Fe/H] and the abundance ratios relative to iron for most elements are estimated to be accurate with a standard deviation of 0.05 dex. We discuss the evolution of α elements, odd-Z elements, iron peak elements and s elements as functions of stellar age and orbital properties in terms of nucleosynthesis in massive stars, in supernovae of Types Ia and II, and in AGB stars. There is a considerable variation in the metallicities of stars formed at a given time in the disk, which means that there is only a weak correlation between age and metallicity. The strongest age-abundance correlation is found for Ba, which is interpreted as the result of the efficient s-element synthesis in low-mass AGB stars which enrich the ISM long after star formation. Metal-poor ([Fe/H] < -0.4) stars are, as previously shown, relatively overabundant in the α elements: [α/Fe] for these metal-poor stars decreases with increasing galactocentric radius of the orbits, implying that the star formation was more vigorous and started first in the inner parts of the galactic disk. The abundances of the two odd-Z light elements sodium and aluminium increase at different rates with metallicity in the disk, which is presumably connected to their respective production in C and Ne burning in massive stars.

The scatter, at a given age and mean distance from the galactic center, in relative abundances like [Si/Fe] is only about 0.05 or less, which is about 4 times less than the corresponding scatter in [Fe/H]. Possible explanations for this are discussed.

Thanks to the high internal accuracy of the analysis and the large sample of programme stars, two groups of chemically mildly peculiar stars have been detected; a group of metal rich stars appear to be enriched in Na, Mg and Al relative to other elements, another group of dwarfs are enriched in s-elements as previously reported by Tomkin et al. (1989). The origins of these peculiarities are discussed.

Send offprint requests to: Bengt Edvardsson

⋆ Based on observations carried out at the European Southern Observatory and the W.J. McDonald Observatory

⋆⋆ Tables 8, 11 and 12 are also available in electronic form: see the editorial in A&A 1992, Vol. 266 No. 2, page E1

Key words: Galaxy: abundances – Galaxy: evolution – Galaxy: kinematics and dynamics – stars: abundances – stars: atmospheres – stars: fundamental parameters

1. Introduction

During the evolution of the galactic disk, nucleosynthesis in successive generations of stars proceeded along with the dynamical interaction of the stars and interstellar gas. A fossil record of the state of the Galaxy at various epochs of its evolution is preserved in the stars surviving from those times until the present. Thus, the determination of chemical abundances of stars has played a significant rôle in the study of the major processes occurring during the evolution of our galaxy.

The early study by Chamberlain & Aller (1951) found that the abundances of iron and calcium in two subdwarfs were probably depleted by an order of magnitude relative to the corresponding abundances in the Sun. Classic papers during the following decade demonstrated that there were abundance differences that seemed to correlate with the stellar kinematic properties, not only between halo and disk stars (Roman 1954, 1955; Eggen et al. 1962), but also within the disk population itself (Gratton 1953; Schwarzschild et al. 1957).

Since then, many more spectroscopic studies of increasing refinement have improved our knowledge of, e.g. the relationships between the abundance variations in different elements. Only relatively limited numbers of stars could, however, be studied with classical spectrographic methods. Much larger samples of stars were accessible to study by photometric techniques, but only one global metallicity parameter could then generally be derived. Moreover, not all photometric systems employed in such large-scale studies are free of systematic errors, e.g., due to interstellar reddening or stellar surface gravity effects. Finally, the accuracy of photometric abundance determinations is limited by the possible galactic scatter in relative abundances, microturbulence parameters, etc.

In the last decade the development of efficient spectrometers like the McDonald 2.7-m coudé and the ESO CES spectrometers, combined with powerful linear detectors such as Reticons and CCD's have revolutionized stellar spectroscopy. Simultaneously, theoretical model atmosphere and synthetic spectrum calculations have been considerably improved, especially with improved treatments of the line blanketing by atoms and molecules. The result has been a considerable improvement in the quality and quantity of stellar chemical abundance determinations, of great importance for our understanding of stellar and galactic evolution. For recent results of studies of disk stars, we refer to the reviews by Lambert (1989), Wheeler et al. (1989), and, for a somewhat broader perspective, the comprehensive summary by Gehren (1988).

Still, previous spectroscopic investigations of galactic evolution have treated rather small numbers of stars. More seriously, the samples have often been selected for study in ways which were statistically poorly defined or susceptible to (kinematical) bias. Also, most previous studies have concentrated on halo stars. These factors have combined to render the results of these investigations less suitable for a more systematic study of galactic evolution, especially that of the galactic disk, than ideally possible with the instruments, observing time, and analysis techniques available.

The present programme was designed to rectify that situation. Our aim has been to provide a homogeneous body of accurate data on the abundances of several key elements in a large enough sample of disk dwarfs that meaningful statistical results can be obtained even after subdivision into several subsamples. Particular attention has been paid to selecting the stars by astrophysically and statistically well-defined criteria. Finally, we have attempted to push the accuracy of the abundance analysis to the point where trends with age or metallicity of not only the average abundance ratios, but also the dispersion about those mean relations could be meaningfully discussed.

Our basic selection of nearly 200 F and early disk G dwarfs for subsequent high-resolution spectroscopic analysis is based on accurate $uvby$ indices and well-defined photometric criteria. These were defined such that disk stars in the full range of metallicities are represented, and so that accurate individual ages can be derived from photometry in combination with stellar evolutionary models and isochrones. As two instruments have been used to cover both celestial hemispheres, we have placed particular emphasis on maintaining identical selection and analysis methods throughout, and on securing a large enough overlap to verify final homogeneity.

In order to maintain a fully homogeneous analysis, both the spectra and the photometry have been analysed using specially designed model atmospheres incorporating a detailed treatment of blanketing from millions of spectral lines. We find that these new models lead to a high degree of internal consistency in the analysis. Based on our measurements of selected weak, unblended lines in the spectra, we have derived individual abundances for a number of chemical elements from oxygen to barium.

To complement the chemical abundance data, accurate kinematical data (radial velocities and proper motions) have been obtained and used to calculate individual galactic orbital parameters for all the stars. In this paper, we discuss the relationships of the chemical and dynamical parameters to each other and to the stellar ages, with the main ambition to put new constraints on any theory for the dynamical and chemical evolution of the Galaxy. A number of new features have been discovered during this study, for some of which we suggest interpretations in terms of specific processes in galactic evolution or nucleosynthesis.

A very large amount of material is presented and discussed in this paper. As will be apparent below, many of the new astrophysical insights provided by our data critically depend on their statistical properties and errors having been correctly assessed. Therefore, much space is devoted to the detailed documentation of the results: Our selection of stars and the observational techniques are presented in Sect. 2, the methods of analysis in Sect. 3, while Sect. 4 contains a detailed analysis of possible errors in the results. The derivation of ages, space motions, and galactic orbital parameters is presented in Sect. 5.

The reader primarily interested in galactic evolution and nucleosynthesis may want to skip directly to Sect. 6, which contains a comprehensive review and discussion of the abundance results and their interpretation. Cross-references are given there to key points covered earlier in the paper. Section 7 summarizes the main conclusions of our work.

The extensive spectral and associated observational data obtained in this investigation are made available in a companion paper in the Supplement Series of this Journal (Edvardsson et al. 1993, Paper II). We emphasize that the definitive results presented here should supersede the preliminary results presented for subsamples of stars in series of earlier reports (Edvardsson et al. 1984; Edvardsson et al. 1985; Nissen et al. 1985; Andersen et al. 1988b; Tomkin et al. 1989; Edvardsson et al. 1990; Gustafsson et al. 1992): Both the observational data and the model atmospheres were then still in a preliminary state, and there are important systematic differences from the final results presented in this paper.

2. Observations

2.1. Selection of stars

The programme stars were selected with the aim of defining a sample of F and early G main sequence stars, evenly distributed over the metal abundance range $-1.0 <$ [Me/H] $< +0.3$, and somewhat evolved away from the ZAMS so that their ages may be estimated. The selection was made by the aid of the large, homogeneous *uvby-β* catalogue of Olsen (1988), which includes nearly all F and early G stars brighter than $V \simeq 8.3$. The original sources of *uvby-β* photometry are: Strömgren & Perry 1965; Crawford et al. 1966; Crawford et al. 1970; Grønbech & Olsen 1976, 1977; Olsen (1983) and Olsen & Perry (1984). From the 19 615 stars in the Olsen (1988) catalogue a subsample fulfilling the criteria

$$2.58 < \beta < 2.72 \qquad (1)$$

and

$$0.04 < (\delta c_1 + 0.5 \cdot \delta m_1) < 0.16 \qquad (2)$$

was first selected. For the definition of δc_1 and δm_1 we refer to Crawford (1975). As discussed in Sect. 3.1.1 β is an indicator of effective temperature, $T_{\rm eff}$, δc_1 gives an estimate of the gravity parameter, log g, or the absolute magnitude, M_V, and δm_1 is closely correlated with the metal abundance parameter, [Me/H]. Criterion (1) means that the stars are confined to the effective temperature range $5600 < T_{\rm eff} < 7000\ K$. Criterion (2) ensures that the stars have evolved a distance of $0\overset{\rm m}{.}4 \lesssim \delta M_V \lesssim 2\overset{\rm m}{.}0$ from the ZAMS relation in the $M_V - \beta$ plane. Thus the stars are situated in a region of the HR diagram where the isochrones are rather well separated, allowing an age determination for the individual stars. Note that by including the term $0.5 \cdot \delta m_1$ in (2) we take into account the shift of the ZAMS in the $c_1 - \beta$ diagram as a function of the metal abundance (see Sect. 3.1.1).

Table 1. The number of stars observed in the 9 metallicity groups and approximate mean values of [Me/H] and limiting magnitudes for the groups

Group	δm_1	N	[Me/H]	$V_{\rm lim}$
1	$< 0\overset{\rm m}{.}000$	29	+0.20	$6\overset{\rm m}{.}5$
2	0.000 - 0.015	23	+0.05	5.7
3	0.016 - 0.030	24	−0.09	5.7
4	0.031 - 0.045	25	−0.23	5.7
5	0.046 - 0.060	25	−0.37	6.4
6	0.061 - 0.075	18	−0.51	7.3
7	0.076 - 0.090	18	−0.65	7.7
8	0.091 - 0.105	18	−0.78	8.2
9	> 0.105	9	−0.90	8.3

Next the subset of stars defined by (1) and (2) was divided into nine metallicity groups according to the δm_1 index. The limits of δm_1 for the groups and the corresponding approximate mean values of [Me/H] are given in Table 1.

In each group we have aimed at observing about 25 of the brightest stars. Known binaries, for which the light from the secondary component was estimated to affect $b-y$, β, m_1 or c_1 by more than $0\overset{\rm m}{.}005$, were excluded. For the brighter stars, information on duplicity (close companions, radial-velocity variability) was available from the Bright Star Catalogue (Hoffleit & Jaschek 1982); for all the fainter stars, accurate photoelectric radial-velocity observations were obtained with CORAVEL (Mayor 1985) concurrently with the present study, and the results were available for this discussion. Moreover, our high-S/N spectra would reveal lines from a secondary star up to 2 mag fainter than the primary if the lines are at least partly resolved.

Stars rotating faster than $v \sin i = 25\ {\rm km\,s^{-1}}$ were also excluded, because the rotational broadening makes the equivalent width measurements too uncertain for such stars. This means that no stars with $T_{\rm eff} > 6800$ K were observed, in spite of the fact that criterion (1) allows hotter stars to be included.

The actual number of stars observed in each group and the limiting magnitudes of the groups are given in Table 1. Only a few stars have been observed in group 9 simply because the limiting magnitude of the catalogue of Olsen (1983) was reached for this group. It is seen that the limiting magnitude for groups 8 and 9 is about $2\overset{\rm m}{.}5$ fainter than the limiting magnitude for groups 2, 3 and 4. Taking into account that the metal deficient stars are intrinsically fainter than the solar abundance stars we estimate that the stars with [Me/H] < -0.7 have been sampled in a volume three times as large as the volume for stars with $-0.3 <$ [Me/H] < 0.1. All stars are, however, within a distance of 60 pc, with the exception of four stars whose distances are between 60 and 80 pc.

The programme stars and their fundamental atmospheric parameters, iron abundances, distances, kinematic and dynamical data, and ages are given in Table 11.

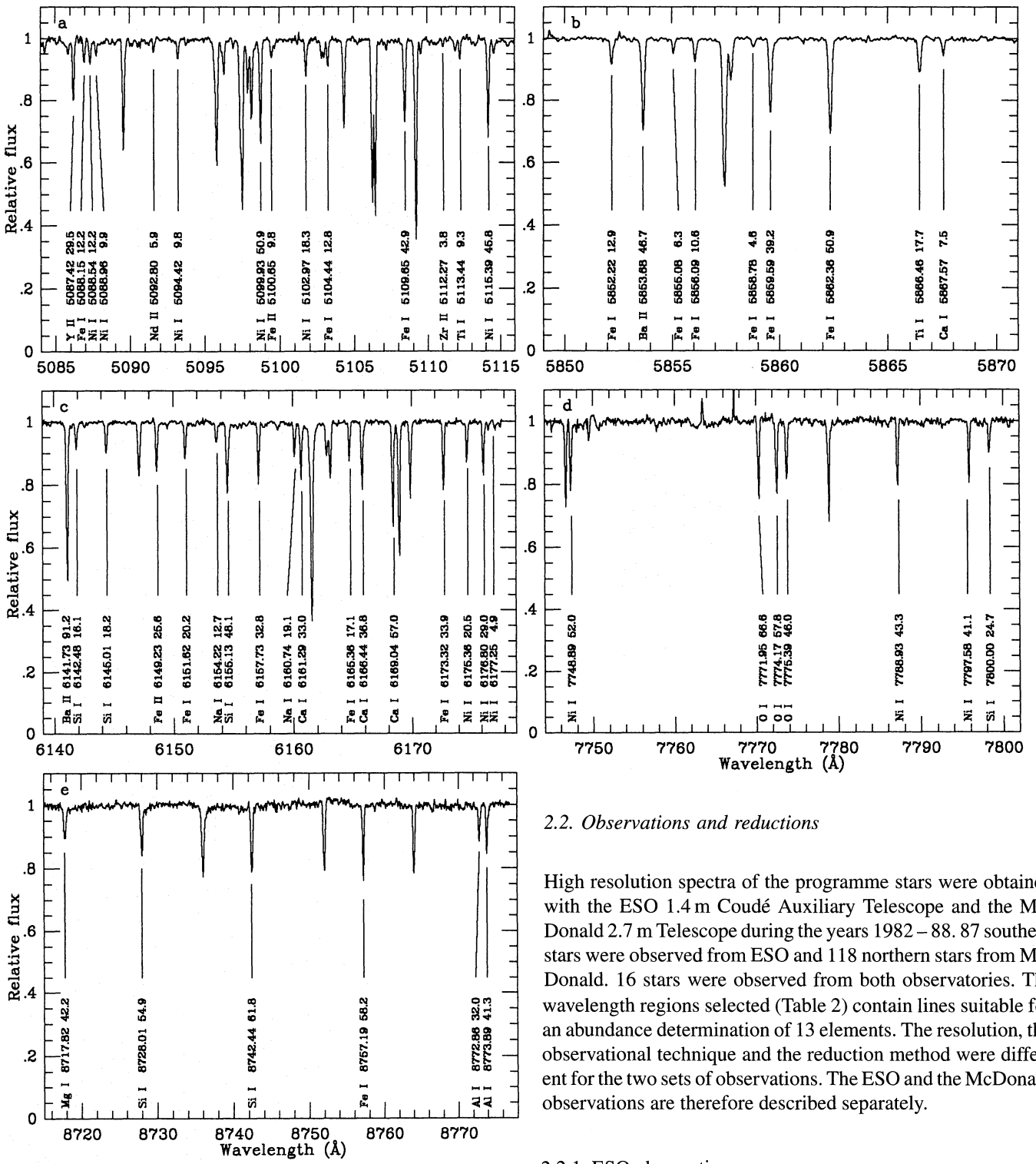

Fig. 1. Spectra obtained with the ESO 1.4 m Coudé Auxillary Telescope and the Coudé Echelle Spectrometer equipped with a CCD detector for one of the faintest stars in our sample, HD 17548, $V = 8.16$. All lines used for the abundance determination are identified and marked with a number equal to the equivalent width of the line in mÅ. Corrections for radial velocity shifts have not been made in all the spectra. In **e** the presence of the Paschen hydrogen line at 8750 Å in the spectrum of the B-type star used for flat-fielding is seen as a broad "emission feature"

2.2. Observations and reductions

High resolution spectra of the programme stars were obtained with the ESO 1.4 m Coudé Auxiliary Telescope and the McDonald 2.7 m Telescope during the years 1982 – 88. 87 southern stars were observed from ESO and 118 northern stars from McDonald. 16 stars were observed from both observatories. The wavelength regions selected (Table 2) contain lines suitable for an abundance determination of 13 elements. The resolution, the observational technique and the reduction method were different for the two sets of observations. The ESO and the McDonald observations are therefore described separately.

2.2.1. ESO observations

The five wavelength regions given in Table 2 were observed with the Coudé Echelle Spectrometer (CES) during a total of about 60 usable nights in the period 1983 – 1986. During the first three years an 1872-element Reticon detector and the long camera of the CES were used: Most of these spectra have a S/N $\approx$ 200. The resolution as measured from the FWHM of lines from a thorium lamp was 80,000. Due to the relatively

Table 2. Approximate wavelength regions and chemical elements investigated

ESO range	McD range	Elements analysed
5085 – 5125	5050 – 5160	Ti, Fe, Ni, Y, Zr, Nd
5835 – 5880	5795 – 5905	Ca, Ti, Fe, Ni, Ba
6130 – 6180	6105 – 6215	O, Na, Si, Ca, Ti, Fe, Ni, Ba
7740 – 7800	Not observed	O, Si, Fe, Ni
8710 – 8780	8690 – 8790	Mg, Al, Si, Fe

Table 3. The IUE ULDA passbands measured for the comparison stars

Passband designation	IUE Camera	Wavelength range (Å)
A	SWP	1550 – 1680
B	SWP	1680 – 1760
C	SWP	1800 – 1900
D	LWR	2200 – 2515
E	LWR	2600 – 2760
F	LWR	2800 – 3100

high read-out noise and dark current of the Reticon detector it was not possible to go fainter than about $V = 6^{m}.5$. In 1986 ESO installed a faster camera with a 640 × 1024 pixel RCA CCD detector, which made it possible to observe the fainter stars in the metal deficient groups. The resolution was degraded to R = 60,000, but as the absorption lines are well separated in these stars this caused no problems.

The raw spectra were reduced for read-out and dark current, divided by flat-fields and wavelength calibrated using standard ESO IHAP routines. Interference fringes on the thinned RCA CCD detector in the near infrared regions (7770 and 8745 Å) caused a special problem. After division by flat-fields from a quartz lamp residual fringes of typically 3% and a period of a few Ångströms remained. In order to get rid of these fringes spectra of fast rotating early B-type stars were taken and divided into the stellar spectra. With some care in focusing and positioning the spectra on the CCD, the residual fringes could be removed in this way to an accuracy better than 1%.

The continuum of the spectra was defined by a number of narrow spectral regions, selected to be free of lines in the solar and Procyon spectra. The resulting rectified spectra for one of the faintest stars in our sample is shown in Fig. 1.

The equivalent widths were measured by interactively fitting single or double Gaussian functions to the line profiles. Lines showing asymmetric line profiles (due to blends) in the high-resolution solar atlas of Delbouille et al. (1973) were excluded.

In course of the analysis we found evidence that the ESO observations are affected by about 1% scattered light in the Coudé Echelle Spectrometer. Therefore the ESO equivalent widths, including the Solar observations, were multiplied by 1.01. For details, see Paper II.

2.2.2. McDonald observations

All observations from McDonald Observatory were made with the 2.7 m telescope, coudé spectrometer and a 1872-element Reticon, self-scanned, silicon photodiode-array detector (Vogt et al. 1978) during the years 1982 – 88. The three wavelength regions 5105, 5850 and 6160 Å were observed at a resolution of 0.20 Å, while the 8740 Å region was observed at a resolution of 0.24 Å. (The 7770 Å wavelength region was not observed at McDonald.) The observations covered 110 Å and had signal-to-noise ratios of between 200 and 500. A few of the observations – the earliest ones in the programme – were made with a 1024-element Reticon, instead of the 1872-element Reticon; their 0.22 Å resolution and 100 Å wavelength coverage were very similar to those of the observations made with the 1872-element Reticon.

Table 4. Stellar identifications and model parameters for the comparison stars, in order of decreasing metallicity

Star ID HD	Star ID HR	$T_{\rm eff}$ (K)	log g	[Me/H]	$\xi_{\rm t}$ (km s^{-1})
186427	7504	5737	4.14	+0.14	1.5
144284	5986	6152	3.96	+0.07	2.1
1671	82	6576	3.62	0.00	2.9
39587	2047	5953	4.46	−0.05	1.2
22001	1083	6769	4.10	−0.08	2.4
16673	784	6287	4.37	−0.09	1.6
11443	544	6352	3.73	−0.14	2.5
1581	77	5989	4.59	−0.18	1.1
109358	4785	5879	4.52	−0.19	1.0
128167	5447	6767	4.27	−0.38	2.1
203608	8181	6139	4.34	−0.73	1.5
110897	4845	5795	4.15	−0.88	1.4
22879		5826	4.27	−0.98	1.3

Lines suitable for measurement were chosen by the requirement that the profiles be sufficiently clean to provide reliable equivalent widths in all, or most of, the programme stars. Inspection of the solar spectrum (Kurucz et al. 1984) and the solar line identifications of Moore et al. (1966) were the main screens against blends. A line's profile did not have to be completely clean in order to be measurable. Some lines, whose profiles were distorted on one side by a nearby line, still provided reliable equivalent widths thanks to the ability of the measuring program (see below) to use only the undistorted part of a partially distorted profile for equivalent width measurement. Fitting of double or triple profiles of closely spaced pairs or triplets of lines allowed a second way of measuring profiles that are influenced by neighbouring lines.

The equivalent widths were measured with a program developed for automatic measurement of Reticon spectra (McWilliam 1988). For each observation, after division by its flat-field lamp, the program used a set of pre-selected continuum windows to set the continuum and then identified and measured the lines on the line list. Least-squares fits of Gaussian profiles to the lines

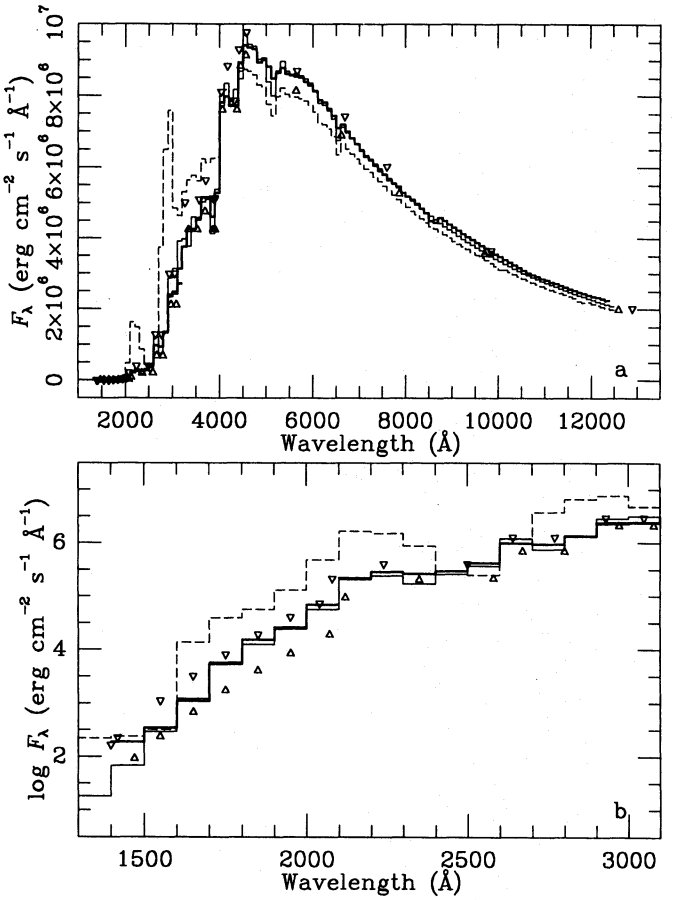

Fig. 2. Solar surface mean fluxes in 100 Å intervals. The thick solid line represents the observations from four sources in different wavelength regions: 1400 - 2100 Å: Samain (1979), 2100 - 3200 Å: Broadfoot (1972), 2900 – 12400 Å: Arvesen et al. (1969) and Neckel & Labs (1964) as quoted by Kurucz et al. (1984). The thin solid line represents the flux of the new solar model with line blanketing data from Kurucz (1989) and the dashed line is the flux of the solar model of Gustafsson et al. (1975). Triangles represent the upper and lower flux limits defined by Vernazza et al. (1976, Table 13). **a** The fluxes of Neckel & Labs redwards of 8700 Å are continuum data only. (In this region Neckel & Labs estimate the line blocking to 2 ± 1%.) **b** An expansion of the UV region of **a** with a logarithmic flux scale. Symbols as in **a**. Note that absorption lines were removed from the observations between 1760 and 2100 Å (Samain) so these should be considered upper limits to the absolute flux. Similarly emission lines were removed from the observations below 1680 Å

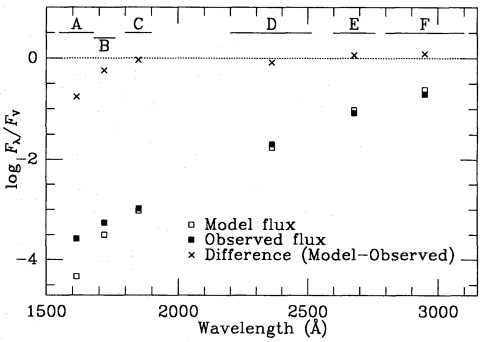

Fig. 3. Comparison of observed and model UV fluxes of HR 7504. Flux units are erg cm^{-2} s^{-1} Å^{-1}. The observed fluxes are mean fluxes measured in six rectangular passbands from absolute calibrated low resolution IUE spectra. The observed and model fluxes were normalized to zero in the V passband near 5500 Å

were used to measure the equivalent widths. The spectral region, continuum and fitted profiles were then displayed on the terminal screen for human inspection and interactive remeasurement of any lines in need of remeasurement.

3. Analysis

3.1. Model atmospheres

A new set of plane parallel, line blanketed, flux constant, LTE model atmospheres was constructed for the abundance analysis. Convection was treated in the mixing-length approximation (ℓ/H_p = 1.5).

The new models derive from a development of the programmes of Gustafsson et al. (1975) and include line blanketing from millions of atomic lines. The line absorption data for Ca through Ni for wavelengths less than 4500 Å were revised (Kurucz 1989). The new line data make a major difference only at shorter wavelengths. For each of these 18 neutral and ionized species the line absorption coefficients were tabulated at 4100 wavelength points, 9 temperatures, 9 gas pressures, and 4 values of the microturbulence parameter. Each of these tables takes about 6 Mbyte in unformatted form. Absorption coefficients of the most important lines of Na I, Mg I and II, Al I and II and Si I and II, with line data adopted from Wiese et al. (1969) were tabulated in the same way. For λ >4500 Å, the ODF opacity tables of Gustafsson et al. (1975) were sampled. Also the continuous absorption coefficients were updated according to Mathisen (1984a, b) and continuous CH and OH absorption coefficients were adopted from Kurucz et al. (1987).

An opacity sampling (OS) version of the original opacity distribution function (ODF) scheme of Gustafsson et al. (1975) was adopted from Plez et al. (1992). The models were calculated with about 4100 OS wavelength points between 1000 and 4500 Å, and 1400 wavelength points between 4500 and 125000 Å. Figure 2 shows the solar model disk integrated flux compared with observations and previous models.

The inclusion of large numbers of previously unknown weak atomic lines obviously seems to solve the problem of the so-called missing ultraviolet opacity, cf. Holweger (1970) and Gustafsson & Bell (1979). This resolution of the problem was in fact suggested already by Holweger (1970). However, a more detailed study of the synthetic solar spectrum indicates the presence of a number of lines which are calculated to be far too strong with Kurucz's gf values (Bell 1993). A careful investigation of the consequences thereof for the general UV flux should be carried out.

Model fluxes were also compared to observed ultraviolet fluxes of 13 F dwarfs, eight of which belong to the main sample of stars investigated in this paper. Mean absolute fluxes in six

passbands were measured from the copy of the IUE Uniform Low Dispersion Archive (ULDA, Wamsteker et al. 1989) at Uppsala Astronomical Observatory and compared to the fluxes of models with parameters obtained from Strömgren photometry exactly as for the programme stars. The UV passbands are defined in Table 3. The model fluxes were scaled to the stellar angular diameters by the factor $f(5500\,\text{Å})/F(5500\,\text{Å})$ where

$$\log f(5500\,\text{Å}) = -0.4 \cdot m_V - 8.43 \quad (3)$$

(Allen 1973), and $F(5500\,\text{Å})$ was taken to be the mean flux of the models between 5400 and 5600 Å in units of erg cm^{-2} s^{-1} Å^{-1}. The stellar identifications and model parameters, obtained with the same criteria as those used for the programme stars (see below), are given in Table 4 and the observed and model fluxes are compared in Table 5. Figure 3 shows an example of the flux comparisons, the flux varying by more than 3 orders of magnitude over the spectral range. As can be seen from the last line of Table 5, the model fluxes agree in the mean very well with the observed fluxes, except for region A, at the shortest wavelength, where the model flux is typically five times lower than the observed fluxes. The cause of this large deviation is not known; it is puzzling since no similar effect was seen for the Sun (Fig. 2b). If the observed fluxes are correct they may indicate the presence of inhomogeneities or a strong overionization effect in Si, since the effective opacity in this wavelength range is dominated by continuous Si I absorption. Alternatively there may be an error in the flux calibration of the IUE spectra below 1650 Å.

The solar model atmosphere of our grid is given in Table 6, and in Fig. 4 it is compared to the solar model of Bell et al. (1976) and to the often used model of Holweger & Müller (1974).

Table 5. Comparison of model UV fluxes with observations. Passband designations as in Table 3. The fluxes were normalized in the V band. The stars are entered in order of decreasing metallicity. The mean deviation for each passband is given at the bottom of the table

Star ID	$\log\left(\frac{\text{model flux}}{\text{observed flux}}\right)$					
HD	A	B	C	D	E	F
186427	−0.76	−0.24	−0.03	−0.08	+0.06	+0.09
144284	−0.79	−0.31	−0.27			
1671	−0.61	+0.11				
39587	−0.77	−0.15	−0.16	−0.09	+0.04	+0.08
22001		+0.22	−0.06			
16673				+0.03	+0.05	+0.09
11443	−0.78	+0.06	+0.02			
1581	−0.52	+0.13	+0.07	−0.01	+0.03	+0.09
109358	−0.62	−0.02	+0.02	−0.03	+0.02	+0.08
128167				−0.02		
203608		+0.48	+0.12			
110897				+0.10	+0.06	+0.11
22879		+0.31	+0.24			
mean	−0.69	+0.06	0.00	−0.01	+0.04	+0.09

3.1.1. Fundamental parameters of model atmospheres

The fundamental atmospheric parameters of the stars have been determined from the Strömgren photometry referred to in Sect. 2.1. The high accuracy of the β, $b-y$, c_1 and m_1 indices makes it possible to determine values of T_{eff}, log g and [Me/H] that are of a relatively high accuracy and internal consistency. The values derived will be checked and systematic errors discussed on the basis of the spectral analysis itself. In the following we briefly outline the calibrations used to determine the three basic parameters.

One star, HR 5459A = α Cen A, was included in our sample, although no $uvby$-β photometry is available, because the star is too bright to be measured with modern pulse counting techniques. Instead we adopted the spectroscopic results of

Table 6. The solar model atmosphere. The model parameters T_{eff}/log g [Me/H]/ξ_t are 5780/4.44/0.00/1.15. τ_R refers to the Rosseland mean optical depth. cgs units are used except for the depth which is given in km

log τ_R	log τ_{5000}	T	log P_g	log P_e	Depth
−4.2	−4.182	4335	2.876	−1.155	0.0
−4.0	−3.983	4369	2.985	−1.048	26.3
−3.8	−3.785	4409	3.095	−0.940	52.9
−3.6	−3.589	4450	3.205	−0.831	79.8
−3.4	−3.392	4491	3.316	−0.722	107.1
−3.2	−3.195	4532	3.426	−0.613	134.5
−3.0	−2.998	4571	3.536	−0.505	162.3
−2.8	−2.800	4609	3.647	−0.398	190.2
−2.6	−2.602	4647	3.757	−0.291	218.4
−2.4	−2.403	4684	3.867	−0.185	246.7
−2.2	−2.204	4721	3.977	−0.079	275.3
−2.0	−2.005	4761	4.087	0.028	304.1
−1.8	−1.805	4806	4.197	0.136	333.2
−1.6	−1.606	4858	4.307	0.246	362.5
−1.4	−1.406	4922	4.417	0.360	392.3
−1.2	−1.207	5005	4.528	0.480	422.5
−1.0	−1.007	5112	4.638	0.609	453.3
−0.8	−0.806	5251	4.748	0.751	484.6
−0.6	−0.606	5439	4.856	0.917	516.5
−0.5	−0.506	5551	4.908	1.014	531.9
−0.4	−0.405	5683	4.958	1.127	547.0
−0.3	−0.305	5833	5.004	1.259	561.4
−0.2	−0.205	6004	5.046	1.411	574.8
−0.1	−0.105	6197	5.083	1.585	587.0
0.0	−0.006	6415	5.114	1.778	597.7
0.1	0.092	6660	5.140	1.987	606.9
0.2	0.190	6935	5.162	2.210	614.8
0.3	0.286	7267	5.178	2.459	621.3
0.4	0.381	7599	5.191	2.691	626.6
0.5	0.474	7887	5.202	2.877	631.1
0.6	0.567	8130	5.212	3.027	635.3
0.7	0.661	8340	5.221	3.149	639.4
0.8	0.751	8526	5.230	3.253	643.4
0.9	0.839	8695	5.239	3.345	647.7
1.0	0.928	8851	5.248	3.428	652.1

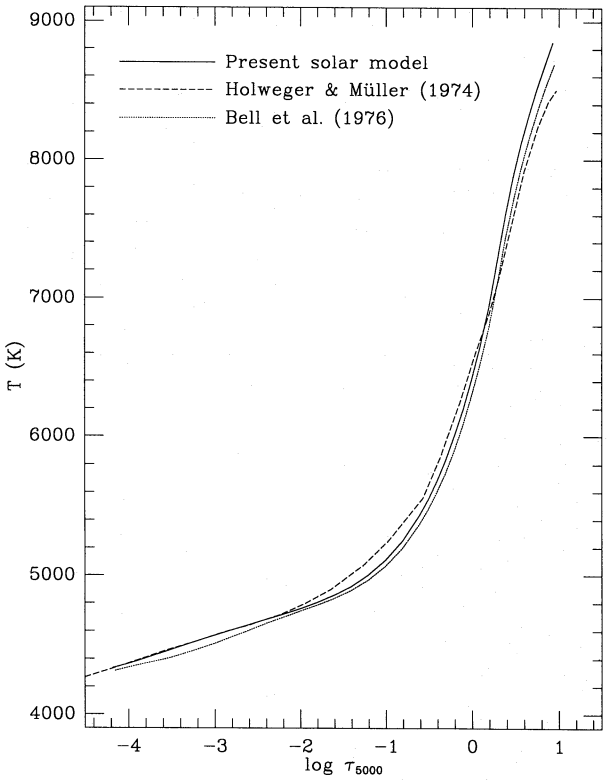

Fig. 4. Comparison of the temperature structure of our new Solar model to two other models. The temperature gradient difference in the deeper layers between the empirical Holweger-Müller model and the two theoretical, flux-constant, models is probably due to differences in the mixing length prescription for convection

Furenlid & Meylan (1990): $T_{\rm eff}$ = 5720 K (solar −60 K), log g = 4.27, from their Table 1, and [Me/H] = +0.12. Chmielewski et al. (1992) recently found a significantly higher $T_{\rm eff}$ (5800 K) for this star. However we find the Furenlid & Meylan effective temperature to be consistent with the $B-V$ value obtained by Flannery & Ayres (1978), an empirical relation between $b-y$ and $B-V$ (cf. Edvardsson & Bell 1989), and our $b-y$ calibration.

The effective temperature Both $b-y$ and the β index may be used to determine $T_{\rm eff}$. β has the advantage of being unaffected by interstellar reddening but is not as sensitive to $T_{\rm eff}$ as $b-y$. For the present sample of stars that are within a distance of 80 pc we expect that the interstellar reddening is negligible. This is confirmed from a comparison of the β and $b-y$ values of the stars. Using the $(b-y)_0$ calibration of Olsen (1988) we get $\langle E(b-y)\rangle = 0.000 \pm 0.009$ for 171 stars with $\delta m_1 > -0.01$. The distribution of $E(b-y)$ is close to a Gaussian and the dispersion is fully explained by the errors in the photometry. For the remaining 16 metal-rich stars having $\delta m_1 < -0.01$ or [Me/H] > +0.20 the calibration of Olsen (1988) is not valid, but all of these stars are closer than 50 pc. Hence, we may assume that all stars in our sample are unreddened (Paresce 1984) and use the uncorrected $b-y$ colour index to determine $T_{\rm eff}$.

For the calibration we used a grid of model atmospheres fully consistent with those used in the abundance analysis. The fluxes

Table 7. Determination of the solar $b-y$ colour from comparison with "solar analogs". Effective temperatures from Hα profiles, surface gravities and metallicities are from Cayrel de Strobel (1990) and the $b-y$ values are from the catalogues referred to in Sect. 2.1. The observed $b-y$ values were corrected for differences relative to the Sun in the metallicity, effective temperature, and surface gravity according to the differentials given in the text. The columns give, respectively, 1) Stellar identification; 2) observed $b-y$; 3) standard deviation in observed $b-y$; 4) metallicity [Fe/H]; 5) error in [Fe/H]; 6-7) effective temperature difference relative to the Sun and standard error; 8) difference in surface gravity relative to the Sun; 9) estimated solar $b-y$; 10) accumulated standard error in $(b-y)_\odot$

HD	$b-y$	σ	[Fe/H]	σ	$\Delta T_{\rm eff}$	σ	$\Delta \log g$	$(b-y)_\odot$	σ
44594	.403	.007	+.15	.06	0	40	+0.06	.398	.009
186427	.418	.0025	+.04	.10	0	50	−0.04	.418	.009
28099	.414	.005	+.14	.04	0	50	+0.06	.409	.009
1835	.422	.007	+.17	.04	0	50	+0.06	.417	.011
76151	.410	.0024	+.06	.05	−60	40	+0.06	.398	.007
20630	.420	.005	.00	.06	−140	40	+0.06	.398	.008

were calculated for these models at 4000 wavelength points distributed across the wavelength interval 1000 – 5000 Å and at most 4.5 Å apart (1.1 Å up to 4526 Å). The opacities considered were those described in Sect. 3.1, including the great number of atomic lines from Kurucz's data bank and additional molecular lines from CH, CN, NH and OH. For $\lambda > 5000$ Å, the Opacity Distribution Functions described by Gustafsson et al. (1975) were used instead. These functions were each calculated for 100 Å broad intervals and based on a smaller number of spectral lines (roughly those identified in the list of Moore et al. 1966). These absorption coefficients were distributed randomly across the corresponding wavelength intervals. As a check we calculated blocking coefficients for the wavelength regions of the b and y passbands, both for our solar model and for the observed solar flux spectrum (Kurucz et al. 1984), sampled in a manner consistent with the model. The line blocking fractions for the b passband are 16.6% and 17.6% for the model and the observations, respectively, and the corresponding figures for the y passband are 7.5% and 7.8%. This difference translates to 0.010 magnitudes in $b-y$ or about 65 K in $T_{\rm eff}$, but since our method is basically differential with respect to the Sun, we expect the systematic errors due to errors in the blocking calculations to be considerably smaller.

Next, the calculated fluxes were multiplied with filter transmission functions (cf. Crawford & Barnes 1970), and synthetic colours were computed. In order to fix the zero point of the colour index we used a set of stars found by Cayrel de Strobel (1990) to have fundamental parameters close to those of the Sun. The effective temperatures derived by Cayrel de Strobel are essentially based on Hα profiles. Of the 10 stars given by Cayrel de Strobel in her Table 3, 7 have been observed in the $uvby$ system. For one of these, HD 89010, the atmospheric parameters depart more than for the others from the solar values, and the uncertainties in its values are also greater.

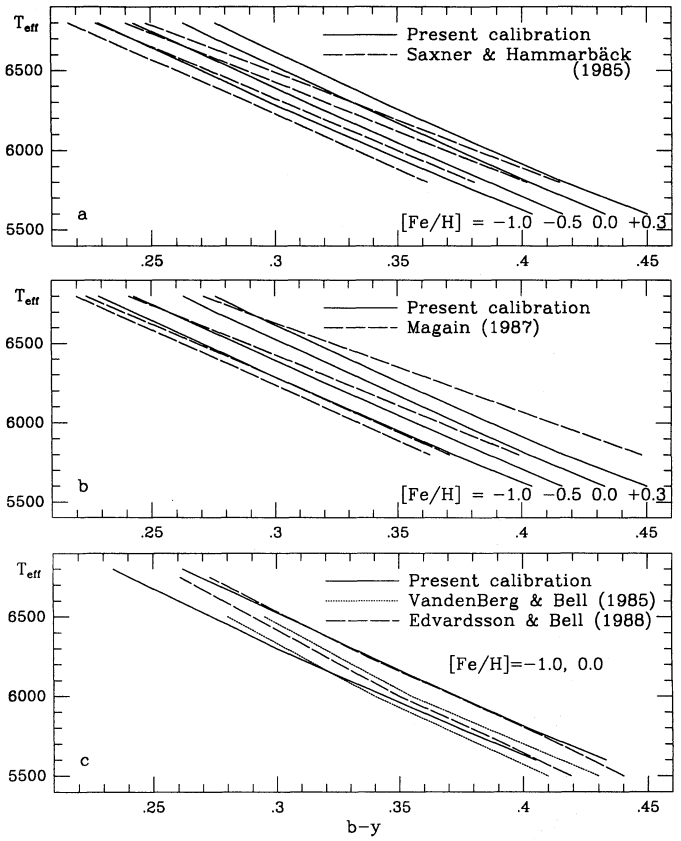

Fig. 5. Comparison of the present effective temperature calibration to some earlier empirical and theoretical calibrations. In panels **a** and **b** the present calibration is plotted for $\log g = 4.2$ and ξ_t according to Eq. (9), while the empirical calibrations were derived from solar type dwarfs with a range in surface gravities. In panel **c** the three theoretical calibrations are plotted for $\log g = 4.5$ and $\xi_t = 1.0\,\mathrm{km\,s^{-1}}$

For the remaining 6 stars we corrected the measured $b-y$ values to solar fundamental parameters, using the differentials $\Delta(b-y)/\Delta T_{\rm eff}$=−0.00015 mag/K, $\Delta(b-y)/\Delta \log g$=+0.015 mag/dex and $\Delta(b-y)/\Delta$[Me/H]=+0.026 mag/dex, as determined from the calculated $b-y$ values. The resulting values of $(b-y)_\odot$ are presented in Table 7.

A mean of these values was adopted as $(b-y)_\odot = 0.406 \pm 0.004$ (mean error). This value is in the middle of the range of recent determinations of the solar colour, see Ardeberg et al. (1983) and Gray (1992). Using the calculated index for our solar model atmosphere the zero-point of the $b-y$ scale was then established and added to the calibration.

The effective temperatures were next derived for each star using values of surface gravity and metallicity derived below.

In Fig. 5 the calibration is compared to the empirical calibrations of Saxner & Hammarbäck (1985) and Magain (1987), which are based on the infrared flux method by Blackwell & Shallis (1977), and to two earlier theoretical calibrations: VandenBerg & Bell (1985) and Edvardsson & Bell (1989). The two empirical calibrations agree with each other for metallicities near [Fe/H]=0.0 and −1.0, but disagree at all other metallicities (sometimes wildly) due to the very different metallicity dependences. The most striking difference among the theoretical calibrations is the larger metallicity sensitivity of the present one, especially at higher temperatures, which is presumably due to the large difference in the adopted metal line absorption data. A general difference between the empirical and the theoretical calibrations, including the present one, is that the former indicate a larger $\Delta(b-y)/\Delta T_{\rm eff}$, i.e. a smaller slope in Fig. 5. A part of the discrepancy between the present calibration and the two empirical ones seems to be due to the small number of stars used in the empirical calibrations. In addition, systematic differences may result from errors in the absolute calibration of the broad-band photometry used in the infrared flux method.

In an attempt to exploit the β measurements and possibly minimize the effects of photometric errors in the observed $b-y$ index and interstellar reddening, we also derived an "empirical" calibration of the β index for our programme stars. Using $T_{\rm eff}$ values as derived from $b-y$ and the calibration described above we found from a regression analysis a polynomial equation, linear in β, δm_1 and δc_1. The standard deviation for a single star from this equation was as large as 81 K.

Since the photometric errors in β are about twice as large as the errors in $b-y$ and the sensitivity of $T_{\rm eff}$ to β is only about half of the sensitivity to $b-y$, and, as shown, the scatter in $T_{\rm eff}(\beta) - T_{\rm eff}(b-y)$ is comparatively large, we finally decided to adopt the $T_{\rm eff}(b-y)$ calibration for our stars.

The errors in the effective-temperature determinations due to errors in measured $b-y$ values are typically about 25 K. Moreover, there is a systematic error of about 30 K, corresponding to an uncertainty in $(b-y)_\odot$ of about 0.005. In addition to that, further systematic errors in $T_{\rm eff}$ may result from errors in the model atmospheres and thus in the calculated $b-y$ values. These errors should, however, largely be compensated for by the fact that the models are used to establish the $T_{\rm eff}$ scale, i.e., even if $T_{\rm eff}$ is not exactly measuring the integrated flux per unit surface area of the stars it is a good measure of the temperature in the flux forming regions, which is of greatest relevance for abundance analysis.

In Sect. 4.3.4 the adopted effective temperatures are confronted with spectroscopic evidence in the form of excitation equilibria.

The surface gravity The surface acceleration of gravity was estimated by means of the Balmer discontinuity index c_1. Differences $\delta c_1 = c_{1,\rm star} - c_{1,\rm ZAMS}$, $\Delta M_V = M_{V,\rm ZAMS} - M_{V,\rm star}$ and $\Delta \log g = \log g_{\rm ZAMS} - \log g_{\rm star}$ were calculated using the respective ZAMS values for the β (or $T_{\rm eff}$) and [Me/H] values of the star. From the relationships between δc_1, ΔM_V and $\Delta \log g$ given below and $\log g_{\rm ZAMS}$ adopted from stellar model calculations, $\log g_{\rm star}$ was then determined.

In order to determine $\log g$ by this method the ZAMS relation between c_1 and β must be known. The standard relation of Crawford (1975) is, by definition, equal to the ZAMS relation for solar metallicities. On the basis of $uvby$-β photometry of a large sample of metal deficient stars by Schuster & Nissen (1988) it was found that the lower envelope of the distribution of stars in the $c_1 - \beta$ diagram (and thus the ZAMS relation)

Table 8. Atomic line data and Solar equivalent widths. The first five columns give, respectively, the line rest wavelength, the excitation energy of the lower level, the logarithm of the product of the oscillator strength and the statistical weight, an enhancement factor multiplied to the classical van der Waals damping constant and the radiation damping constant. Columns 6 and 7 give the Solar equivalent width and identifies whether it was measured from ESO (E) or McDonald (M) spectra. The measured equivalent widths were corrected for 1% scattered light as described in Sect. 2 of Paper II. In the last column we indicate whether the line was frequently measured in the data sets from ESO (E), McDonald (M) or both (B)

λ [Å]	χ_l [eV]	$\log gf$	$\delta\Gamma_6$	$\Gamma_{\rm rad}$ [s^{-1}]	$W_{\lambda\odot}$ [mÅ]	Obs. $\odot$	Used
O I $\log\epsilon_\odot = 8.93$							
6158.17	10.74	−0.32	2.5	5.4+7	5.3	E	E
7771.95	9.14	+0.25	2.5	4.8+7	69.9	E	E
7774.17	9.14	+0.11	2.5	4.7+7	60.9	E	E
7775.39	9.14	−0.11	2.5	4.5+7	47.8	E	E
Na I $\log\epsilon_\odot = 6.33$							
6154.22	2.10	−1.61	2.0	6.4+7	38.2	E	B
6160.75	2.10	−1.31	2.0	6.6+7	58.6	E	B
Mg I $\log\epsilon_\odot = 7.58$							
8712.69	5.93	−1.26	2.5	1.4+7	55.6	E	B
8717.82	5.93	−0.97	2.5	1.4+7	88.3	E	B
Al I $\log\epsilon_\odot = 6.47$							
8772.87	4.02	−0.41	2.5	2.3+8	80.4	E	B
8773.90	4.02	−0.25	2.5	2.3+8	98.1	E	B
Si I $\log\epsilon_\odot = 7.55$							
6125.03	5.61	−1.54	1.3	1.1+6	32.7	M	M
6142.49	5.62	−1.48	1.3	8.4+5	35.4	E	B
6145.02	5.61	−1.43	1.3	9.6+5	38.8	E	B
6155.14	5.62	−0.77	1.3	3.6+6	85.4	E	E
7760.64	6.20	−1.28	1.3	6.6+5	21.5	E	E
7800.00	6.18	−0.72	1.3	3.3+6	55.9	E	E
8728.01	6.18	−0.36	1.3	6.6+6	89.3	E	B
8742.45	5.87	−0.51	1.3	8.2+7	95.6	E	B
Ca I $\log\epsilon_\odot = 6.36$							
5867.57	2.93	−1.61	1.8	2.6+8	26.2	E	B
6161.30	2.52	−1.27	1.8	1.9+7	66.5	E	B
6166.44	2.52	−1.20	1.8	1.9+7	70.8	E	B
6169.04	2.52	−0.82	1.8	2.0+7	95.6	E	B
Ti I $\log\epsilon_\odot = 4.99$							
5087.06	1.43	−0.84	2.5	3.3+7	30.0	E	E
5113.45	1.44	−0.88	2.5	3.6+7	27.7	E	E
5866.46	1.07	−0.87	2.5	6.4+7	48.5	E	B
6126.22	1.07	−1.46	2.5	7.1+6	21.0	M	M
Fe I $\log\epsilon_\odot = 7.51$							
5067.16	4.22	−0.93	1.4	2.1+8	71.3	M	M
5083.34	0.96	−3.11	1.2	1.5+7	108.	M	M
5088.16	4.15	−1.59	1.4	2.6+8	39.6	E	E
5090.78	4.26	−0.53	1.4	2.1+8	93.7	E	B
5104.44	4.28	−1.54	1.4	2.1+8	36.0	E	E
5109.66	4.30	−0.73	1.4	2.1+8	78.8	E	B
5126.20	4.26	−0.65	1.4	2.1+8	85.7	M	M
5127.37	0.91	−3.32	1.2	1.7+7	99.8	M	M
5141.75	2.42	−2.19	1.4	1.5+8	88.1	M	M
5809.22	3.88	−1.76	1.4	5.1+7	45.1	M	M
5849.69	3.69	−2.97	1.4	5.5+7	8.0	E	B
5852.22	4.55	−1.22	1.4	1.9+8	41.0	E	B
5855.08	4.61	−1.56	1.4	1.9+8	22.7	E	B
5856.09	4.29	−1.60	1.4	5.6+7	33.8	E	B
5858.78	4.22	−2.19	1.4	2.7+8	14.0	E	B
5859.59	4.55	−0.61	1.4	1.9+8	74.4	E	B
5861.11	4.28	−2.34	1.4	2.1+8	9.2	E	B
5862.36	4.55	−0.42	1.4	1.9+8	87.0	E	B
6151.62	2.18	−3.33	1.4	1.6+8	50.3	E	B
6157.73	4.08	−1.24	1.4	5.0+7	62.5	E	B
6159.38	4.61	−1.88	1.4	1.9+8	12.8	E	B
6165.37	4.14	−1.53	1.4	8.8+7	44.8	E	B
6173.34	2.22	−2.90	1.4	1.7+8	68.5	E	B
6187.99	3.94	−1.70	1.4	4.6+7	45.9	M	M
6200.32	2.61	−2.45	1.4	1.0+8	71.7	M	M
7745.52	5.08	−1.18	1.4	6.4+8	22.9	E	E
7746.60	5.06	−1.29	1.4	6.3+8	19.4	E	E
7751.11	4.99	−0.77	1.4	6.4+8	47.1	E	E
7802.51	5.08	−1.37	1.4	6.3+8	16.2	E	E
8713.20	2.95	−2.51	1.4	9.3+7	62.5	E	E
8747.44	3.02	−3.29	1.4	8.0+7	20.6	E	E
8757.19	2.84	−2.02	1.4	7.7+6	94.2	E	B
Fe II $\log\epsilon_\odot = 7.51$							
5100.66	2.81	−4.13	2.5	3.4+8	22.8	E	E
6149.23	3.89	−2.80	2.5	3.4+8	36.3	E	B
Ni I $\log\epsilon_\odot = 6.25$							
5082.35	3.66	−0.63	2.5	1.8+8	68.4	M	M
5084.11	3.68	−0.18	2.5	1.3+8	98.2	M	M
5088.54	3.85	−1.09	2.5	1.6+8	33.1	E	E
5088.96	3.68	−1.33	2.5	1.3+8	29.5	E	E
5094.42	3.83	−1.17	2.5	1.2+8	30.4	E	B
5099.94	3.68	−0.25	2.5	1.3+8	92.4	E	E
5102.97	1.68	−2.81	2.5	1.3+8	50.3	E	B
5115.40	3.83	−0.34	2.5	7.3+7	77.8	E	B
5847.00	1.68	−3.43	2.5	7.4+7	23.3	E	B
5857.75	4.17	−0.39	2.5	2.2+8	57.4	E	E
6111.08	4.09	−0.96	2.5	1.5+8	30.2	M	M
6130.14	4.27	−1.04	2.5	2.8+8	20.0	M	M
6133.98	4.09	−1.77	2.5	1.4+8	6.4	E	M
6175.37	4.09	−0.59	2.5	2.3+8	50.0	E	E
6176.82	4.09	−0.37	2.5	1.5+8	63.4	E	B
6177.25	1.83	−3.53	2.5	4.3+7	15.5	E	E
6204.61	4.09	−1.17	2.5	1.8+8	21.2	M	M
7748.89	3.71	−0.37	2.5	9.5+7	90.6	E	E
7788.93	1.95	−1.99	2.5	1.0+8	90.7	E	E
7797.58	3.90	−0.40	2.5	1.0+8	76.8	E	E
Y II $\log\epsilon_\odot = 2.24$							
5087.43	1.08	−0.36	2.5	1.3+7	47.3	E	B
Zr II $\log\epsilon_\odot = 2.60$							
5112.27	1.66	−0.76	2.5	1.1+7	9.8	E	B
Ba II $\log\epsilon_\odot = 2.13$							
5853.68	0.60	−0.97	3.0	6.4+7	63.3	E	B
6141.73	0.70	−0.06	3.0	7.3+7	117.	E	B
Nd II $\log\epsilon_\odot = 1.50$							
5089.83	0.20	−1.14	2.5	2.1+6	3.4	E	E
5092.80	0.38	−0.51	2.5	6.1+6	9.0	E	E

shifts according to the equation

$$c_{1,\mathrm{ZAMS}}(\beta) =$$

$$\begin{cases} c_{1,\mathrm{STD}}(\beta) + 0.055\,([\mathrm{Me/H}] + 0.2), & \text{if } [\mathrm{Me/H}] < -0.2; \\ c_{1,\mathrm{STD}}(\beta) & \text{otherwise.} \end{cases} \quad (4)$$

The difference in absolute, visual magnitude, corresponding to δc_1, was calculated as

$$\Delta M_V = (9.0 + 50\,(2.72 - \beta)) \cdot \delta c_1 \quad (5)$$

where the coefficient of δc_1 has been determined empirically by Nissen (1988) from a study of *uvby-β* photometry of open clusters.

Neglecting the small change in bolometric correction as a function of M_V at a given effective temperature but taking into account that a star in the main-sequence band above the ZAMS has a somewhat larger mass than a star with the same T_{eff} on the ZAMS we get

$$\Delta \log g = 0.35 \cdot \Delta M_V . \quad (6)$$

Finally, the ZAMS relation

$$\log g_{\mathrm{ZAMS}} = 4.45 - 2.583\,(\log T_{\mathrm{eff}} - 3.80) - 0.1 \cdot [\mathrm{Me/H}], \quad (7)$$

derived from the stellar models of VandenBerg (1985), was used to determine $\log g_{\mathrm{star}}$ from $\Delta \log g$.

It should be emphasized that this gravity calibration is valid only for main sequence stars with $5600 < T_{\mathrm{eff}} < 7000$ K and [Fe/H] > -1.0.

The error of $\log g$ corresponding to the photometric errors of β and c_1 is of the order of ± 0.07 dex. However, systematic errors in the calibration equations may be larger. The position of the $c_{1,\mathrm{ZAMS}}(\beta)$ relation for the metal deficient stars is uncertain by as much as $\pm\ 0\overset{\mathrm{m}}{.}02$ in c_1, corresponding to an error of $\pm$ 0.1 dex in $\log g$. Furthermore, it is known that cluster sequences of unevolved F stars do not always follow the same $c_1 - \beta$ relation even if the clusters have the same metallicity. Most notable is the Hyades anomaly of $\delta c_1 \approx 0.03$ with respect to Coma (Strömgren et al. 1982). Similar large differences of c_1 occur between other pairs of clusters with identical metal abundances (Nissen 1988). This suggests that the c_1 index is affected by parameters other than T_{eff}, $\log g$ and [Me/H] causing errors of the order of $\pm$ 0.1 dex in $\log g$.

As a check of our method of determining the surface gravity, we have computed $\log g$ for a sample of F-type binary stars for which accurate *uvby-β* photometry exists and for which $\log g$ has been determined to an accuracy better than 0.02 dex from the binary data directly (mass and radius). The sample consists of the following binary components: UX Men A and B (Andersen et al. 1989), DM Vir A=B (Andersen et al. 1984), RZ Cha A=B (Jørgensen & Gyldenkerne 1975; Andersen et al. 1975) and V1143 Cyg A=B (Andersen et al. 1987). The mean difference between the two sets of $\log g$ values is 0.04 dex with a rms deviation of only 0.05 dex. Thus this comparison confirms the estimated accuracy of the surface gravity determination, although it should be admitted that the comparison covers only a limited range in T_{eff} (6100-6600 K) and [Me/H] (-0.15 to $+0.10$).

The metal abundance The metal abundance parameter [Me/H] was determined from the δm_1 index using the equation

$$[\mathrm{Me/H}] = -(10.5 + 50\,(\beta - 2.626)) \cdot \delta m_1 + 0.12 . \quad (8)$$

The coefficient of δm_1 is the same as derived empirically from very narrow band photometry by Nissen (1981). The constant, however, has been changed from 0.16 to 0.12 in accordance with the determination of the Hyades iron abundance by Cayrel et al. (1985). In calculating δm_1 we used the Hyades relation between m_1 and β published by Crawford & Barnes (1969). It is slightly different from the standard relation of Crawford (1975) but gives a somewhat better fit to the observed Hyades sequence in the range $2.62 < \beta < 2.66$ (Nissen 1988).

The error in [Me/H] corresponding to the mean error of δm_1 is about $\pm$ 0.05 dex, while Nissen (1981) estimated the total error in [Me/H] to be 0.10 dex. For the δm_1 calibration of Nissen (1981) only a few stars with [Me/H] < -0.6 were available, and one may therefore question the validity of the linear expression in Eq. (8) for the most metal deficient stars in our sample. However, as we shall see, the spectroscopic values of [Fe/H] derived in the present paper agree well with [Me/H] determined from Eq. (8), except for the most metal rich stars, for which the equation overestimates the metallicity by 0.1 to 0.3 dex. For the metal rich stars, the exact metallicity is rather important for the line blanketing and the structure of the atmosphere, and thus the derived atmospheric parameters and abundances may be expected to be sensitive to this parameter. Therefore, we decreased the metallicities of the 15 metal rich stars with the largest differences [Fe/H]$-$[Me/H] to the values of [Fe/H] derived in a preliminary abundance analysis, and reiterated the determination of model parameters and the abundance analysis. Although the procedure of abundance analysis and determination of model parameters was not iterated to full consistency, this has a negligible effect on the finally derived abundances.

3.1.2. The microturbulence parameter

The microturbulence parameters, ξ_{t}, for the individual stars were determined from an empirically derived relation between ξ_{t}, T_{eff} and $\log g$. This relation was derived during the abundance analysis and the microturbulence parameters are therefore (in contrast to the photometric determination of T_{eff} and $\log g$) not independent of the details of this analysis.

Originally the relation found by Nissen (1981) was adopted for the Sun and the programme stars and abundances of Fe I and Ni I were derived for all stars as described in Sect. 3.2. These two species are the best observed, as regards the number of spectral lines, and they both contain lines of a range of different equivalent widths and excitation energies. 17 Fe I and Ni I lines were observed in the majority of stars in both the ESO and the McDonald samples, and these lines were chosen for determination of microturbulence parameters. For each of the stars with at least 12 of these common lines observed (157 stars) a linear relation was sought between abundance and line

strength; ($\log \epsilon_{line} - \langle \log \epsilon \rangle_{species}$ vs $\log W/\lambda$ where the theoretical equivalent widths were used, following Magain (1984)). The slope coefficients thus obtained were then plotted against $T_{\rm eff}$, $\log g$ and [Me/H]. After some experimenting with the parameters of Eq. 2 of Nissen (1981) and iteration of the described procedure we found a relation that minimized the dependence of the slope coefficients on the fundamental stellar atmospheric parameters:

$$\xi_{\rm t} = 1.25 + 8 \cdot 10^{-4}(T_{\rm eff} - 6000) - 1.3\,(\log g - 4.5)\ {\rm km\,s^{-1}}. \quad (9)$$

This relation (which was used for the final abundance analysis) was derived for stars in the parameter range $5550 < T_{\rm eff} < 6800$; $3.8 < \log g < 4.5$; $-1.1 <$ [Me/H] < 0.3. No significant metallicity dependence was found, and the rms scatter of individual stars from this relation is about 0.3 km s^{-1}. This relation departs from that of Nissen (1981) by having a larger $T_{\rm eff}$ coefficient.

3.2. *Abundances*

The abundance analysis was made with model atmospheres constructed individually for each star, see Sect. 3.1. Theoretical equivalent widths were calculated and the model abundance iterated until the calculated equivalent width was equal to the measured width. When more than one line of the same species was measured for a star, a mean abundance value and the standard deviation of the mean were calculated.

To avoid uncertainties due to statistical noise in weak lines, a lower limit was set to the acceptable line strength, $\log(W_\lambda/\lambda) = -6.1$ (5 mÅ at 6000 Å), and weaker lines were excluded from the final abundance determinations. Similarly, an upper limit to the line strength was set in order to avoid excessive uncertainty due to the increasing microturbulence sensitivity of stronger lines. This limit was set at $\log(W_\lambda/\lambda) = -4.8$ (95 mÅ at 6000 Å), but Ba II lines were excluded from this cut in order to allow barium abundances to be determined for all stars. To avoid systematic errors (Magain 1984), the line strength cuts were applied not to the measured equivalent widths but rather to the "theoretical" equivalent widths; this is the equivalent width the line would have in order to give the mean abundance obtained for the species.

3.2.1. Atomic line data

The 86 spectral lines used in the abundance analysis were selected after inspection of solar and stellar spectra. The lines were chosen to be as free as possible of blends affecting the measurements of equivalent widths. A few lines, although showing no line asymmetry, were excluded when it became clear from the abundance analysis that they were probably blended, i.e. when the abundance derived for a certain line differed from the abundance of other lines of the same species by an amount correlated with the stellar effective temperature.

Solar oscillator strengths (gf values) were used for all the lines. They were determined by requiring that the equivalent width calculated for the solar model of our grid, $T_{\rm eff} = 5780$ K, $\log g = 4.44$, [Me/H] = 0.0 and $\xi_{\rm t} = 1.15$ km s^{-1}, be equal to the equivalent width observed in the solar spectrum. The fact that our lines are weak or only moderately saturated not only in the programme stars, but also in the Sun, suggests that their solar equivalent widths provide reliable oscillator strengths. Solar chemical abundances were adopted from Anders and Grevesse (1989) except for iron for which the meteoritic value of $\log \epsilon = 7.51$ was adopted, which agrees well with recent photospheric abundances (Holweger et al. 1991, Biémont et al. 1991). The solar observations and data reduction are described in Paper II.

Atomic line broadening by radiation damping and van der Waals damping (as well as from thermal Doppler broadening and microturbulence) was considered in the calculation of equivalent widths and abundances. Radiation damping parameters for Ca through Ni lines were adopted from Kurucz (1989). For the remaining species, published oscillator strengths of strong lines were used for determination of life times and thus radiation damping for relevant energy levels. Correction factors to the classical van der Waals damping widths (Γ_6) were taken from the literature: Na I: Holweger (1971), Si I: Holweger (1973), Ca I: O'Neill & Smith (1980), Ba II: Holweger & Müller (1974), Fe I: Simmons & Blackwell (1982) and Magain & Zhao (1992), Fe II: Holweger et al. (1990). For all other species a correction factor of 2.5 was applied to the classical Γ_6 ($\Delta \log C_6 = +1.0$), following Mäckle et al. (1975). Stark broadening was found to have negligible effects on our lines in these stars, except possibly for our two Mg lines.

The atomic line data are presented in Table 8.

3.2.2. Scaling of oxygen abundances

It is well known both theoretically and empirically (cf. Eriksson & Toft 1979; Nissen et al. 1985; Kiselman 1991, 1993) that oxygen abundances derived from the high excitation O I infrared triplet lines near 7773 Å are affected by non-LTE effects and possibly also by convective inhomogeneities. This recently motivated a special investigation of the [O I] 6300 Å line (Nissen & Edvardsson 1992) in 23 of our programme stars. This line is expected to suffer far less from effects of non-LTE and inhomogeneities than the triplet lines. The oxygen abundances derived from the [O I] line were found to be different from those derived from high excitation lines, suggesting an abundance pattern more similar to that of the other α elements (cf. Sect. 6). This result was used to derive simple, empirical corrections to our results: For the 6158.17 Å line we found

$$[{\rm O/Fe}]_{6300} = -0.025 + 0.4657\ [{\rm O/Fe}]_{6158} \quad (10)$$

from 15 stars with a standard deviation $\sigma = 0.050$, and for the triplet lines at 7771.95, 7774.17 and 7775.39 Å

$$[{\rm O/Fe}]_{6300} = -0.078 + 0.6794\ [{\rm O/Fe}]_{7773} \quad (11)$$

from 20 stars with $\sigma = 0.091$.

These scaled oxygen abundances are the ones used in the following, except in the calculation of Z in the age determinations which were made before these results were available (cf. Sect. 5.1).

4. Errors in resulting abundances

4.1. Effects of errors in equivalent widths

Comparisons of data from ESO spectra of the same star but independently observed, reduced and measured by two persons show that for most stars the equivalent widths are generally reproduced with a standard deviation of 2 mÅ. The resulting abundance errors are significant (up to 0.05 dex) only for elements with one or two weak lines measured (Fe II, Zr II and Nd II). Effects of systematic errors in equivalent widths, e.g., due to undiscovered blends or errors in continuum definition, are more difficult to evaluate. In general, however, they should be small. Possible exceptions are the abundances of Y, Zr and Nd that are based on measurements in the regions at the shortest wavelengths where the continuum location is difficult and risk of blending is obviously higher in the most metal-rich stars. There are also systematic differences between equivalent widths measured from ESO and those measured at McDonald Observatory. These are discussed in Paper II, and their possible small effects on abundances will be discussed in Sect. 4.3.

4.2. Errors in models and in calculated equivalent widths

The errors in the abundances induced by errors in model atmospheres and calculated equivalent widths may be of different types: errors in fundamental parameters ($T_{\rm eff}$, log g, [Me/H], $\xi_{\rm t}$), errors in the temperature structures, e.g., due to missing opacity sources, and errors due to oversimplifying basic assumptions concerning convective flux, plane-parallel stratification, or LTE. Another type of error is that caused by representing spectra of unresolved binary stars with models of single stars. Further errors are due to errors in gf values. In the following, effects of these different types of errors will be commented upon.

4.2.1. Errors in fundamental parameters of the model atmospheres

As discussed above, we estimate errors in the $T_{\rm eff}$ values due to errors in observed $b-y$ values and in $(b-y)_\odot$ to be about 50 K. Moreover, the excitation equilibria may indicate that there are further systematic $T_{\rm eff}$ errors of 50-100 K; see Sect. 4.3.4, below. It seems realistic to consider the possible total errors in $T_{\rm eff}$ to range from −50 K to +100 K.

In log g the total errors may approach 0.2 dex, resulting from errors in observations of β and c_1, from systematic errors in the $c_{1,\rm ZAMS}(\beta)$ relation and influences on δc_1 by "non-classical effects".

The errors in the first photometric estimates of [Me/H] were estimated to 0.10 dex. As described above, for 15 metal rich stars with strongly deviating spectroscopic metallicities the procedure was iterated with these new [Me/H] values to achieve consistency. After these corrections, the final errors in the abundances resulting from errors in the choice of [Me/H] for the models were found to be negligible.

Errors in the microturbulence parameters were estimated to 0.3 km s^{-1}. In most stars, however, only a few lines are seriously affected by microturbulence and only the Ba abundance is sensitive to the microturbulence.

The consequences on the abundance estimates of changing the fundamental parameters within the error estimates above are illustrated for four different stars in Table 9.

It is seen that the errors are, at the most, about 0.10 dex in the abundances relative to hydrogen, and generally less in the abundances relative to Fe. For the elemental abundances derived from lines of neutral atoms the effective-temperature uncertainty is the most important one, leading to abundance errors of typically 0.05 dex, while for the abundances derived from ions, notably those of the s-elements, the errors in log g may be

Table 9. Effects on derived abundances resulting from model changes for four typical programme stars. The model parameters ($T_{\rm eff}$/log g/[Me/H]) are given after the stellar identifications. The table entries show the effects on the logarithmic abundances relative to hydrogen, Δ[X/H], of changes in effective temperatures and surface gravities, and also the effects of using scaled Solar (Holweger-Müller) models in the analysis. Note that the effects on "relative" abundances, for example [X/Fe], are often considerably smaller than abundances relative to hydrogen, [X/H]

	HR 4903 (5953/4.00/+0.26)			HR 784 (6287/4.37/−0.09)			HD 98553 (5907/4.38/−0.53)			HD 22879 (5826/4.27/−0.98)		
Ion	Δ$T_{\rm eff}$ +100 K	Δ log g −0.2 dex	Scaled model	Δ$T_{\rm eff}$ +100 K	Δ log g −0.2 dex	Scaled model	Δ$T_{\rm eff}$ +100 K	Δ log g −0.2 dex	Scaled model	Δ$T_{\rm eff}$ +100 K	Δ log g −0.2 dex	Scaled model
Fe I	+.06	+.01	+.02	+.06	+.01	−.01	+.06	+.01	0.00	+.06	0.00	0.00
O I	−.06	−.04	+.09	−.05	−.03	0.00	−.06	−.03	−.05	−.05	−.03	−.06
Na I	+.05	+.01	−.03	+.05	−.01	−.01	+.05	0.00	−.01	+.04	0.00	−.01
Mg I	+.03	+.04	−.11	+.03	+.03	−.01	+.02	+.01	−.01	+.03	+.01	−.03
Al I	+.03	+.04	−.12	+.04	+.03	−.02	+.04	+.03	−.02	+.04	+.02	−.03
Si I	+.03	+.01	−.02	+.03	+.03	0.00	+.01	0.00	0.00	+.02	0.00	−.01
Ca I	+.06	+.02	−.04	+.06	+.02	−.01	+.07	+.02	0.00	+.06	+.01	−.02
Ti I	+.08	0.00	−.02	+.08	0.00	−.01	+.09	0.00	+.01	+.09	0.00	+.02
Ni I	+.06	0.00	−.02	+.06	+.01	0.00	+.06	0.00	0.00	+.06	0.00	+.01
Fe II	−.03	−.09	+.17	−.02	−.08	+.02	−.02	−.08	+.01	−.02	−.09	+.05
Y II	+.01	−.09	+.15	+.02	−.08	+.03	+.02	−.08	+.02	+.06	−.07	+.10
Zr II	0.00	−.08	+.16	+.01	−.08	+.02	0.00	−.09	+.03	+.02	−.08	+.07
Ba II	+.02	−.06	+.06	+.04	−.02	0.00	+.04	−.02	+.01	+.05	−.04	+.01
Nd II	+.02	−.09	+.15	+.03	−.08	+.02	+.03	−.09	+.04			

more significant. The microturbulence parameter uncertainties may lead to uncertainties in the Ba abundances of between 0.05 and 0.10 dex.

4.2.2. Errors in temperature structure

In spite of the fact that the "theoretical" or "flux-constant" models used in the present study should be among the most sophisticated ones calculated for F-type stars they may still be inadequate, e.g. due to the basic assumptions behind them. The use of flux-constant plane-parallel models for the analysis of solar-type spectra may therefore be questioned (see, e.g. Steffen 1985 or Spite 1990) and several authors prefer to use the simpler scaled solar model atmospheres instead. Although the present differential approach (i.e. all gf values were determined by requiring the calculated equivalent widths for a model of the solar atmosphere, consistent with the models for the stars, to agree with the observations) should minimize the errors, it is still of interest to study the effects on the abundances of using scaled solar models. We calculated a set of such models with temperature structures according to the relation

$$T(\tau_{5000}) = \frac{T_{\rm eff}}{T_{\rm eff\odot}} \cdot T_{\odot}(\tau_{5000}) \qquad (12)$$

where $T_{\odot}(\tau_{5000})$ is the Holweger & Müller (1974) model. After integration of the hydrostatic equilibrium equation for the appropriate metal abundance the models were used for deriving abundances of four stars with different fundamental parameters. The gf values were next obtained by applying the Holweger & Müller model to the solar equivalent widths. The results are given in Table 9. It is seen that the effects on the abundances are, not unexpectedly, largest for the stars with the extreme metallicities. Typically, they are less than 0.1 dex; the abundances of O, Mg and Al may, however, be significantly affected for metal-rich stars. It is also noteworthy that the abundances as derived from ions are more severely affected as a result of the neglect of the temperature structure sensitivity to metal-line absorption. In fact, the good consistency between the Fe I and Fe II abundances when the flux constant models are used (cf. Sect. 4.3.3) indicates that the differential metal-line blanketing is indeed significant for the analysis of solar-type stars. We assert that the differences between the abundances derived from the flux constant and the matching scaled models are a reasonable measure of the errors from a failure of the flux constant models to represent the true atmospheres correctly within the assumption of homogeneous plane-parallel layers.

We also tested the sensitivity of the abundances to the mixing-length parameter of convection by increasing ℓ/H_P from 1.5 to 3.0. The maximum effects of 0.04 dex were obtained for oxygen, which reflects the great temperature sensitivity and deep formation layers of these high-excitation lines. However, these small effects of convection uncertainties may well be underestimated since convection should penetrate to shallower depths in the F star atmospheres.

4.2.3. Non-LTE effects

All abundances have been derived on the assumption that LTE prevails. This is known to be a questionable assumption for solar-type stars. In particular, for the more metal-poor stars the hot UV radiation field might lead to non-local (over-)ionization and also affect the excitation equilibria. For G-type subdwarfs significant departures from LTE for Fe I were reported by Magain (1988) and Magain & Zhao (1992). These authors found abundances systematically smaller by 0.2 dex when derived from low-excitation lines than from high-excitation lines of iron. The effect was interpreted as the result of over-ionization; the low-excitation lines being formed systematically further out in the atmosphere where the over-ionization effect is more significant.

In his calculation for a 17 level Fe I model atom in F-dwarf model atmospheres with different metal abundances Saxner (1984) found over-ionization effects which caused errors in LTE-abundances by -0.3 dex for models with [Fe/H]$=-1.0$, and much less for more metal-rich stars. More recently, Gratton et al. (1992), using models and UV fluxes of the present study, found that the effects were considerably reduced when the number of atomic levels was increased, due to a more efficient collisional coupling. Gratton et al. obtained negligible abundance effects for an Fe I model atom with 40 levels in a solar model while corrections of up to 0.2 dex were derived for a model with ($T_{\rm eff}$/log g/[Me/H]) = (5690/4.0/-2.0). The corresponding results obtained for a Mg I atom were < 0.04 dex for the solar case while they may amount to about 0.1 dex for the subdwarf. In another study, Lemke (1992) has studied Fe I with a more extensive Fe I atom (according to Gigas 1986) in a sequence of solar-type model atmospheres and varying [Fe/H], again with model atmospheres and UV fluxes consistent with those of the present study. The non-LTE effects obtained are smaller or of the same order of magnitude as those obtained by Gratton et al.; for the model with the greatest effects (6500/4.5/-1.0) the absolute effects are still less than 0.1 dex. Typical effects on [Fe/H] are 0.04 dex and increase with increasing effective temperature and decreasing metallicity. The use of Kurucz ODF UV fluxes leads to marginally greater effects; the maximum correction being 0.15 dex. Gehren et al. (1991) recently calculated departures from LTE of iron with a similar model atom for solar-type Population I stars and also found only marginal effects.

Gehren et al. (1991), however, found considerable non-LTE effects due to over-ionization for resonance Al I lines in metal-poor dwarf models, amounting to 0.5 dex. This result reflects the strong photo-ionization edge of Al I at 2078 Å, and the sparse term structure, which makes the coupling to the continuum by collisions weak. For the more mildly metal poor stars of our sample and the excited lines we use, however, the effects are expected to be considerably smaller.

For oxygen, Kiselman (1991, 1993) has studied the departures from LTE in abundances derived from the infrared triplet and the 6158 Å lines. The non-LTE corrections are considerable (typically -0.4 dex) but get less significant with decreasing [Fe/H] for models in the present [Fe/H] interval. This work shows that there is still a significant discrepancy between observed and calculated solar triplet lines - the latter being about 50% too strong. We note that collisions with neutral hydrogen atoms were not included in these calculations. Kiselman speculates that the discrepancy might be due to effects of inhomo-

geneities. In Sect. 3.2.2 we discuss the scaling of our oxygen abundances to the results of Nissen & Edvardsson (1992) for the [O I] 6300 Å line, which should be formed in LTE.

In concluding the discussion on non-LTE effects on the abundances we find that the abundances based on neutral lines may be somewhat underestimated, as a result of the over-ionization effects dominating over departures from the Boltzmann distribution. However, the effects are probably close to negligible for complex atoms, such as iron. Also for simpler atoms, like Mg I they are at most on the order of 0.1 dex in the abundances, and probably only significant for the most metal-poor stars. Greater effects are possible for aluminium and probably for oxygen, prior to our scaling to the [O I] line abundance scale.

The second order effects, on the model atmospheres and thus only indirectly affecting the line strengths, are probably considerably smaller than the direct ones. This is, however, not quite certain since there is a positive feed-back in the sense that an increased ionization enhances the UV flux which in turn increases the over-ionization. Some experiments to consider this in the model atmospheres (Saxner 1984; Gratton et al. 1993) indicate, however, that this is not very important.

Further non-LTE studies are urgently needed but are not thought to alter the main conclusions of the present paper. The likely corrections to the abundances for the non-LTE effects are small enough to rival the present uncertainties in the non-LTE calculations themselves!

4.2.4. Inhomogeneities

One of the least studied possible sources of systematic errors in the chemical analysis of solar-type stars is the effect of thermal inhomogeneities, presumably induced by convection. Existing simulations of convection (Nordlund & Dravins 1990; Steffen et al. 1989) have not yet, to our knowledge, been used for a systematic study of such effects. Some guidance may be obtained from Steffen's work, as quoted by Holweger et al. (1990), where the effects of granular inhomogeneities on strengths of some different solar absorption lines were investigated. The errors in the abundances are typically 30% or less. A characteristic feature is also that lines of different excitation and from different ionization stages behave similarly; what matters for the absolute line strength is the temperature gradient rather than the temperature itself. Therefore, the effects on abundance ratios [X/Fe] ought to be small. In general, one may expect that effects of thermal inhomogeneities on relative abundances should be most serious for lines that are strongly temperature dependent, and in particular for those that show a pronounced non-linear behaviour on temperature. This means in practice lines of high excitation from elements that are mainly neutral or lines of low excitation from elements that are mainly ionized (in this latter case the difference in $\chi_{\rm ionization} - \chi_{\rm excitation}$ is particularly important). We have investigated these effects when studying the errors due to errors in effective temperature. For the model of a typical star, the effects were found to be greatest for the following elements ($\Delta[N_{\rm el}]$ for $\Delta T_{\rm eff}$ = 100 K given within parenthesis): O I (−0.08), Ti I (+0.08), Ca I (+0.06), Fe I (+0.06) and Ni I (+0.06). Obviously, the ratio [O/Fe] is particularly vulnerable to the effects of inhomogeneities.

Kiselman (1991) has studied the behaviour of the oxygen triplet lines in solar type dwarfs of different metal abundances. He concludes that the line strengths cannot be fully explained as the result of (non)-LTE line formation in plane-parallel model atmospheres, neither in the solar spectrum nor in the spectra of Population II dwarfs, and suggests the discrepancies between calculated and observed line widths be due to inhomogeneities. These discrepancies amount to about 20% for disk stars, relative to the Sun. Ascribing all this to inhomogeneities we would estimate an upper limit of the effects for Ca, Fe and Ni to be less than 15% in the abundances and that ratios like Ca/Fe are not significantly affected by inhomogeneities. The fact that the oxygen lines are formed at much greater depths than the other lines may imply that this is an overestimate of the effects since the thermal fluctuations due to convection are greater there (cf. Nordlund & Dravins 1990). This conclusion is, however, very tentative, and a detailed study based on hydrodynamical simulations of inhomogeneities would be highly worthwhile. Cf. also note added in proof.

4.2.5. Oscillator strengths

The solar observations are discussed in Paper II, where the errors in the solar equivalent widths are estimated to be about 1%. For lines on the linear part of the curve of growth, the resulting errors in the gf values are also 1% and, hence, negligible, while they may rise to 0.03 dex for stronger lines on the flat part of the curve of growth.

Undetected line blends and uncertainties in the solar continuum level may introduce errors in the solar gf values. Since the Sun is cooler than most programme stars, and also of higher surface gravity, this might be a significant source of error. This is difficult to evaluate, in particular for abundances derived from a small number of spectral lines. In the present case, however, we do not believe that significant errors in excess of about 0.1 dex have been introduced due to this for the abundance of any element.

4.2.6. Duplicity

Undiscovered binary components contributing significantly to the total light will cause four main types of errors:

1. An erroneous effective temperature may be estimated from the colours and be used for the model atmosphere;
2. inappropriate equivalent widths, hence erroneous abundances, may be derived;
3. the age estimate based on these temperatures and abundances may be wrong, and
4. the assumed distance, and thus the tangential velocity and computed galactic orbital parameters, may be incorrect.

The number of undiscovered binaries in the sample may be estimated as follows: The 46 stars below the Bright Star Catalogue (BSC) magnitude limit were selected without previous duplicity information. The CORAVEL observations of these stars, which have typical errors below 0.5 km s^{-1}, reveal seven spectroscopic binaries among them. Three of them have large enough amplitudes that they would have been detected if in the BSC, while the other four (10%) have low amplitudes (5-6 km s^{-1}) and might well have passed undetected. Similarly,

Table 10. Mean differences in abundances, Δ = $[X/H]_{McD} - [X/H]_{ESO}$, derived for 16 stars observed both from ESO and McDonald. The first set of data shows the differences using all available lines, while the second set shows the abundances derived using only lines common to spectra from both sites for those elements for which the line data sets differ (labeled "B" in the last column of Table 8). The standard deviation (σ) of Δ and the number of stars used to calculate the mean are also given

Species	Δ_{all}	σ	N	Δ_{common}	σ	N
Fe I	−0.03	0.03	16	−0.02	0.04	16
Fe II	−0.02	0.06	16	−0.01	0.05	16
Na I	+0.00	0.06	16			
Mg I	+0.04	0.06	13			
Al I	+0.00	0.07	14			
Si I	−0.03	0.06	16	−0.03	0.06	16
Ca I	−0.04	0.03	16			
Ti I	+0.01	0.09	13	+0.00	0.08	12
Ni I	+0.00	0.08	16	−0.01	0.06	16
Y II	−0.05	0.13	10			
Zr II	+0.09	0.10	5			
Ba II	−0.08	0.05	16			

among 28 BSC stars with existing velocity data, we find only one new (also low-amplitude) binary. In all, among 89 stars with CORAVEL data, we find 5 low-amplitude binaries. Thus, we can expect of the order of 8-10 undetected binaries in the sample.

How many of these binaries have secondary components of significant luminosity? A simple estimate, based on the binary statistics by Abt & Levy (1976) and Abt (1983) (but see also Morbey & Griffin (1987) and Abt (1987)) leads to the conclusion that there should be only about one star in the sample for which an undiscovered binary companion would lead to significant errors in the parameters of interest in this paper.

4.3. Consistency checks

Abundances derived from different lines of the same element should ideally be identical. If there are differences which are correlated with ionization state, excitation energy, wavelength or line strength one may suspect systematic errors in the basic assumptions, in the input data, or in the analysis. Below we will discuss a few simple checks of our results along these lines.

4.3.1. ESO vs McDonald

Small discrepancies were found between ESO and McDonald equivalent widths measured from spectra of the Sun and of 16 stars observed from both sites (see Paper II). These are generally due to differences either in the observations or in the data reductions and are discussed in Paper II. Here the resulting abundance differences will be discussed.

Firstly, the two sets of abundances derived for the 16 stars are compared in Table 10. The largest differences appear for Zr II and Ba II. For Zr II only the rather weak 5112.27 Å line has been observed. The weakness of this line makes it especially sensitive to continuum location. This combined with the fact that in the McDonald spectra the highest points in the immediate neighbourhood of the line often do not reach the continuum, means that the fitted Gaussian may have been too wide at the continuum and so slightly overestimated some of the McDonald equivalent widths. The higher resolution of the ESO spectra makes them always come close to, or reach, the continuum in the immediate neighbourhood of the line so that one has much less of a tendency to overestimate its equivalent width. We think that the 0.09 dex greater Zr abundance (Table 10) obtained from the McDonald spectra is, therefore, a result of their lower resolution.

Both Ba II lines (5853.68 and 6141.73 Å) were measured for all stars except for one line for two ESO stars. The Ba II lines' location on the flat portion of the curve of growth, which was avoided for other lines (cf. Sect. 3.2) has the consequence that small errors in their equivalent widths results in comparatively large abundance errors. The differences in resolution may have caused some differences in the measurements of the contribution to equivalent widths from the damping wings of the two samples of stars.

Secondly, since we expect the northern and southern samples to be statistically equivalent, the abundance trends for all stars in the two samples can be compared. When comparing plots of [X/Fe] vs [Fe/H] for all stars in both samples, some small differences may be traced. These can partly be related to the somewhat different line samples measured for the two sets, while the rest is probably due to differences in the observations and data reduction procedures.

For Na I, Al I, Ca I and (in spite of what was found for the 16 stars in Table 10) Ba II, the same lines are measured at both observatories, and the abundance trends are in excellent agreement.

For Mg I, the same two lines are measured, but the ESO abundances fall a little bit lower than the McDonald abundances; the difference is at the most 0.05 dex for the metal rich stars. Scrutiny of the two lines shows that they both give very nearly the same abundances in the McDonald sample (standard deviation only 0.047 dex), and the 8717.82 Å line in the ESO spectra gives a 0.04 dex lower abundance compared to the McDonald observations. The 8712.69 Å line, however, gives in the ESO results systematically lower abundances for the high-metallicity stars. The cause of the difference seems to be that the higher resolution of the ESO spectra will cause the Gaussian line measurement fits to avoid more of the often rather pronounced wings of the lines, thereby underestimating the true equivalent widths. Both lines have high excitation energies and are rather strong in the Sun (55.0 and 87.4 mÅ), therefore we expect the line wings in many of the spectra to be caused by the quadratic Stark effect. The mismatch of the Stark wings by the Gaussian fits is likely to introduce some line-strength dependent errors in the resulting Mg abundances, making our Mg abundances less accurate than those of other elements. Tests show that the fine structure splitting of the lines does not affect our abundance measurements.

For Ti I the McDonald abundances fall about 0.04 dex higher than the ESO abundances for the metal rich stars, and this differ-

ence is only marginally reduced when the only line in common between the two data sets, 5866.46 Å, is used alone.

For Si I and Ni I the McDonald abundances are a few hundredths of a dex higher than those of ESO for the more metal poor stars, but the samples meet at intermediate values when only the lines in common are used.

Fe I is naturally the best represented species in the survey, and here it has been used for normalization of the other abundances. Only the lines in common between the two samples have been used for that purpose. However, the $[Fe/H]_{ESO}$ is in the general analysis based on a sample of Fe I lines significantly different from the $[Fe/H]_{McDonald}$. The effects of these differences in the Fe I line data samples have also been been investigated: For the ESO stars, the iron abundances are the same for the "common lines" and the "all lines" samples, with a standard deviation of only 0.012 dex, while for the McDonald sample the $[Fe/H]_{Fe\,I,\,all\,lines}$ agrees very well with $[Fe/H]_{Fe\,I,\,common\,lines}$ at solar metallicity but is about 0.02 dex higher for the metal poor stars.

4.3.2. Photometric vs spectroscopic metallicities

One may also compare the $[Fe/H]_{Fe\,I}$ values with the photometrically derived metallicities. The iron abundances derived from Fe I lines deviate somewhat from the original [Me/H] values derived from Eq. (8), Sect. 3.1.1. A linear regression fit to the McDonald data gives

$$[Me/H] = 1.144\,[Fe/H] + 0.018; \quad \sigma = 0.088\,, \tag{13}$$

whereas the corresponding ESO regression gives

$$[Me/H] = 1.086\,[Fe/H] - 0.014; \quad \sigma = 0.098\,. \tag{14}$$

The largest deviations from a linear relation were found for 15 of the most metal rich stars (cf. Sect. 3.1.1). For these it appears that the photometric metallicities are overestimated by 0.1 to 0.3 dex. The removal of these 15 stars gives for the remaining 174 ones the relation

$$[Me/H] = 1.049\,[Fe/H] - 0.030; \quad \sigma = 0.074\,. \tag{15}$$

The differences [Me/H] – [Fe/H] are shown in Fig. 6. The small scatter in the relations above underlines the high precision possible in the photometric metallicity determination, especially since part of the scatter must be caused by random errors in the spectroscopic analysis. The 5% difference from unity slope is probably due to our revised temperature scale, and secondary consequences of this.

4.3.3. Ionized vs neutral species

There are two Fe II lines available in our spectra, λλ 5100.66 and 6149.23 Å. Both lines are accompanied by weak, unidentified features in high resolution solar atlases. The 5100.66 Å line was measured only in the ESO Reticon spectra; a neighbouring, fainter, high excitation Fe II line 0.20 Å towards the red forces us to reject the Fe II line in the less resolved ESO CCD or McDonald spectra. There are also numerous C_2 lines in the vicinity.

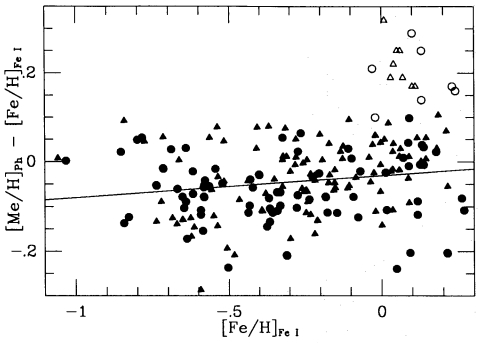

Fig. 6. The differences between photometric metallicities and spectroscopic iron abundances vs spectroscopic iron abundance. ESO stars are shown as circles and McDonald stars as triangles. The rms scatter from the linear fit is 0.074 dex. The open symbols show the 15 metal rich stars discussed in Sect. 3.1.1 and indicated in Table 11. These were not included in the derivation of the least squares fit of Eq. (15)

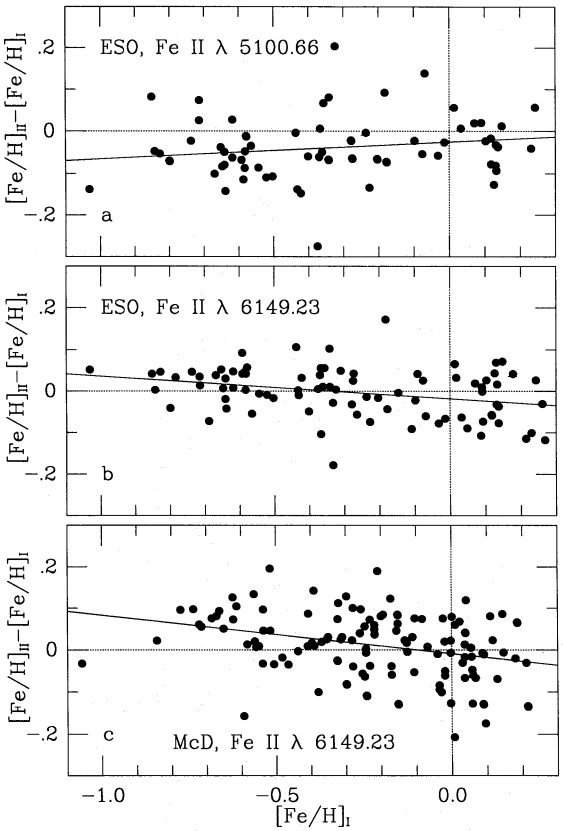

Fig. 7a–c. Comparison of iron abundances determined from Fe I and Fe II lines for northern and southern stars. **a** ESO stars, for Fe II only the line at λ 5100.66 Å. **b** ESO stars, for Fe II only λ 6149.23 Å. **c** McDonald stars, for Fe II only λ 6149.23 Å. Linear least squares fits are shown as solid lines, and the stars scatter around these with standard deviations of 0.074, 0.056 and 0.072 dex, respectively, in the three panels

The 6149 Å line appears much more isolated from obviously disturbing lines. Plots of [Fe II/Fe I] vs [Fe I/H] for the different lines are shown in Fig. 7. There are only weak trends in the diagrams, indicated by the linear least squares fits. In general the consistency between the Fe I and Fe II lines is very satisfac-

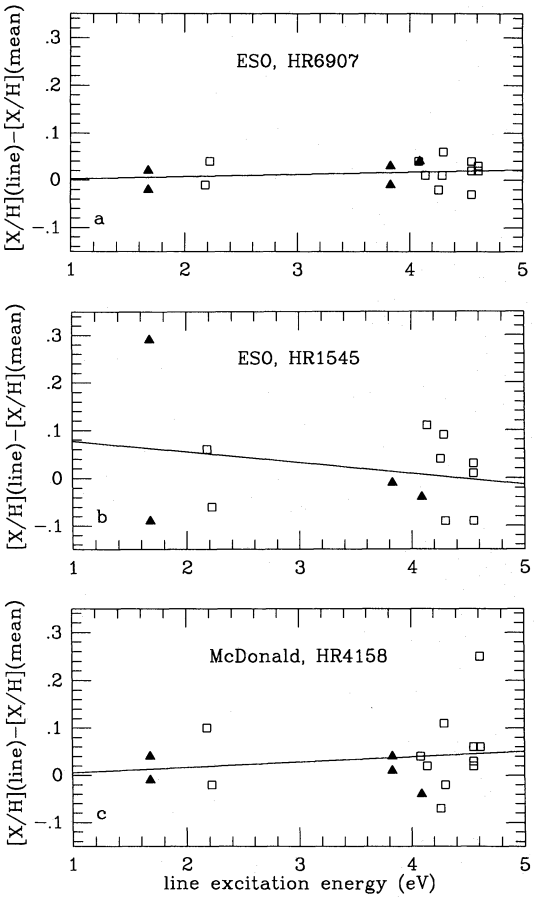

Fig. 8. Variations in derived nickel (triangles) and iron (squares) abundances as a function of excitation energy of the lower line state. From panels **b** and **c**, it is obvious that the slope for a single star may be seriously affected by an error in the measured equivalent width of one line

tory, indicating that the log g values derived from the Strömgren photometry are accurate to within 0.15 dex rms as estimated in Sect. 3.1.1 (c.f. Table 9 for iron abundance effects of variations in log g).

4.3.4. Excitation equilibrium

In a perfect abundance analysis, the abundance of an element as derived from different lines should be independent of the excitation energy. We have investigated the excitation balance for a sample of 17 lines of Fe I and Ni I which were observed in most stars. The use of both these species together is motivated by a wish to have as many lines as possible for statistical reasons. The ionization energies and ranges in excitation energies are similar for Fe and Ni, and the iron to nickel abundance ratio in all the stars is almost identical (see below, Sect. 6.2).

For all stars with at least 12 of these 17 lines observed (80 ESO stars and 77 McDonald stars), the abundance from each of the selected lines *minus* the mean abundance derived for the species were plotted against excitation energy of the lower line energy level, and linear least squares fits were derived. Rather small slopes were found in most of these plots. Examples of such diagrams are shown in Fig. 8. The slope parameter of the fit for each star was then plotted against the fundamental atmospheric parameters. This is shown in Fig. 9. Apparently, there are some small but systematic deviations from excitation equilibrium, which seem to vary with model atmosphere parameters. The deviations differ between the two samples of stars, being smaller for the ESO stars. This is most likely explained by the differences in the observations and data reductions. The mean values of the deviations are +0.007 and +0.015 dex eV^{-1}, respectively, for the two samples of stars, which, translated into errors in effective temperatures, correspond to underestimates by 50 and 100 K. It should be pointed out that these results are based on gf values derived from observed solar equivalent widths and the solar model, which was assumed to be in perfect LTE excitation equilibrium. We conclude that systematic errors in the effective temperatures may be typically 50 K, with a possible dependence on effective temperature.

4.3.5. Summary

The consistency checks indicate a high internal consistency between the two sets of observations. Differences between results for ionized and neutral lines for Fe are very minor. The dependence of abundance on excitation is rather small and not very significant. Systematic errors due to data reduction uncertainties, blends, line saturation and other systematic errors discussed above lead to an error of at most 0.05 to 0.10 dex in the abundance ratios [X/Fe] in almost all cases. Also [Fe/H] is judged to be accurate to this degree.

5. Stellar ages and dynamics

5.1. The stellar ages

Ages of the stars were estimated by comparing their position in the $\Delta M_V - \log T_{\rm eff}$ diagram with theoretical isochrones. Procedures for determining $T_{\rm eff}$ and ΔM_V (defined with respect to the $M_{V,\rm ZAMS}(\beta)$ relation for the metal abundance of the star) are described in Sect. 3.1.1. The isochrones were adopted from VandenBerg (1985), and refer to stellar models with helium mass fraction Y = 0.25 and heavy element mass fractions of Z = 0.0169, 0.01, 0.006, 0.003 and 0.0017. Using the $M_{V,\rm ZAMS}(\log T_{\rm eff})$ relations computed by VandenBerg for the various Z values, we transformed his isochrones given in the $M_V - \log T_{\rm eff}$ plane to the $\Delta M_V - \log T_{\rm eff}$ plane.

The models of VandenBerg (1985) were computed with a mixing-length parameter of α = 1.6. This value is required to match the shapes of observed ZAMSs and the effective temperatures of globular cluster giants. On the other hand α = 1.6 leads to a solar model which is too hot by $\delta \log T_{\rm eff}$ = 0.009. As discussed by VandenBerg & Poll (1989) this mismatch is probably due to the fact that VandenBerg (1985) used underblanketed theoretical model atmospheres to provide the boundary conditions of his models. If instead the empirical model of the solar atmosphere by Holweger & Müller (1974) is adopted, the effective temperature of the solar model agrees with the effective temperature of the Sun. Also, a good agreement is obtained if the present model atmospheres are used as boundary conditions

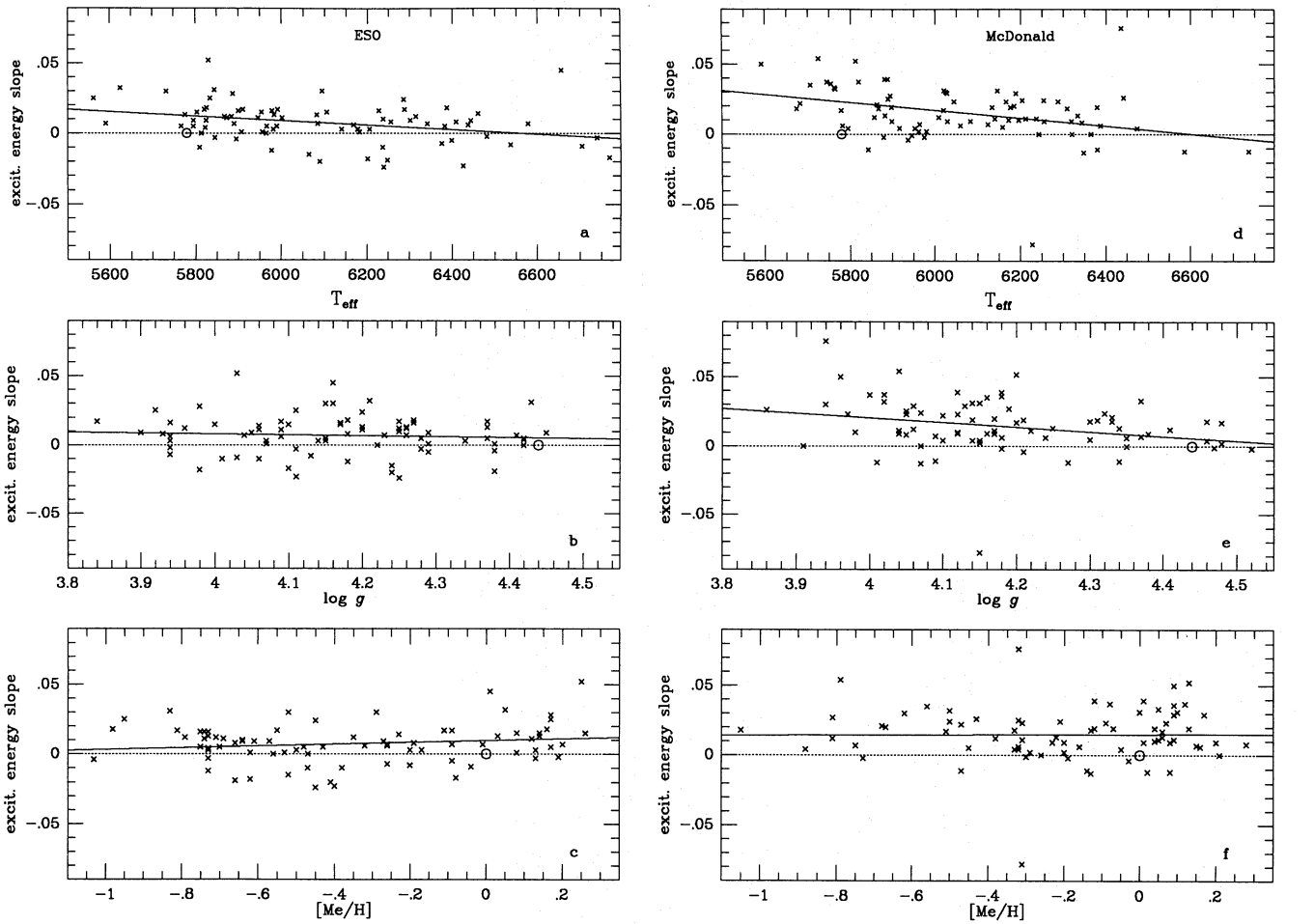

Fig. 9a–f. Residual deviations from excitation equilibria of Fe I and Ni I. See text for explanations. **a-c**: ESO observations, **d-f**: McDonald observations

for new VandenBerg models (Gustafsson 1992). This suggests that the models of VandenBerg (1985) are slightly too hot for the disk stars, and we have therefore shifted his isochrones by $\delta \log T_{\rm eff} = -0.009$. In Fig. 10 the resulting isochrones corresponding to ages of 2, 4, 8 and 15 Gyr are shown for the heavy element mass fractions of $Z = Z_\odot = 0.0167$ and $Z = 0.006$.

The mass fraction of elements heavier than helium in a given star was calculated from the abundance ratios determined in the present work. If data for [O/H] are missing or of low accuracy, as is the case for stars observed from McDonald, we have used [O/H] = 0.4 · [Fe/H]. For the heavier unobserved elements we have assumed that the abundance relative to iron is the same as in the Sun. The solar composition of heavier elements was adopted from Table 1 of VandenBerg (1983).

The five Z-values of the isochrone sequences of VandenBerg (1985) correspond to values of $\log Z/Z_\odot$ of 0.0, −0.23, −0.45, −0.75 and −1.0, whereas the range in $\log Z/Z_\odot$ of the stars goes from about 0.2 to −0.7. For each star the sequence of isochrones for the $\log Z/Z_\odot$ value closest to that of the star was selected and the star plotted in the corresponding $\Delta M_V - \log T_{\rm eff}$ diagram. By graphical interpolation the value of the logarithmic age ($\log \tau$), corresponding to the chosen $\log Z/Z_\odot$ value, was assigned to the star, and then corrected for the difference between the heavy element abundance of the star and that of the set of isochrones. This rather small correction was determined from the shift of the isochrones as a function of $\log Z$. The resulting individual stellar ages are given in Table 11.

In Fig. 10 the isochrone sequences corresponding to Z = 0.0169 and Z = 0.006 are shown together with stars having Z-values in narrow ranges around these values. The error bars given correspond to the mean errors of $T_{\rm eff}$ and ΔM_V, $\sigma(\log T_{\rm eff}) = 0.007$ and $\sigma(\Delta M_V) = 0.3$, as estimated from the photometric errors and possible errors in the calibration of the photometry. The corresponding error of the logarithmic age is $\sigma(\log \tau) = 0.07$ to 0.15, depending on the position of the star in the $\Delta M_V - \log T_{\rm eff}$ diagram, in good agreement with the error estimates of Strömgren (1987). A few stars in our sample lie rather close to the ZAMS (they were observed at McDonald before the final selection criteria were set up) and have errors in $\log \tau$ considerably larger than 0.15 dex. For these stars the ages have not been derived. Furthermore, a number of the younger stars lie in the so-called "hook-region" of the isochrones, where the age determination is ambiguous. In these cases, which are marked in Table 11, we have assumed that the star is in the core hydrogen burning phase and used the age resulting from interpolation between the redder part of the isochrones.

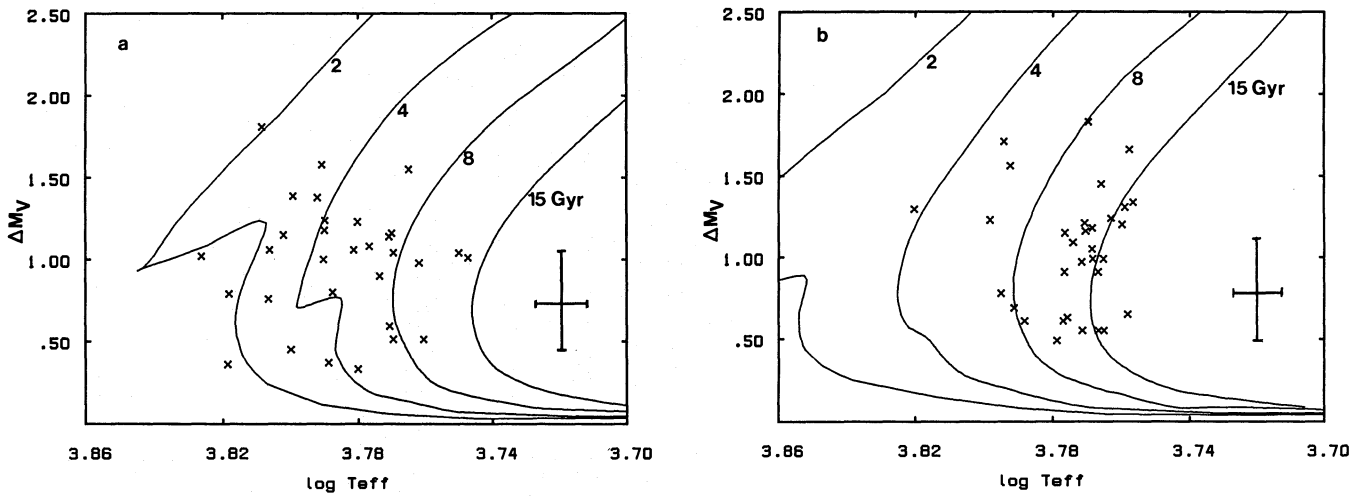

Fig. 10a and b. The ΔM_V–$\log T_{\rm eff}$ diagram with isochrones from VandenBerg (1985) for 2, 4, 8 and 15 Gyr. In **a** the isochrones correspond to $Z = Z_\odot = 0.0169$ and the stars plotted have $-0.05 \leq \log Z/Z_\odot \leq +0.05$. In **b** the isochrones correspond to $Z = 0.006$ (i.e. $\log Z/Z_\odot = -0.45$), and the stars plotted are within the range $-0.55 \leq \log Z/Z_\odot \leq -0.35$. The error bars correspond to $\pm$ the estimated mean errors of $\log T_{\rm eff}$ and ΔM_V

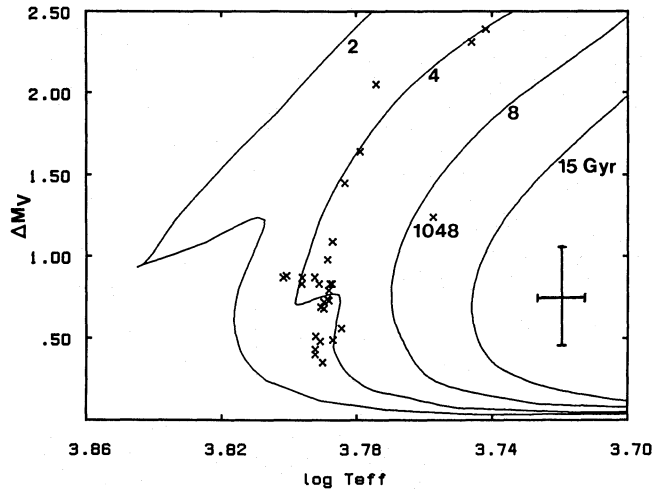

Fig. 11. The $\Delta M_V - \log T_{\rm eff}$ diagram for stars in M67. Only stars with $\Delta M_V \gtrsim 0.4$ have been plotted and known binaries and suspected variables have been excluded. The position of the possible non-member (ID 1048) is indicated. For comparison the isochrones of VandenBerg (1985) corresponding to $Z = 0.0169$ are shown

The ages derived are somewhat sensitive to the chemical composition of the stars, in particular to the abundance of oxygen, because this element contributes about half of the total mass of elements heavier than helium. The oxygen abundances derived directly from the high excitation O I lines were used when the age determinations were made. If instead the (more correct) scaled oxygen abundances (cf. Sect. 3.2.2) would have been used, the ages of some metal deficient stars would increase by up to 0.10 dex. In most cases, however, these changes are less than 0.05 dex.

The error, $\sigma(\log \tau) = 0.07$ to 0.15, is estimated from the errors of the photometric determination of $T_{\rm eff}$ and ΔM_V. Errors in the computed isochrones will also contribute to the uncertainty of the derived ages. It is therefore important to get an independent check of the accuracy of the ages. Such a check is indeed possible on the basis of *uvby-β* photometry of the open cluster M67 by Nissen et al. (1987).

M67 is an intermediate-age cluster of solar metallicity with a turn-off effective temperature close to the average $T_{\rm eff}$ of our sample of stars. From the *uvby-β* data of Nissen et al. we have derived $T_{\rm eff}$ and ΔM_V using the calibrations in Sect. 3.1.1, and have plotted the stars with $0.4 \lesssim \Delta M_V < 2.5$ in Fig. 11. As can be seen all stars except one fall relatively close to the 4 Gyr isochrone. Spectroscopic binaries and photometric variables as listed in Table III of Nissen et al. are excluded. The exception (ID 1048) has a distance modulus of $V_0 - M_V = 10.1$ which is considerably higher than the average distance modulus of 9.6 for M67. Probably ID 1048 is a field star, despite the fact that the proper motion study of Sanders (1977) gives a membership probability of 84%. Excluding this star we derive a mean logarithmic age of $< \log \tau >= 9.58$ (corresponding to an age of M67 of 3.8 Gyr) and a rms deviation of $\sigma(\log \tau) = 0.07$, showing that the theoretical isochrones are close to having the correct shape.

Still, our age determinations for stars with non-solar abundances may have systematic errors because the VandenBerg (1985) models did not have quite the correct chemical composition. First, a rather large extrapolation in $\log Z/Z_\odot$ is necessary for the most metal-rich stars. Second, the models for metal-poor stars do not take into account the enhancement of O and the α-elements. Recent models by VandenBerg (1992) and corresponding isochrones by Bergbusch & VandenBerg (1992) do include enhanced O, with scaled solar abundances for all other heavy elements. We have compared the models adopted here with the new set for the same total content of those heavy elements which are important for the opacities and hence for the temperatures used to estimate ages. The new 16-Gyr isochrone for $Z = 0.006$ coincides almost exactly with the 15-Gyr standard isochrone in the $\log T_{\rm eff} - \Delta M_V$ diagram (Fig. 10b). Thus, oxygen enhancement alone seems not to imply any major revision of our age estimates for the oldest stars. In particular,

our conclusion that field star ages seem to range up to those of globular clusters appears to be a fairly robust result.

Nonetheless, the possibility of systematic errors in the $T_{\rm eff}$ values of both the observed stars and the models advises caution in accepting the absolute values of the ages derived here. Important sources of systematic errors are convective overshoot and opacities. Although the empirical tests based on binaries that have been performed (e.g. Popper & Ulrich 1986; Andersen et al. 1988a, 1989) suggest that the standard evolutionary models work very well for main-sequence stars with $M \lesssim 1.3 M_{\odot}$ there may be considerable effects of convective overshoot and opacity uncertainties for higher masses (Andersen 1991; Andersen et al. 1991). The new grid of models by Schaller et al. (1992), containing improved opacity tables as well as some numerical refinements, greatly reduces the age discrepancy between standard and overshooting models (cf. also Bertelli et al. 1992). Ages derived from those models seem to agree with our present estimates within 10%.

We conclude that the differential ages should be accurate to within 0.10 dex at least when stars with similar abundances are compared.

5.2. Kinematic data and galactic orbital parameters

5.2.1. Distances and space motions

The sample of stars studied here occupies a small, local volume. Their precise present locations relative to the Sun are not in themselves of particular interest because the stars were born elsewhere in the Galaxy. Some stars, in fact, have travelled over a wide range of Galactocentric distances before making their current appearance in the solar neighbourhood (see, e.g. Grenon 1987). Hence, their abundances carry information about spatial variations in the production of the chemical elements as well as their evolution with time. The space motions of the stars in our sample are the clue to their origin in the Galaxy, and we have made an effort to determine these motions as accurately as possible.

In order to derive space motions we need distances, proper motions, and radial velocities for all the stars. Photometric distances on a uniform scale were determined by computing the absolute magnitudes with the $\delta c_1 - \beta$ method of Crawford (1975), using the improved scale factor f by Nissen (1988) and the slightly revised $M_{\rm V,ZAMS}(\beta)$ relation by Olsen (1989). As an independent check on the photometric distance scale, absolute trigonometric parallaxes were available for many of our stars from the new catalogue by van Altena et al. (1993), kindly made available before publication. Mean trigonometric and photometric parallaxes for groups of successively more distant stars were compared, and excellent agreement was found. We thus estimate that our distances are without appreciable systematic error and accurate to within about $\pm 15\%$ (Crawford 1975). Possible exceptions may be the spectroscopic binaries which are marked in Table 11.

Proper motions have been compiled from a variety of sources retrieved from the SIMBAD data base. They are thus

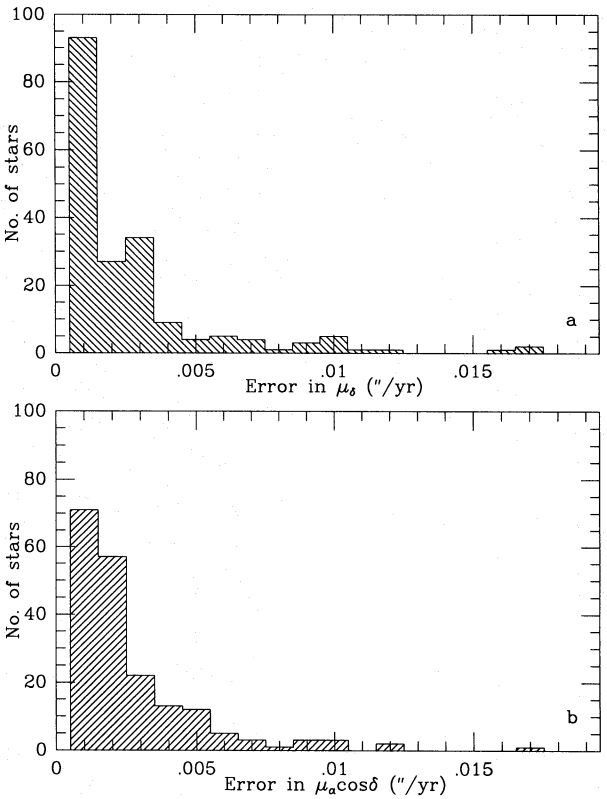

Fig. 12. The distribution of proper motion errors for the 189 programme stars

of somewhat heterogeneous origin and accuracy. Many of our bright stars are, however, found in the FK5 fundamental catalogue (Fricke et al. 1988) and thus have proper motions of excellent quality. Moreover, modern positions on the FK5 system have been observed for all the stars north of declination $-45°$ by the Carlsberg Automatic Meridian Circle (CAMC) at La Palma, Spain. Improved proper motions based on these observations are included in the Carlsberg Meridian Catalogues (1989, 1991). As appears from Fig. 12, the vast majority of our stars have proper motions better than about $\pm 0\farcs005\ {\rm yr}^{-1}$; the few exceptions are stars below the declination limit of the CAMC. These exceptions are marked in Table 11. Corresponding typical errors in the tangential velocity are only $\pm 1\ {\rm km\ s}^{-1}$.

Radial velocities for most of the brighter stars are found in the Wilson (1953) General Catalog, with quality "a" or "b". In addition, precise measurements of radial velocity have been made with the CORAVEL photoelectric scanners (Mayor 1985) in both hemispheres in several programmes overlapping with the sample discussed here (see Andersen et al. 1985; Nordström & Andersen, 1989). Mean radial velocities have been extracted from the CORAVEL data base and have kindly been made available for the present study before publication. These data are complete for all stars for which previous radial velocities were of quality "c" or missing, and have also clarified a few dubious cases of alleged or real variability. Thus, radial velocities are also known to about $\pm 1\ {\rm km\ s}^{-1}$ for almost all the stars.

Table 11 contains the computed distances and space motion components U (positive towards the anticentre), V, and W,

Table 11. Data for the programme stars. $T_{\rm eff}$, log g and [Me/H] are the parameters used for the model atmospheres. ([Me/H] values closer to the resulting [Fe/H] values were used for the models of 15 stars, cf. Sect. 3.1.1. [Me/H] values for these 15 are given within parentheses.) [Fe/H]: resulting spectroscopic iron abundance. Dist.: distance from the Sun. U, V, W: space motions relative to the Sun (U is positive towards the galactic anti-centre). $R_{\rm p}$: perigalactic distance. $R_{\rm m}$: straight mean of the perigalactic and the apogalactic distances. Z_{max}: maximum distance from the galactic plane. e: orbital eccentricity as projected on the galactic plane. Ages are determined from isochrones and in the last column spectroscopic binaries "SB" (with possibly uncertain distances), stars with uncertainties in proper motions "pm" significantly above 0.″005 year^{-1} and possible hook stars "h" (for which the ages may be underestimated by 0.15 dex) are indicated

ID	$T_{\rm eff}$ [K]	log g [cgs]	[Me/H]	[Fe/H]	Dist. [pc]	U [km s^{-1}]	V [km s^{-1}]	W [km s^{-1}]	$R_{\rm p}$ [kpc]	$R_{\rm m}$ [kpc]	$Z_{\rm max}$ [kpc]	e	log Age [Gyr]	Rem.
HR 17	6192	4.13	−0.39	−0.35	29.7	−24.5	−9.8	−7.9	7.15	8.05	0.02	0.11	0.74	
HR 33	6204	4.07	−0.50	−0.38	19.6	−19.3	−14.0	−18.7	7.11	7.90	0.13	0.10	0.74	
HR 35	6577	4.26	−0.09	−0.10	22.6	21.9	3.2	−2.3	7.90	8.48	0.04	0.07	0.29	SB
HR 107	6488	4.08	−0.29	−0.37	37.8	−13.6	−35.1	−17.3	6.23	7.23	0.11	0.14	0.53	
HR 140	6408	4.18	−0.19	0.05	27.1	17.1	−22.7	−35.2	7.01	7.57	0.33	0.07	0.46	
HR 145	6176	4.06	−0.36	−0.25	39.3	−43.0	−23.3	−2.8	6.36	7.70	0.03	0.17	0.68	
HR 203	5809	4.06	−0.38	−0.28	29.9	−20.5	−24.7	4.8	6.65	7.56	0.10	0.12	0.93	
HR 219	5946	4.47	−0.30	−0.31	5.0	25.8	−7.9	−13.3	7.59	8.10	0.07	0.06		
HR 235	6254	4.32	−0.21	−0.15	17.0	−23.8	−2.8	−12.7	7.36	8.28	0.07	0.11	0.49	
HR 244	6196	3.98	0.04	0.00	21.1	5.8	21.3	16.2	8.00	9.12	0.27	0.12	0.54	
HR 340	5804	3.88	−0.34	−0.21	34.3	−24.8	2.1	−5.2	7.46	8.45	0.01	0.12	0.69	
HR 366	6474	4.10	−0.32	−0.32	24.9	34.9	21.2	−8.3	7.84	9.16	0.02	0.14	0.54	
HR 368	6517	4.01	−0.24	−0.24	40.4	25.1	38.2	−4.0	7.96	9.93	0.02	0.20	0.49	
HR 370	6081	4.26	0.03	0.12	17.3	51.6	−23.4	−10.5	6.53	7.64	0.04	0.15	0.54	
HR 448	5820	3.84	−0.11	0.09	33.0	9.6	−30.5	13.0	6.60	7.30	0.20	0.10	0.53	
HR 458	6212	4.17	0.05	0.09	13.3	−28.3	−22.1	−14.6	6.64	7.67	0.08	0.13	0.46	h
HR 483	5898	4.31	0.04	−0.02	14.5	44.4	−35.5	−0.7	6.11	7.26	0.05	0.16	0.88	
HR 573	6239	4.25	−0.45	−0.34	28.1	57.0	−10.4	−4.3	6.90	8.08	0.02	0.15	0.77	pm
HR 646	6358	4.07	−0.38	−0.32	28.4	19.3	−11.8	3.2	7.57	7.98	0.09	0.05	0.59	
HR 672	6045	4.12	0.07	0.06	26.9	68.9	10.6	17.1	7.17	8.93	0.28	0.20	0.70	
HR 720	5857	4.06	−0.38	−0.22	25.6	25.7	29.5	−14.9	7.95	9.50	0.10	0.16	0.87	
HR 740	6436	3.94	−0.32	−0.25	25.8	−28.2	−2.6	19.1	7.29	8.31	0.29	0.12	0.49	
HR 784	6287	4.37	−0.09	0.02	23.0	−15.3	3.1	−7.8	7.66	8.47	0.02	0.10		SB
HR 799	6309	4.30	−0.13	−0.02	11.0	30.8	2.0	−0.5	7.73	8.43	0.05	0.08	0.46	
HR 962	6104	4.10	0.08	0.09	22.6	20.0	−19.2	−6.1	7.18	7.69	0.00	0.07	0.57	
HR 1010	5889	4.41	−0.26	−0.23	13.1	76.3	−49.4	18.3	5.18	7.05	0.26	0.26	0.94	
HR 1083	6769	4.10	−0.08	−0.11	23.2	54.1	−24.0	−3.2	6.47	7.64	0.02	0.15	0.26	
HR 1101	5981	4.15	−0.20	−0.11	13.8	−1.5	−14.7	−42.2	7.39	7.86	0.44	0.06	0.77	
HR 1173	6739	4.11	0.13	0.09	17.7	−35.6	−21.9	−21.4	6.53	7.70	0.15	0.15	0.22	
HR 1257	6301	3.97	−0.07	0.04	31.6	−15.3	−26.8	15.2	6.62	7.49	0.22	0.12	0.48	
HR 1294	5732	4.16	−0.29	−0.18	29.9	51.1	−30.8	−13.7	6.23	7.41	0.07	0.16	1.03	
HR 1489	6028	4.06	0.09	0.06	29.9	54.7	−18.9	12.1	6.66	7.80	0.19	0.15	0.69	
HR 1536	5886	3.98	0.17	0.14	33.9	50.7	−86.3	−17.8	3.83	6.03	0.10	0.36	0.64	
HR 1545	6425	4.11	−0.40	−0.33	37.7	−27.6	−5.9	−25.8	7.21	8.19	0.22	0.12	0.59	
HR 1673	6442	4.05	−0.27	−0.30	25.5	9.9	−6.2	1.6	8.00	8.26	0.08	0.03	0.55	
HR 1687	6596	4.15	0.18	0.26	35.9	27.8	−18.6	−1.8	7.11	7.73	0.04	0.08	0.19	
HR 1729	5889	4.12	0.01	−0.03	15.9	77.6	−48.0	5.4	5.22	7.09	0.10	0.26	0.85	
HR 1780	6152	4.36	−0.14	0.00	14.8	36.9	−14.5	7.5	7.14	7.89	0.14	0.09	0.55	
HR 1983	6398	4.29	−0.09	−0.07	9.1	−18.6	4.7	−12.3	7.62	8.53	0.06	0.11	0.43	
HR 2047	5953	4.46	−0.05	−0.03	9.2	−13.5	3.1	−8.2	7.69	8.47	0.02	0.09		
HR 2141	5917	4.14	−0.33	−0.24	24.7	−6.5	−23.6	−30.9	6.88	7.56	0.27	0.09	0.91	
HR 2220	6587	4.27	0.02	0.04	22.7	32.9	−18.8	−17.9	7.02	7.73	0.12	0.09	0.24	

all relative to the Sun. From the discussion above, it follows that radial velocities and proper motions contribute only about 1 km s^{-1} each to the uncertainty of U, V, and W; for stars with large tangential velocities, the ±15% uncertainty in the distance will be the dominant contribution to the total error.

5.2.2. Galactic orbital parameters

From the U, V, W velocity components of Table 11 the main parameters of the galactic orbits of our programme stars have been computed by Dr. M. Grenon, Geneva Observatory, using methods developed earlier (Grenon 1987). The results are used

Table 11. (continued)

ID	$T_{\rm eff}$ [K]	log g [cgs]	[Me/H]	[Fe/H]	Dist. [pc]	U [km s^{-1}]	V [km s^{-1}]	W [km s^{-1}]	$R_{\rm p}$ [kpc]	$R_{\rm m}$ [kpc]	$Z_{\rm max}$ [kpc]	e	log Age [Gyr]	Rem.
HR 2233	6347	4.07	−0.13	−0.17	32.3	−45.0	3.3	−31.7	7.10	8.60	0.31	0.17	0.55	
HR 2354	5803	4.17	(0.27)	0.13	35.4	−18.1	−17.0	−16.3	7.01	7.80	0.10	0.10	0.84	pm
HR 2493	6063	4.24	−0.52	−0.38	27.3	25.3	24.6	17.2	7.94	9.27	0.28	0.14	0.94	
HR 2530	6595	4.16	−0.47	−0.43	33.0	−24.7	−16.2	−11.4	6.93	7.85	0.05	0.12	0.42	h
HR 2548	6460	4.06	−0.23	−0.20	26.3	48.5	−12.3	6.3	6.99	7.98	0.12	0.12	0.50	
HR 2601	6025	3.94	−0.62	−0.56	34.2	13.1	22.9	−16.6	8.00	9.18	0.12	0.13	0.84	
HR 2721	5963	4.48	−0.29	−0.28	14.6	79.5	0.3	33.5	6.78	8.63	0.54	0.21		
HR 2835	6184	4.17	−0.67	−0.55	30.4	62.4	−3.3	−25.6	6.99	8.35	0.22	0.16	0.81	
HR 2883	5976	4.18	−0.73	−0.75	23.2	31.4	−48.2	−13.8	5.60	6.86	0.07	0.18	1.03	
HR 2906	6167	4.09	−0.26	−0.18	19.8	37.3	−48.2	−3.6	5.57	6.89	0.02	0.19	0.62	
HR 2943	6704	4.03	(0.08)	−0.02	3.6	−4.6	−8.9	−19.0	7.58	8.07	0.13	0.06	0.22	h
HR 3018	5822	4.42	−0.73	−0.78	12.1	122.8	−66.4	24.1	4.14	7.06	0.37	0.41	1.18	SB
HR 3176	5779	4.20	(0.26)	0.04	23.3	−32.4	4.4	−16.0	7.36	8.57	0.10	0.14	0.94	
HR 3220	6536	4.13	−0.20	−0.26	20.5	−17.3	−15.3	−33.1	7.10	7.85	0.31	0.10	0.49	
HR 3262	6365	4.35	−0.26	−0.26	17.7	24.0	−38.1	7.0	6.15	7.12	0.12	0.14	0.48	
HR 3271	5955	4.07	0.08	0.07	37.8	−4.6	−18.4	1.1	7.16	7.73	0.07	0.07	0.70	
HR 3538	5763	4.37	(0.33)	0.01	21.9	47.0	−18.7	−17.8	6.79	7.77	0.11	0.13	0.95	
HR 3578	5965	4.37	−0.75	−0.82	16.2	48.9	−93.3	61.2	3.56	5.88	0.97	0.39	1.11	
HR 3648	5881	4.18	−0.12	−0.08	20.2	−8.4	−7.1	−9.1	7.57	8.13	0.03	0.07	0.90	
HR 3775	6380	4.09	−0.14	−0.20	10.9	48.7	−27.3	−17.6	6.41	7.51	0.11	0.15	0.40	h
HR 3881	5899	4.12	0.08	0.04	20.5	−13.7	−6.3	18.8	7.48	8.15	0.28	0.08	0.81	
HR 3951	5746	4.02	(0.27)	0.10	25.1	71.2	−67.6	4.7	4.49	6.55	0.09	0.31	0.81	
HR 3954	6403	4.05	0.06	0.04	36.5	−6.3	−4.6	−14.7	7.69	8.22	0.09	0.06	0.31	h
HR 4012	6124	4.09	0.15	0.14	38.5	25.2	−22.4	−3.6	6.96	7.60	0.02	0.08	0.59	
HR 4027	5820	4.00	−0.08	−0.04	37.4	20.9	−22.2	18.0	7.00	7.59	0.26	0.08	0.79	
HR 4039	6158	4.30	−0.45	−0.38	22.1	49.9	−29.0	5.3	6.33	7.47	0.11	0.15	0.79	
HR 4067	6320	4.07	0.21	0.18	34.9	9.3	−25.6	−13.6	6.87	7.45	0.07	0.08	0.32	h
HR 4150	6488	3.92	−0.35	−0.23	48.4	−20.1	−2.9	−16.2	7.44	8.27	0.10	0.10	0.43	
HR 4158	6140	4.22	−0.31	−0.24	24.4	−67.1	−34.7	−36.7	5.60	7.53	0.36	0.26	0.78	
HR 4277	5882	4.34	0.06	0.01	14.8	25.8	−2.6	1.4	7.74	8.28	0.07	0.07	0.84	
HR 4285	5890	4.05	−0.32	−0.30	32.0	6.3	−22.4	−8.7	7.05	7.57	0.02	0.07	0.88	
HR 4395	6643	3.98	−0.01	−0.10	32.7	39.5	−28.2	−11.9	6.50	7.45	0.05	0.13	0.25	h
HR 4421	6610	3.99	−0.46	−0.54	41.2	23.7	28.1	−37.6	7.96	9.43	0.41	0.16	0.52	
HR 4529	6083	4.04	0.20	0.16	41.7	6.1	−30.7	−6.9	6.58	7.30	0.01	0.10	0.58	
HR 4533	6387	4.18	0.16	0.24	37.2	32.7	−15.9	−7.5	7.15	7.82	0.01	0.09	0.30	
HR 4540	6176	4.14	0.13	0.13	11.0	−40.8	3.4	6.7	7.18	8.59	0.13	0.16	0.57	
HR 4657	6247	4.38	−0.66	−0.70	21.9	−51.3	−68.1	−61.2	4.47	6.54	0.76	0.32	0.73	SB
HR 4683	6394	4.07	−0.57	−0.54	41.1	−41.0	11.0	−0.4	7.32	8.88	0.06	0.18	0.64	
HR 4688	6343	4.05	0.28	0.21	42.3	22.3	−40.6	−12.7	6.03	7.05	0.06	0.14	0.32	h
HR 4734	5776	4.20	(0.39)	0.10	32.5	67.6	−75.7	−14.6	4.18	6.34	0.07	0.34	0.93	
HR 4767	6060	4.35	−0.16	−0.11	23.8	1.2	11.3	−28.1	7.97	8.74	0.26	0.09	0.71	
HR 4785	5879	4.52	−0.19	−0.19	8.1	29.9	−3.3	2.3	7.64	8.25	0.08	0.07		
HR 4845	5795	4.15	−0.88	−0.59	16.8	40.1	6.8	75.7	7.62	8.60	1.38	0.11	1.12	
HR 4903	5953	4.00	(0.40)	0.24	40.1	10.9	−58.7	−28.4	5.15	6.57	0.23	0.22	0.54	
HR 4981	6375	3.94	−0.26	−0.17	29.2	−19.5	−8.2	−38.1	7.31	8.10	0.38	0.10	0.48	
HR 4983	6029	4.38	0.01	0.03	10.0	54.6	12.6	9.2	7.45	8.90	0.17	0.16	0.64	
HR 4989	6314	4.25	−0.35	−0.28	18.0	55.8	37.6	−14.5	7.68	10.08	0.10	0.24	0.64	
HR 5011	6021	4.15	0.00	0.10	20.9	43.5	1.1	−15.1	7.46	8.41	0.09	0.11	0.66	
HR 5019	5590	4.23	(0.18)	−0.03	12.6	33.6	−71.3	−45.1	4.52	6.31	0.45	0.28	1.15	

in this study with his kind permission, and were obtained as follows.

A Myamoto-type potential with three components (nucleus-disk-halo) representing the observed galactic rotation curve is assumed. For a fixed grid of (U, V, W) values, orbits were computed by numerical integration for a sufficient number of revolutions to define the main orbital parameters with adequate precision. For real stars, individual orbital parameters were then derived by interpolation in the results of this grid of computed orbits. The corrections applied to the observed velocities for the

Table 11. (continued)

ID	$T_{\rm eff}$ [K]	log g [cgs]	[Me/H]	[Fe/H]	Dist. [pc]	U [km s^{-1}]	V [km s^{-1}]	W [km s^{-1}]	$R_{\rm p}$ [kpc]	$R_{\rm m}$ [kpc]	$Z_{\rm max}$ [kpc]	e	log Age [Gyr]	Rem.
HR 5235	6068	3.83	0.29	0.19	10.7	−8.7	−16.1	−2.6	7.21	7.82	0.03	0.08	0.44	
HR 5323	6237	4.04	(0.26)	0.07	30.1	36.6	−28.2	−26.5	6.54	7.45	0.21	0.12	0.57	
HR 5338	6177	3.94	−0.17	−0.11	17.8	−21.7	−29.1	−11.0	6.43	7.43	0.04	0.13	0.48	
HR 5353	5562	3.92	(0.38)	0.13	49.3	−56.6	7.2	−61.8	6.97	8.86	0.87	0.21	0.74	
HR 5423	5593	3.96	(0.30)	0.05	41.3	−52.5	−5.8	−4.5	6.75	8.34	0.01	0.19	0.84	
HR 5447	6767	4.27	−0.38	−0.41	17.5	−2.5	18.3	−5.8	7.95	9.01	0.00	0.12	0.32	
HR 5459	5720	4.27	0.20	0.15	1.3	30.3	3.6	13.6	7.76	8.49	0.22	0.09	0.62	
HR 5542	6001	4.09	0.12	0.13	39.8	58.3	−33.7	10.4	6.02	7.37	0.16	0.18	0.69	
HR 5691	6172	4.12	0.04	−0.02	23.2	−56.3	−28.4	−24.8	5.98	7.64	0.20	0.22	0.65	
HR 5698	6341	4.04	−0.01	0.01	26.9	21.5	−14.1	−6.8	7.42	7.89	0.01	0.06	0.51	
HR 5723	6532	3.93	−0.09	−0.13	29.6	4.8	−19.9	−13.3	7.18	7.65	0.07	0.06	0.41	
HR 5868	5937	4.21	−0.03	−0.04	13.2	49.5	−24.5	−39.5	6.52	7.60	0.39	0.14	0.86	
HR 5914	5843	4.34	−0.47	−0.52	11.4	34.1	−0.8	−61.1	7.60	8.33	0.78	0.09	1.13	
HR 5933	6333	4.25	−0.22	−0.16	11.1	−56.1	−33.0	−25.0	5.81	7.50	0.20	0.23	0.53	
HR 5968	5782	4.24	−0.32	−0.26	17.1	−53.5	−34.8	20.1	5.78	7.43	0.29	0.22	1.07	
HR 5996	5831	4.03	(0.40)	0.23	42.6	33.6	−30.3	29.2	6.47	7.38	0.41	0.12	0.72	
HR 6189	6200	3.98	−0.62	−0.56	39.7	6.6	−20.3	−24.6	7.16	7.63	0.20	0.06	0.74	
HR 6202	6442	3.86	−0.43	−0.37	42.2	−9.6	11.0	3.4	7.84	8.74	0.10	0.10	0.40	SB
HR 6243	6435	3.80	−0.01	0.00	31.6	−6.9	−2.0	−19.2	7.73	8.30	0.14	0.07	0.28	
HR 6315	6284	4.38	−0.22	−0.17	14.6	−1.1	−7.5	−27.4	7.72	8.14	0.24	0.05		
HR 6409	6480	3.94	0.19	0.09	38.9	37.9	−13.6	6.0	7.15	7.91	0.12	0.10	0.38	
HR 6458	5676	4.33	−0.33	−0.41	15.5	−29.9	−82.8	−66.9	3.98	6.10	0.84	0.35	1.24	
HR 6541	6243	3.91	−0.26	−0.23	37.1	27.5	−47.1	−27.5	5.68	6.89	0.22	0.18	0.53	
HR 6569	6675	4.15	−0.25	−0.27	22.1	2.9	−10.7	−17.5	7.67	8.03	0.12	0.04	0.33	h
HR 6598	5765	4.02	−0.50	−0.39	33.8	−40.1	−45.9	−17.2	5.49	7.04	0.10	0.22	0.94	
HR 6649	6088	4.24	−0.41	−0.34	28.6	23.4	−8.1	−29.2	7.64	8.10	0.26	0.06	0.86	
HR 6701	6170	3.89	−0.25	−0.22	28.6	26.0	−24.0	−20.5	6.87	7.55	0.14	0.09	0.55	
HR 6775	6020	4.48	−0.51	−0.56	12.5	2.4	0.2	6.6	7.95	8.40	0.13	0.05		
HR 6850	6587	4.09	−0.24	−0.31	23.1	5.8	−13.1	−49.9	7.57	7.93	0.57	0.05	0.51	
HR 6907	6382	4.15	0.17	0.13	33.7	17.3	2.1	2.5	7.96	8.46	0.09	0.06	0.35	h
HR 7061	6369	4.02	−0.17	−0.11	19.4	−37.7	2.2	−8.5	7.21	8.51	0.02	0.15	0.53	
HR 7126	6655	4.16	0.01	0.21	31.8	31.8	−39.1	−3.4	6.05	7.12	0.02	0.15	0.19	
HR 7232	5625	4.21	(0.22)	0.03	25.0	−57.5	−49.3	−15.4	5.17	7.05	0.08	0.27	1.08	
HR 7322	6319	4.17	−0.23	−0.28	34.3	52.1	−37.8	7.0	5.92	7.22	0.12	0.18	0.65	
HR 7534	6379	4.21	−0.12	−0.13	21.3	−37.6	−7.3	−24.4	6.98	8.19	0.20	0.15	0.45	
HR 7560	6146	4.14	0.10	0.09	21.3	3.6	−2.4	−28.2	7.95	8.34	0.25	0.05	0.63	
HR 7766	5964	4.22	−0.47	−0.36	28.6	−33.5	−43.6	27.2	5.65	7.07	0.38	0.20	0.94	
HR 7875	5991	4.09	−0.55	−0.44	20.4	59.1	−38.8	2.3	5.79	7.22	0.07	0.20	0.87	
HR 7955	6188	4.13	0.17	0.12	17.7	−21.1	−28.1	−13.1	6.49	7.46	0.06	0.13	0.59	
HR 8027	6285	4.20	−0.45	−0.37	27.7	5.4	19.8	23.0	7.99	9.06	0.37	0.12	0.73	
HR 8041	5813	4.20	(0.28)	0.11	35.3	6.7	−28.8	−6.9	6.69	7.36	0.01	0.09	0.89	
HR 8077	6166	4.05	−0.09	−0.07	35.8	−7.8	−35.7	10.6	6.25	7.20	0.16	0.13	0.62	
HR 8181	6139	4.34	−0.73	−0.67	8.8	13.5	41.8	6.2	8.00	10.10	0.15	0.21	0.96	
HR 8354	6285	4.09	−0.66	−0.66	28.7	−13.9	15.7	−7.8	7.81	8.93	0.02	0.12	0.75	
HR 8472	6249	3.86	0.04	0.06	35.2	39.3	−27.9	−5.8	6.52	7.47	0.00	0.13	0.40	
HR 8665	6228	4.15	−0.31	−0.32	13.9	−3.0	−27.7	−24.1	6.70	7.42	0.19	0.10	0.72	
HR 8697	6288	3.97	−0.31	−0.25	26.4	57.6	−6.7	−33.8	6.99	8.20	0.33	0.15	0.56	
HR 8729	5755	4.18	(0.31)	0.06	22.4	22.3	−29.6	12.2	6.60	7.36	0.19	0.10	0.93	
HR 8805	6597	4.21	−0.11	−0.13	34.3	30.2	−9.1	10.2	7.47	8.06	0.17	0.07	0.32	

solar motion were (−10,+6,+6) km s^{-1} in (U, V, W), and the solar galactocentric distance and circular velocity were taken to be 8.0 kpc and 226.0 km s^{-1}, respectively.

The parameters of particular interest here are $R_{\rm p}$ and $R_{\rm a}$ (peri- and apo-galactic distances), $Z_{\rm max}$ (maximum distance from the plane), e (projected orbital eccentricity), and the mean Galactocentric distance $R_{\rm m} \equiv (R_{\rm p} + R_{\rm a})/2$. Table 11 lists these data for the stars in our programme. Propagated uncertainties in the orbital parameters from errors in the space velocities are well below ±10%. The orbit of HD 148816 has a very large ec-

Table 11. (continued)

ID	$T_{\rm eff}$ [K]	log g [cgs]	[Me/H]	[Fe/H]	Dist. [pc]	U [km s^{-1}]	V [km s^{-1}]	W [km s^{-1}]	$R_{\rm p}$ [kpc]	$R_{\rm m}$ [kpc]	$Z_{\rm max}$ [kpc]	e	log Age [Gyr]	Rem.
HR 8853	6134	4.21	−0.07	0.00	24.6	−6.9	−27.8	−28.0	6.66	7.43	0.23	0.10	0.69	
HR 8885	6579	4.12	0.11	0.02	34.6	12.3	−17.9	−13.5	7.31	7.73	0.07	0.05	0.27	
HR 8969	6255	4.16	−0.20	−0.17	13.2	7.8	−25.0	−25.3	6.91	7.47	0.20	0.08	0.64	
HD 2615	6255	3.93	−0.66	−0.58	82.0	63.0	41.0	−9.1	7.61	10.34	0.03	0.26	0.60	
HD 6434	5813	4.42	−0.56	−0.54	35.7	−74.0	−61.6	−6.0	4.55	6.87	0.00	0.34	1.10	
HD 14938	6164	4.09	−0.47	−0.37	52.5	−8.9	−30.3	−3.0	6.52	7.36	0.03	0.11	0.67	SB
HD 17548	5977	4.27	−0.74	−0.59	54.6	12.4	27.0	31.4	8.00	9.36	0.50	0.15	1.06	
HD 18768	5725	4.04	−0.79	−0.62	33.4	85.7	43.1	−19.2	7.33	10.74	0.16	0.32	1.04	
HD 22879	5826	4.27	−0.98	−0.84	21.7	107.6	−78.0	−49.0	3.85	6.60	0.56	0.42	1.21	
HD 25704	5844	4.43	−0.83	−0.85	42.0	105.5	−64.3	−12.9	4.35	6.91	0.06	0.37	1.22	pm
HD 30649	5736	4.22	−0.70	−0.51	29.6	59.3	−78.1	−9.9	4.13	6.24	0.03	0.34	1.18	
HD 38007	5684	4.10	−0.47	−0.35	35.9	69.5	−9.4	11.9	6.70	8.19	0.19	0.18	1.07	SB
HD 43947	5945	4.28	−0.47	−0.30	29.1	39.1	−10.6	−2.6	7.23	8.01	0.03	0.10	1.00	
HD 51929	5845	4.28	−0.73	−0.64	33.5	96.0	−61.4	−2.3	4.54	6.89	0.03	0.34	1.14	pm
HD 62301	5895	4.19	−0.81	−0.69	28.3	3.7	−90.4	−20.6	3.73	5.86	0.13	0.36	1.10	
HD 66573	5730	4.37	−0.63	−0.58	27.9	−56.2	20.1	13.5	7.20	9.41	0.23	0.23	1.25	SB2
HD 68284	5883	3.96	−0.71	−0.59	66.0	54.8	−23.4	26.4	6.49	7.66	0.38	0.15	0.86	
HD 69611	5795	4.29	−0.64	−0.58	43.5	43.1	−137.1	−38.3	2.05	5.08	0.33	0.60	1.08	pm
HD 74011	5741	4.15	−0.78	−0.65	38.9	36.8	−57.3	28.8	5.15	6.65	0.39	0.23	1.17	
HD 78558	5767	4.28	−0.43	−0.40	36.2	69.0	−72.8	−63.6	4.30	6.42	0.80	0.33	1.05	
HD 78747	5824	4.45	−0.61	−0.64	35.7	−12.4	2.2	−18.6	7.70	8.44	0.13	0.09	1.08	pm
HD 89707	5989	4.42	−0.48	−0.42	32.7	67.4	−49.8	55.7	5.25	6.97	0.90	0.25	0.91	pm
HD 91347	5872	4.24	−0.69	−0.48	36.2	−50.2	29.3	−3.0	7.41	9.78	0.03	0.24	1.07	
HD 98553	5907	4.38	−0.53	−0.43	34.0	−11.9	27.2	−26.5	7.89	9.40	0.25	0.16	1.09	
HD 114762	5871	4.24	−0.87	−0.74	33.7	67.4	−58.0	55.9	4.91	6.76	0.90	0.27	1.14	
HD 126512	5753	4.20	−0.75	−0.63	36.3	−60.7	−63.8	−68.3	4.57	6.70	0.93	0.32	1.18	
HD 130551	6237	4.25	−0.64	−0.62	46.9	−40.1	−6.2	14.8	6.96	8.24	0.23	0.15	0.85	pm
HD 134169	5834	4.11	−0.95	−0.83	44.2	−13.4	0.6	13.4	7.65	8.38	0.21	0.09	1.08	SB
HD 144172	6330	4.03	−0.48	−0.44	51.6	−20.1	−11.2	−3.6	7.19	7.99	0.02	0.10	0.63	
HD 148211	5899	4.17	−0.75	−0.65	46.6	23.1	−87.3	−4.1	3.85	5.94	0.01	0.35	1.07	
HD 148816	5867	4.26	−0.79	−0.74	34.3	−64.9	−220.5	−73.2	0.27	4.35	5.44	0.94	1.13	
HD 155358	5868	4.19	−0.81	−0.67	36.6	−25.2	−44.0	17.7	5.71	7.03	0.24	0.19	1.11	pm
HD 157089	5795	4.15	−0.70	−0.59	33.5	162.9	−42.3	−17.1	4.50	8.50	0.13	0.47	1.07	
HD 159307	6227	3.94	−0.73	−0.71	73.5	13.5	−22.1	0.1	7.07	7.57	0.06	0.07	0.68	SB
HD 165401	5758	4.31	−0.55	−0.47	25.3	79.2	−89.1	−41.2	3.61	6.11	0.39	0.41	1.18	
HD 174912	5863	4.33	−0.68	−0.54	29.5	22.1	8.4	−42.3	7.93	8.65	0.46	0.08	1.13	
HD 184499	5711	4.15	−0.76	−0.61	28.0	65.1	−161.3	46.6	1.37	4.82	0.66	0.72	1.16	
HD 188815	6181	4.29	−0.62	−0.58	47.2	16.9	6.9	−15.5	7.98	8.60	0.10	0.07	0.86	pm
HD 198044	6093	4.15	−0.52	−0.31	48.0	17.9	−46.2	−5.4	5.76	6.89	0.00	0.16	0.74	SB
HD 199289	5894	4.38	−1.03	−1.03	40.9	38.1	−57.0	−24.9	5.15	6.66	0.18	0.23	1.26	pm
HD 200973	6301	3.90	−0.57	−0.52	74.3	59.1	40.8	−63.0	7.66	10.28	0.93	0.26	0.51	
HD 201099	5872	4.06	−0.74	−0.50	47.9	115.3	−19.2	39.8	5.71	8.38	0.70	0.32	0.93	
HD 201891	5867	4.46	−1.05	−1.06	24.7	−58.8	−92.0	−38.5	3.51	6.06	0.35	0.42	1.23	
HD 205294	6236	4.01	−0.47	−0.36	54.4	−16.1	−27.6	−31.4	6.57	7.46	0.28	0.12	0.64	
HD 208906	6009	4.41	−0.81	−0.72	25.5	−63.5	−0.8	−11.4	6.68	8.63	0.05	0.23	1.02	
HD 210752	5910	4.25	−0.81	−0.64	34.8	9.6	27.6	−62.3	8.00	9.39	0.83	0.15	1.15	
HD 215257	5983	4.37	−0.73	−0.65	36.5	54.4	11.2	42.1	7.44	8.84	0.68	0.16	1.06	
HD 218504	5945	4.20	−0.69	−0.62	57.8	−14.8	−14.5	32.4	7.17	7.88	0.48	0.09	1.03	
HD 221830	5707	4.16	−0.56	−0.52	34.1	70.0	−115.7	61.3	2.70	5.54	0.99	0.51	1.13	

centricity (low angular momentum); such orbits show stochastic behaviour, and the value of $Z_{\rm max}$ then refers to that point of the orbit when the inclination is also largest.

The stellar orbits were also calculated by Dr. J. Sommer-Larsen (Copenhagen) using an empirical dynamical model for the galactic disk (Sommer-Larsen & Antonuccio-Delogū 1993). The results agree within 5% with the orbital parameters derived by Dr. M. Grenon.

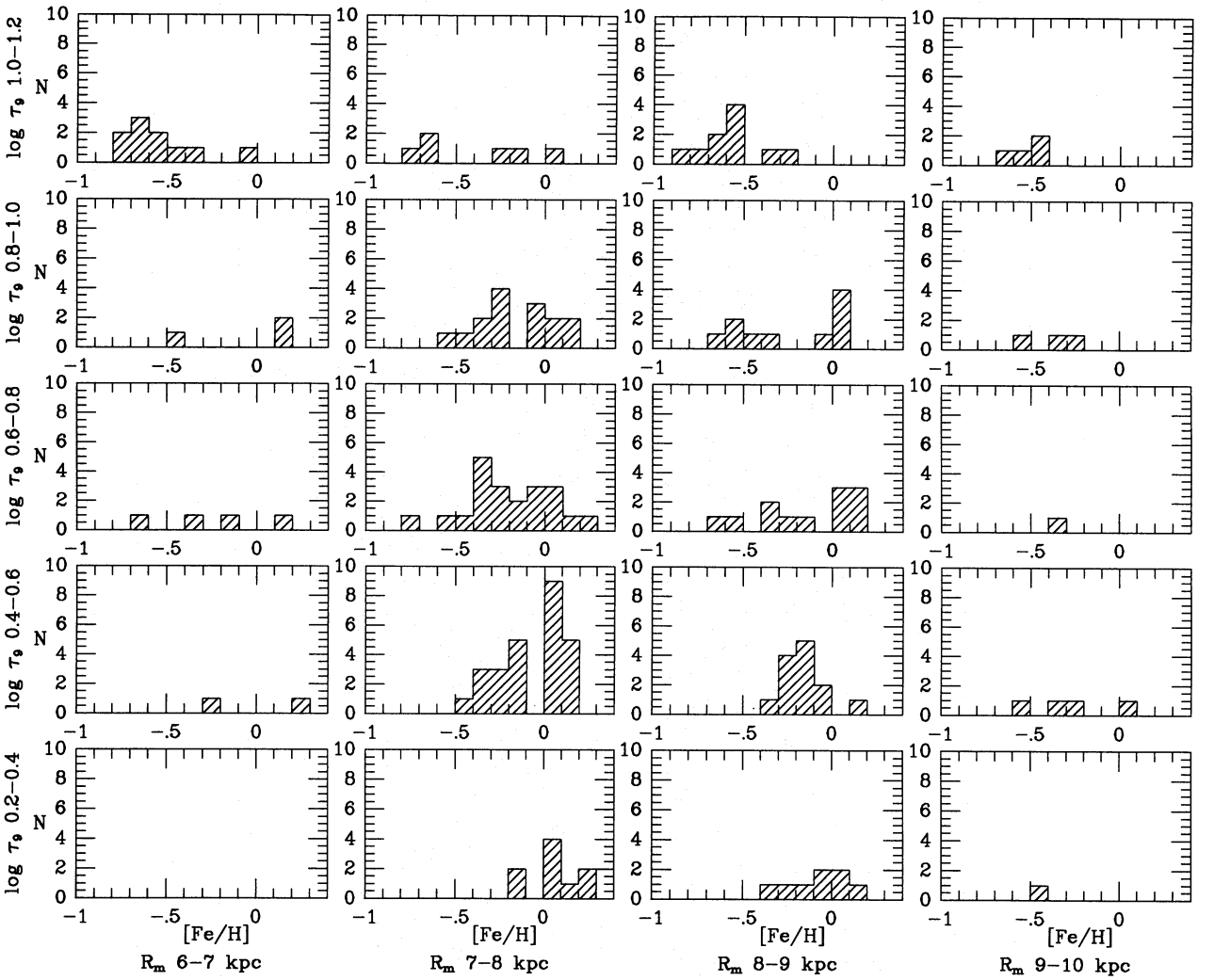

Fig. 13. Histograms of the metallicity distribution of 162 of our 189 stars for different intervals in logarithmic age and R_m. Of the remaining 27 stars, 7 lack age determinations and 20 fall outside the range of the boxes shown

6. Results and discussion

6.1. Introduction

The chemical abundances (relative to the Sun) are given in Table 12 for our stars. These abundances are a record of the history of stellar nucleosynthesis of the galactic disk over the last 10 to 15 billion years. Except for a few photometric surveys of stellar metallicity, no previous work on the composition of disk stars has covered such a large sample of stars and of elements sampling most of the major processes of stellar nucleosynthesis. In this section we describe our results by detailing the principal trends and correlations among the elemental abundances and between the abundances, the stellar ages, and the stellar kinematics. In addition, we relate the observed trends and correlations to some of the proposed theories of the galactic disk's evolution. A fully systematic comparison of our results to contemporary models of galactic evolution is, however, beyond the scope of the present paper.

Galactic evolution models predict that the compositions of interstellar gas clouds, the birth sites of stars, will depend on the age of the Galaxy and the location of the cloud in the Galaxy. It is assumed that the photospheres of the F and G dwarfs comprising our sample reflect faithfully the compositions of their birth sites, at least for the elements examined here. The age of the Galaxy at the birth of a star, t, is not measureable. What we can measure is the age of a star, τ, with respect to the appropriate ZAMS; the time taken by the star to collapse to the ZAMS is a minor fraction of the main sequence lifetime.

Simple theories generally suppose that chemical evolution at a given galactic epoch will be more advanced in the inner regions and less advanced in the outer Galaxy; i.e., there is a radial abundance gradient at a given epoch. Thanks to efficient mixing, it is thought that chemical compositions of interstellar clouds at a given galactocentric radius, R, are unlikely to depend greatly on galactic longitude. Then, a reasonable supposition is that the metallicity may be expressed as

$$[\mathrm{Fe/H}] = F(R, t).$$

The metallicity is the cumulative effect of stellar nucleosynthesis (and other effects, such as infall) over several stellar generations. This effect is likely to vary with t and R and, hence, relative abundances, say [X/Fe], will also vary:

$$[\mathrm{X/Fe}] = F'(R, t).$$

For the local disk stars, we adopt the mean galactocentric distance R_m (see Sect. 5.2.2) as a substitute for R. Grenon (1987) shows that R_m is rather constant for long periods of time. By replacing t by τ, we assume that a gas cloud is not dormant and isolated for long periods of time; a consequence of dormancy is, for example, to introduce scatter into what otherwise might be a tight relation between age and metallicity. With these substitutions, we expect [Fe/H] = $G(R_\mathrm{m}, \tau)$ and [X/Fe] = $G'(R_\mathrm{m}, \tau)$.

In studies of chemical evolution involving local disk stars, the traditional observational tests are four:

1. The age-metallicity relation:
   [X/H] vs τ at a fixed R_m, where X is, for obvious observational reasons, usually identified with Fe;
2. The galactic abundance gradient:
   [X/H] vs R_m at a given τ;
3. The variation of the relative abundances with metallicity:
   most often [X/Fe] vs [Fe/H] is considered;
4. The frequency distribution of the metallicities:
   N([Fe/H]) vs [Fe/H] for a given R_m and τ, a test whose outcome is often referred to as the G-dwarf problem.

Clearly, these tests may give erroneous or misleading results unless the stellar samples are selected carefully. To the extent that is possible with our modest sample, we apply these traditional tests on appropriate subsamples. The tests sample in different ways the primary influences on the disk's chemical composition such as the star formation rate, the initial mass function, the infall rate, and the nucleosynthetic yields.

In what follows, it is necessary to keep in mind that although our sample spans the intervals $-1.1 \leq$ [Fe/H] < 0.25, $4 < R_\mathrm{m}$(kpc) < 11, and $0.2 \leq \log \tau_9 < 1.25$, τ_9 being the stellar age in 10^9 years, coverage is far from uniform over these intervals (as Fig. 13 shows). Selection effects and the structure of the Galaxy dictate the coverage. When appropriate, we make explicit corrections for observational selection effects.

As a guide to the detailed discussion, we first show three traditional modes of displaying the abundances:

— The age-metallicity relation is shown in Fig. 14 for [Fe/H], [α'/H], and [Ba/H] where [α'/H] is the mean of the logarithmic Si and Ca abundances. The scatter in these relations is primarily real and *not* observational. This has not been clearly demonstrated for field stars before, but is known for open clusters (Nissen 1988; Boesgaard 1989, Friel & Janes 1991). The overall trend of a slowly increasing abundance with decreasing age is consistent with photometric surveys (Twarog 1980; Meusinger et al. 1991). [Ba/H] shows the steepest slope of the three relations and [α'/H] the shallowest slope.

— Relative abundances ([X/Fe]) as a function of [Fe/H] are shown in Fig. 15. These results generally confirm published trends of [X/Fe] based on lower quality spectroscopic analyses

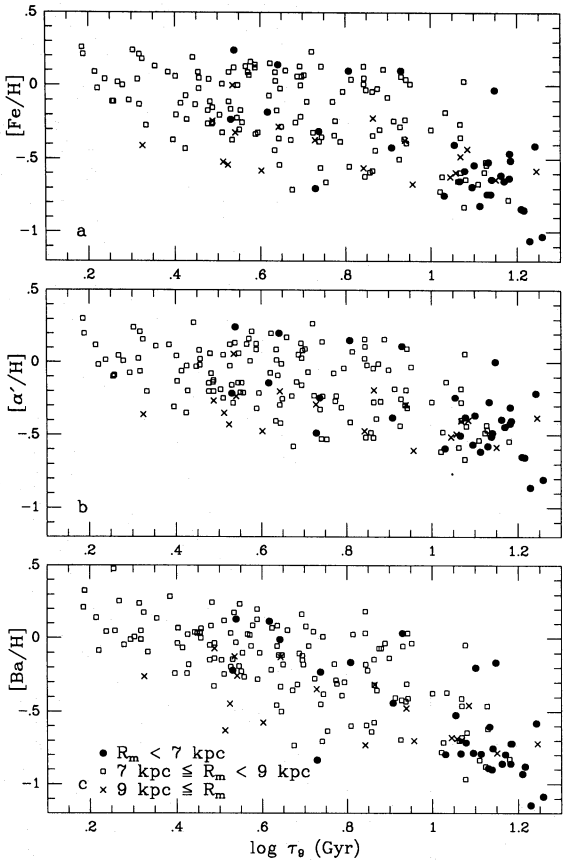

Fig. 14a–c. The abundances of iron **a**, α'-elements (the mean of the logarithmic silicon and calcium abundances) **b** and barium **c** as a function of logarithmic age. The symbols identify stars of different R_m

- see reviews by Lambert (1989) and Wheeler et al. (1989). Several new features are obvious by inspection and other novelties require the detailed scrutiny given below. Among the obvious features, we note that the trend of [Mg/Fe] vs [Fe/H] for [Fe/H]< -0.4 has a steeper slope and shows more scatter than the trends of the other α-elements Si, Ca and Ti.

— To illustrate the relation between the kinematics and the abundances, we show in Fig. 16 the W velocity (perpendicular to the galactic plane) as a function of [Fe/H] and $\log \tau$. This shows, as is well known, an increase of the W dispersion with decreasing [Fe/H] and with increasing age. However, no trend of an increasing velocity dispersion with age in the interval 3–10 Gyr is seen. On the basis of these data Freeman (1991) has suggested that the heating of the disk saturates at about 20 km s^{-1} in W after about 3 Gyr. The thick disk, being at least 10 Gyr old and with $\sigma_W \approx 40$ km s^{-1} then needs to be explained by another heating process, or else the stars in the thick disk were formed with a velocity dispersion of this magnitude.

6.2. The relative abundances

6.2.1. Sites of stellar nucleosynthesis

The trends displayed in Fig. 15 indicate that the compositions of the most metal-poor disk stars appear to resemble those of

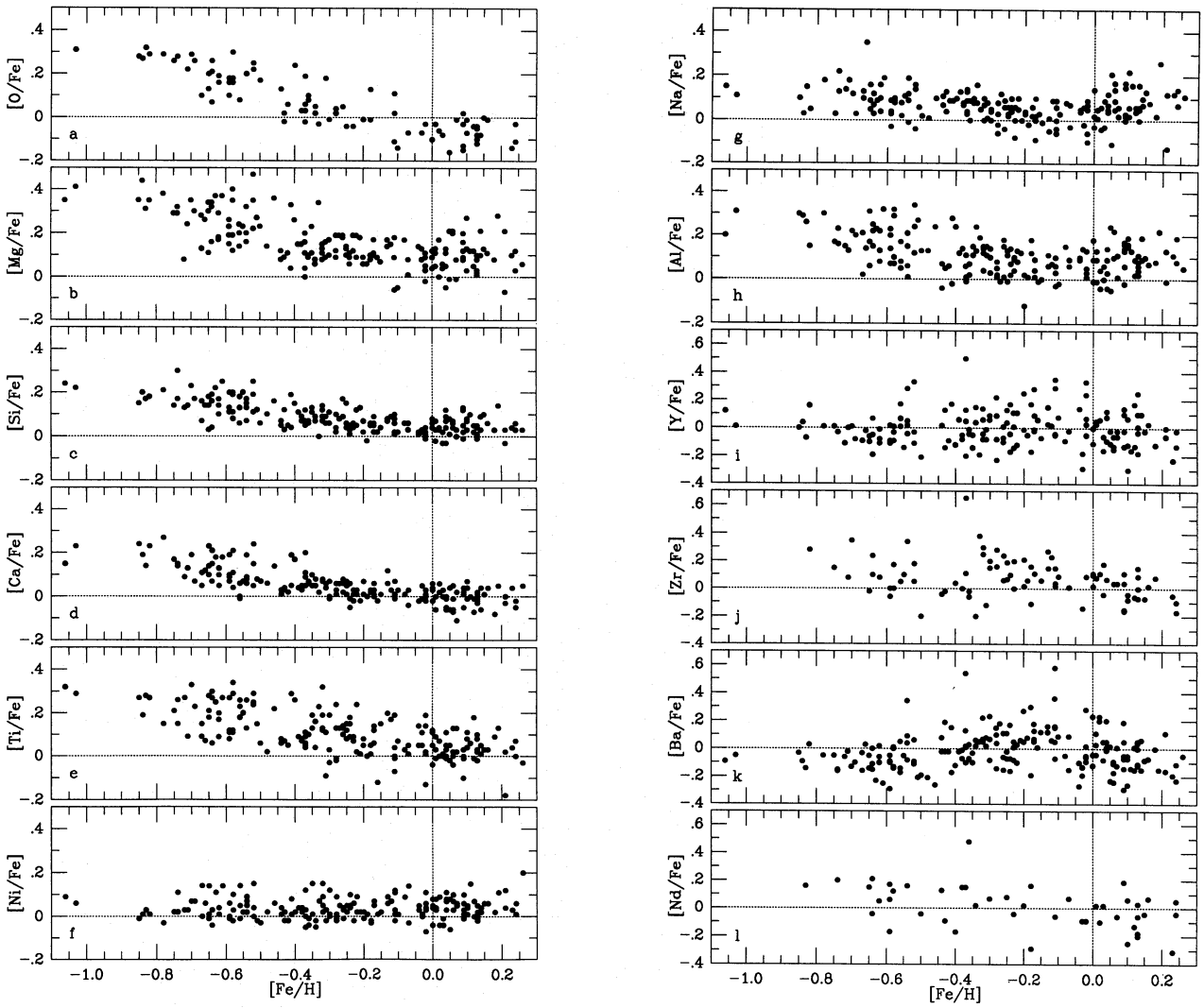

Fig. 15a-l. Abundances relative to iron vs the iron abundance. The solar position is at the origin in all the panels. In **a** the scaled oxygen abundances from Sect. 3.2.2 are used. Note that the vertical scale is expanded in panels **i, j, k** and **l**

the halo dwarfs and giants, i.e., [α/Fe] approaches 0.4 as [Fe/H] decreases towards [Fe/H] values typical for halo stars. For the α elements in halo stars this excess relative to iron was first traced by Aller & Greenstein (1960) and more firmly established by Wallerstein (1962) and Pagel (1970). The gradual change is, in terms of stellar nucleosynthesis, broadly attributed to the fact that the leading stellar contributors of different elements have different lifetimes. This was originally proposed as an explanation for the corresponding phenomenon for oxygen by Tinsley (1979). Three sites of stellar nucleosynthesis are generally recognized:

1. Massive (short-lived) stars ($M > 8M_{\odot}$) are considered to be the dominant sources of O and the α-elements and the light odd Z-even N elements Na and Al. These stars return newly synthesised material via stellar winds and terminal explosions as Type II Supernovae.
2. Type Ia Supernovae are supposed to be a major source of iron-group elements. Return of synthesised material to the interstellar medium is slow relative to the "instantaneous" return from massive stars. Type Ia SNe are considered to have contributed to the present interstellar medium but not much to the halo. The delayed contribution from SNe Ia is responsible for the transition in [α/Fe] from 0.4 in the halo to about 0.0 at present.
3. Asymptotic giant branch (AGB) stars contribute heavy elements synthesised by the s-process in the AGB stars' H-burning shells. These stars run in mass up to about $8M_{\odot}$ but it is probably the lower mass (M about 1–3 $M_{\odot}$) and longer lived stars that dominate the synthesis of elements like Y, Zr, Ba and Nd. The newly synthesised heavy elements are returned to the interstellar medium via stellar winds and the superwinds that lead to ejection of the envelope and creation of a planetary nebula.

This synopsis serves as a reminder that the elements examined by us were provided by at least three types of stars with different lifetimes. It is for this reason, presumably, that

Table 12. Abundances relative to hydrogen [X/H] derived for 14 neutral and ionized species for the programme stars. $[\alpha/H] = \frac{1}{4}([Mg/H] + [Si/H] + [Ca/H] + [Ti/H])$

ID	Fe I	O I	Na I	Mg I	Al I	Si I	Ca I	Ti I	Fe II	Ni I	Y II	Zr II	Ba II	Nd II	α
HR 17	−0.35		−0.25	−0.12	−0.20	−0.22	−0.25	−0.16	−0.32	−0.20	−0.40		−0.38		−0.19
HR 33	−0.38	−0.35	−0.30	−0.23	−0.24	−0.30	−0.35	−0.29	−0.40	−0.35	−0.45	−0.38	−0.45	−0.23	−0.29
HR 35	−0.10	−0.24	−0.06	−0.15	−0.12	−0.08	−0.07	−0.03	−0.12	−0.09	−0.02	−0.01	−0.01		−0.08
HR 107	−0.37		−0.24	−0.17	−0.31	−0.25	−0.32	−0.33	−0.35	−0.25	0.13	0.28	0.17		−0.27
HR 140	0.05	−0.12	−0.06	0.04	−0.01	0.06	−0.01	0.03	−0.04	−0.01	0.03		0.06		0.03
HR 145	−0.25		−0.19	−0.11	−0.13	−0.10	−0.17	−0.13	−0.19	−0.20			−0.31		−0.13
HR 203	−0.28	−0.23	−0.30	−0.19	−0.26	−0.25	−0.25	−0.30	−0.31	−0.29	−0.51		−0.42		−0.25
HR 219	−0.31		−0.30	−0.15	−0.16	−0.26	−0.25	−0.20	−0.28	−0.28	−0.32		−0.29		−0.21
HR 235	−0.15		−0.16	−0.08	−0.15	−0.11	−0.14	0.00	−0.28	−0.14	−0.22	−0.09	−0.04		−0.08
HR 244	0.00	−0.11	0.02	0.12	0.17	0.06	0.05	0.12	−0.13	0.05	−0.11	0.11	−0.13		0.09
HR 340	−0.21		−0.21	−0.03	−0.09	−0.08	−0.23	−0.20	−0.02	−0.19			−0.15		−0.13
HR 366	−0.32		−0.22	−0.24	−0.21	−0.23	−0.24	−0.19	−0.35	−0.31	−0.40	−0.07	−0.25		−0.23
HR 368	−0.24		−0.14	−0.15	−0.22	−0.24	−0.30	−0.15	−0.25	−0.15	−0.07		−0.07		−0.21
HR 370	0.12	0.08	0.18	0.16	0.13	0.17	0.11	0.11	0.05	0.12	−0.01	0.06	−0.03	−0.01	0.14
HR 448	0.09	0.06	0.24	0.30	0.25	0.21	0.04	0.12	0.02	0.09			−0.19		0.17
HR 458	0.09		0.11	0.25	0.23	0.08	0.09	0.12	0.08	0.09			0.04		0.13
HR 483	−0.02		0.08	0.09	0.11	−0.01	−0.01	0.17	−0.07	0.05	−0.07		−0.07		0.06
HR 573	−0.34	−0.32	−0.26	−0.28	−0.10	−0.28	−0.26	−0.18	−0.30	−0.36	−0.19		−0.29		−0.25
HR 646	−0.32		−0.25	−0.19	−0.19	−0.18	−0.25	0.00	−0.25	−0.28	−0.26	−0.02	−0.10		−0.16
HR 672	0.06		0.19			0.11	0.05	0.06	−0.07	0.13	0.00		−0.18		0.07
HR 720	−0.22		−0.16	−0.13	−0.14	−0.17	−0.21	−0.19	−0.16	−0.20	−0.34		−0.31		−0.18
HR 740	−0.25	−0.29	−0.23	−0.15	−0.26	−0.21	−0.19	−0.09	−0.27	−0.23	−0.12	−0.06	−0.14	−0.17	−0.16
HR 784	0.02	−0.04	−0.02	0.02	−0.02	0.05	0.08	0.02	0.05	−0.02	0.08	0.13	0.22	−0.08	0.04
HR 799	−0.02		−0.08	0.01	−0.01	−0.03	−0.01	−0.15	−0.08	0.01	0.01		0.00		−0.04
HR 962	0.09	0.11	0.26	0.21	0.26	0.22	0.11	0.08	0.11	0.15	0.07	−0.07	0.02		0.15
HR 1010	−0.23	−0.27	−0.22	−0.11	−0.14	−0.19	−0.20	−0.15	−0.33	−0.25	−0.37	−0.23	−0.31	−0.27	−0.16
HR 1083	−0.11	−0.22	−0.17	−0.17	−0.14	−0.09	−0.09	−0.18	−0.20	0.01	0.18	−0.07	0.05		−0.13
HR 1101	−0.11	−0.09	−0.05	−0.02	−0.01	−0.04	−0.11	−0.10	−0.08	−0.08	−0.16	−0.09	−0.17	−0.17	−0.07
HR 1173	0.09	−0.06	0.11	0.17	0.06	0.14	0.11	0.09	−0.02	0.14	0.23	0.13	0.14		0.13
HR 1257	0.04		0.09	0.17	0.07	0.13	−0.01	0.15	0.02	0.10			0.09		0.11
HR 1294	−0.18	−0.19	−0.12	−0.10	0.00	−0.12	−0.15	−0.16	−0.23	−0.20	−0.35	−0.29	−0.37	−0.47	−0.13
HR 1489	0.06		0.11			0.12	−0.01	0.02	0.00	0.09	−0.09	0.10	−0.10		0.05
HR 1536	0.14	0.06	0.20	0.34	0.32	0.23	0.18	0.15	0.06	0.17			−0.01		0.22
HR 1545	−0.33	−0.36	−0.28	0.01	−0.14	−0.33	−0.31	−0.10	−0.51	−0.27	−0.52	0.05	−0.28		−0.18
HR 1673	−0.30	−0.31	−0.26	−0.14	−0.16	−0.19	−0.23	−0.11	−0.25	−0.19	−0.25	−0.15	−0.23	−0.23	−0.17
HR 1687	0.26		0.37	0.32	0.31	0.30	0.31	0.23	0.23	0.46			0.21		0.29
HR 1729	−0.03		0.04	0.10	0.11	0.00	−0.04	0.02	−0.13	−0.01	−0.32		−0.22		0.02
HR 1780	0.00		−0.03	0.04	−0.01	0.09	0.04	−0.04	0.08	−0.04			0.23		0.03
HR 1983	−0.07	−0.14	−0.09	−0.06	0.00	−0.01	−0.04	−0.02	−0.03	−0.10	−0.09	−0.06	0.02	0.00	−0.03
HR 2047	−0.02		−0.13	−0.04	0.01	−0.01	0.01	−0.01	0.05	−0.09	0.31		0.26		−0.01
HR 2141	−0.24		−0.20	−0.14	−0.11	−0.19	−0.18	−0.09	−0.35	−0.19	−0.41		−0.41		−0.15
HR 2220	0.04		0.11	−0.01	0.06	0.00	0.03	0.03	−0.03	0.12	0.16		0.05		0.01

[Fe/H], [α/H] and [Ba/H] show different age-abundance relations (Fig. 14). The relative contributions of the three types of stars may well vary with galactic age and location in the Galaxy. One might imagine that the ejecta from Type II SNe, Type Ia SNe and AGB stars might not be thoroughly mixed everywhere in the Galaxy and, hence, stars of a given metallicity might show a spread in (say) [α/Fe] or [Ba/Fe]. With but a single qualification, it is remarkable that the spread which we dub "galactic" scatter, is very small for the sampled portions of the disk at a given age.

With this introduction, we turn to a detailed examination of our abundances.

6.2.2. Oxygen and α-elements in the disk at [Fe/H] > -0.2

The general shape of the [α/Fe] vs [Fe/H] relation is in fact well described by models of chemical evolution that take into account the time delay of SNe I relative to SNe II; see e.g. the analytical models of Pagel (1989), which account for the break in [α/Fe] at [Fe/H] ≈ -1. If there is a real "kink" in the relation for the disk, e.g. at [Fe/H] $\simeq -0.2$ (cf. the [Si/Fe] and [Ca/Fe]

Table 12. (continued)

ID	Fe I	O I	Na I	Mg I	Al I	Si I	Ca I	Ti I	Fe II	Ni I	Y II	Zr II	Ba II	Nd II	α
HR 2233	−0.17		−0.16	−0.06	−0.14	−0.15	−0.14	−0.05	−0.21	−0.10	−0.08		−0.10		−0.10
HR 2354	0.13	0.08	0.29	0.21	0.21	0.18	0.14	0.11	0.13	0.14	0.38	0.28	0.19	0.07	0.16
HR 2493	−0.37	−0.40	−0.34	−0.26	−0.26	−0.30	−0.28	−0.31	−0.51	−0.42	−0.57		−0.48	−0.22	−0.29
HR 2530	−0.43	−0.41	−0.31		−0.38	−0.31	−0.39		−0.44	−0.41	−0.30		−0.24		−0.35
HR 2548	−0.20	−0.22	−0.16	−0.14	−0.18	−0.19	−0.19	−0.16	−0.25	−0.21	−0.21	−0.18	−0.15	−0.18	−0.17
HR 2601	−0.56		−0.54	−0.32	−0.39	−0.38	−0.57	−0.30	−0.54	−0.51	−0.49	−0.51	−0.73		−0.39
HR 2721	−0.28		−0.35	−0.16	−0.26	−0.24	−0.27	−0.15	−0.26	−0.30	−0.36	−0.12	−0.24		−0.20
HR 2835	−0.55		−0.44	−0.32		−0.35	−0.48	−0.35	−0.54	−0.53	−0.69	−0.45	−0.60		−0.37
HR 2883	−0.75	−0.49	−0.72	−0.46	−0.58	−0.60	−0.58	−0.54	−0.67	−0.72	−0.74	−0.60	−0.79		−0.54
HR 2906	−0.18	−0.06	−0.16	−0.09	−0.06	−0.12	−0.16	−0.14	−0.05	−0.22	−0.01	−0.02	0.11	−0.02	−0.13
HR 2943	−0.02	−0.05	0.04	0.07	0.00	0.01	−0.04	0.12	−0.08	0.02	0.04	0.06	−0.09	−0.11	0.04
HR 3018	−0.78	−0.50	−0.60	−0.40	−0.49	−0.57	−0.52	−0.64	−0.75	−0.81	−0.77		−0.83		−0.53
HR 3176	0.04		0.17	0.15	0.19	0.16	0.03	0.07	0.16	0.15	0.12		0.04		0.10
HR 3220	−0.26	−0.22	−0.17	−0.08	−0.08	−0.09	−0.18	−0.13	−0.32	−0.22	−0.36		−0.32		−0.12
HR 3262	−0.26		−0.19		−0.25	−0.17	−0.23	−0.12	−0.16	−0.27	−0.25	−0.02	−0.15		−0.17
HR 3271	0.07	0.06	0.09	0.06	0.09	0.10	0.09	0.09	0.09	0.12	0.01	0.11	0.08	0.01	0.08
HR 3538	0.01		0.02	0.12	0.14	−0.01	−0.05	0.04	−0.20	0.05	0.04		−0.03		0.02
HR 3578	−0.82	−0.54	−0.77	−0.47	−0.67	−0.64	−0.59	−0.56	−0.84	−0.81	−0.66	−0.54	−0.79		−0.56
HR 3648	−0.08		0.00	0.09	0.07	−0.03	−0.07	−0.05	−0.01	0.00	−0.17		−0.13		−0.02
HR 3775	−0.20		−0.17	−0.11	−0.32	−0.13	−0.13	−0.12	−0.12	−0.18	0.05	0.01	0.07		−0.12
HR 3881	0.04		0.08	0.17	0.13	0.11	0.04	0.09	0.08	0.07	−0.05	0.11	0.02		0.10
HR 3951	0.10		0.32	0.37	0.29	0.17	0.14	0.14	−0.08	0.15	−0.20		−0.16		0.20
HR 3954	0.04			0.09	0.00	0.08	−0.02	0.04	0.05				0.24		0.05
HR 4012	0.14		0.25	0.24	0.23	0.18	0.08	0.19	0.23	0.17	0.24		0.20		0.17
HR 4027	−0.04		0.00	0.11	0.05	−0.03	−0.06	0.01	−0.13	−0.01			−0.30		0.01
HR 4039	−0.38		−0.30			−0.29	−0.33	−0.31	−0.48	−0.34	−0.43		−0.39		−0.31
HR 4067	0.18		0.20	0.26	0.26	0.21	0.11	0.27	0.16	0.20	0.06	0.26	0.18		0.21
HR 4150	−0.23		−0.31		−0.19	−0.17	−0.22		−0.27	−0.18	−0.22		−0.18		−0.20
HR 4158	−0.24		−0.19	−0.19	−0.17	−0.21	−0.26	−0.06	−0.24	−0.20	−0.28	−0.14	−0.31		−0.18
HR 4277	0.01		0.05	0.06	0.00	0.04	0.01	0.00	0.07	0.09			0.04		0.03
HR 4285	−0.30		−0.30	−0.20	−0.26	−0.24	−0.30	−0.32	−0.17	−0.29	−0.21	−0.10	−0.07		−0.27
HR 4395	−0.11		−0.02		−0.14	−0.10	−0.10	0.08	−0.03	0.00			0.47		−0.04
HR 4421	−0.54		−0.55		−0.52	−0.41	−0.44		−0.57	−0.46	−0.49		−0.44		−0.43
HR 4529	0.16	0.15	0.24	0.27	0.23	0.23	0.20	0.19	0.18	0.22	0.19	0.18	0.09	0.23	0.22
HR 4533	0.24	0.13	0.31	0.27	0.31	0.27	0.22	0.31	0.12	0.29	0.22	0.14	0.01	0.20	0.27
HR 4540	0.13	0.05	0.18	0.17	0.19	0.14	0.11	0.17	0.09	0.16	0.11	0.13	0.03	−0.05	0.15
HR 4657	−0.70	−0.42	−0.58	−0.36	−0.48	−0.47	−0.51	−0.38	−0.71	−0.64	−0.69	−0.35	−0.83		−0.43
HR 4683	−0.54		−0.35	−0.38	−0.48	−0.39	−0.45		−0.49	−0.45	−0.52		−0.50		−0.41
HR 4688	0.21		0.33	0.42	0.34	0.24	0.18	0.23	0.18	0.25	0.15		0.05		0.27
HR 4734	0.10	0.03	0.13	0.13	0.25	0.14	0.09	0.21	0.10	0.14	0.17	0.06	0.04	0.16	0.14
HR 4767	−0.11		−0.15			−0.03	−0.10	−0.07	−0.16	−0.13	−0.15	0.04	−0.05		−0.07
HR 4785	−0.19		−0.22	−0.13	−0.19	−0.21	−0.20	−0.19	−0.11	−0.18	−0.24	−0.13	−0.11		−0.18
HR 4845	−0.59		−0.63	−0.33	−0.39	−0.46	−0.51	−0.49	−0.75	−0.53	−0.70		−0.88		−0.45
HR 4903	0.24	0.22	0.38	0.36	0.43	0.30	0.19	0.24	0.29	0.26	0.11	0.07	0.13	0.29	0.27
HR 4981	−0.17		−0.18	−0.01	−0.14	−0.11	−0.17	−0.11	−0.17	−0.12	−0.18		−0.05		−0.10
HR 4983	0.03		0.00	0.07	0.03	0.00	0.03	0.04	0.00	−0.01	−0.03	0.21	0.09		0.04
HR 4989	−0.28	−0.25	−0.25	−0.09	−0.22	−0.18	−0.22	−0.29	−0.30	−0.26	−0.18		−0.13		−0.19
HR 5011	0.10	0.10	0.17	0.23	0.26	0.18	0.17	0.18	0.08	0.12	−0.02	0.03	0.05	−0.15	0.19
HR 5019	−0.03	−0.10	−0.05	0.05	0.11	−0.01	0.02	0.07	−0.10	−0.04	−0.21	−0.17	−0.16	−0.12	0.03

panels in Fig. 15), one might invoke a rather abrupt change in the relative role of these types of supernovae: the SNe I production again declining relative to that of SNe II, or retention by the thin galactic disk of the ejecta from the supernovae was different for the two supernova types compared to the situation in the older thick disk. The dynamical data show a demarcation between the thin ($\sigma(W)$ about 20 km s^{-1}) and the thick ($\sigma(W) \simeq 40$ km s^{-1}) disks around [Fe/H] = −0.2 to −0.3 (cf. Figs. 16a and 15).

Table 12. (continued)

ID	Fe I	O I	Na I	Mg I	Al I	Si I	Ca I	Ti I	Fe II	Ni I	Y II	Zr II	Ba II	Nd II	α
HR 5235	0.19		0.45	0.47	0.41	0.33	0.23	0.32	0.25	0.30			0.04		0.34
HR 5323	0.07		0.13	0.15	0.17	0.06	−0.05	0.20	0.00	0.13	0.05	0.11	−0.05		0.09
HR 5338	−0.11	0.00	−0.11	0.07	−0.09	−0.03	−0.12	−0.12	−0.07	−0.14	0.24		0.25		−0.05
HR 5353	0.13	0.09	0.19	0.23	0.24	0.17	0.12	0.21	0.09	0.12	0.23	0.13	0.01	0.16	0.18
HR 5423	0.05		0.26	0.26	0.30	0.13	0.09	0.10	0.06	0.13	−0.06		−0.18		0.15
HR 5447	−0.41		−0.32	−0.37	−0.43	−0.36	−0.36		−0.40	−0.40	−0.24		−0.26		−0.36
HR 5459	0.15	0.15	0.28	0.28	0.25	0.25	0.16	0.18	0.19	0.20	0.13	0.08	0.07	0.11	0.22
HR 5542	0.13	0.03	0.18	0.14	0.17	0.12	0.15	0.15	0.09	0.10	−0.05	0.06	0.16	−0.07	0.14
HR 5691	−0.02		0.04	0.03	0.02	0.00	−0.02	−0.01	0.00	0.09	0.22		−0.11		0.00
HR 5698	0.01	−0.02	0.06	0.14	0.10	0.09	0.01	0.10	0.08	0.05	0.06	0.09	0.12	0.03	0.09
HR 5723	−0.12		−0.03	0.03	−0.05	−0.03	−0.09	0.05	−0.13	−0.06	−0.10	0.11	−0.06		−0.01
HR 5868	−0.04		0.00	0.10	0.06	−0.02	−0.06	0.09	−0.05	0.01	0.10		−0.14		0.03
HR 5914	−0.52		−0.55	−0.30	−0.40	−0.40	−0.47	−0.28	−0.32	−0.48	−0.19		−0.46		−0.36
HR 5933	−0.16		−0.13	−0.07	−0.17	−0.14	−0.18	−0.28	−0.11	−0.14	−0.10		−0.15		−0.17
HR 5968	−0.26		−0.30	−0.07	−0.11	−0.17	−0.20	−0.16	−0.22	−0.23	−0.33	−0.20	−0.41		−0.15
HR 5996	0.23	0.09	0.36	0.33	0.34	0.27	0.27	0.27	0.16	0.26	0.00	0.18	0.05	−0.08	0.28
HR 6189	−0.56	−0.48	−0.48	−0.36	−0.51	−0.50	−0.56	−0.38	−0.59	−0.57	−0.55		−0.70		−0.45
HR 6202	−0.37	−0.34	−0.28	−0.32	−0.36	−0.30	−0.32	−0.26	−0.37	−0.34	−0.32		−0.24		−0.30
HR 6243	0.00		0.14		0.09	0.04	−0.02	0.05	0.02	0.08		0.02	−0.05		0.02
HR 6315	−0.17		−0.26	−0.07	−0.16	−0.13	−0.16	−0.03	−0.05	−0.12	0.11		0.00		−0.10
HR 6409	0.09	−0.04	0.09	0.21	0.22	0.11	0.14	−0.01	0.09	0.19	0.19	−0.06	0.29	0.28	0.11
HR 6458	−0.41		−0.31	−0.08	−0.13	−0.22	−0.21	−0.12	−0.32	−0.33			−0.58		−0.16
HR 6541	−0.23		−0.17	−0.04	−0.13	−0.18	−0.25	−0.14	−0.16	−0.18	−0.12	−0.03	−0.22		−0.15
HR 6569	−0.27		−0.16	−0.08	−0.28	−0.19	−0.21	−0.14	−0.23	−0.22			−0.09		−0.16
HR 6598	−0.39		−0.26	−0.25	−0.27	−0.28	−0.35	−0.30	−0.25	−0.35	−0.33		−0.41		−0.29
HR 6649	−0.34	−0.29	−0.19	−0.26	−0.21	−0.26	−0.29	−0.30	−0.32	−0.39	−0.30	−0.54	−0.32	−0.32	−0.28
HR 6701	−0.22		−0.12	−0.02	−0.08	−0.10	−0.19	0.02	−0.17	−0.13	−0.11		−0.19		−0.07
HR 6775	−0.56		−0.55	−0.43	−0.48	−0.43	−0.50	−0.33	−0.43	−0.42	−0.39		−0.51		−0.42
HR 6850	−0.32		−0.32	−0.21	−0.28	−0.25	−0.25	−0.13	−0.29	−0.22	−0.18		−0.25		−0.21
HR 6907	0.13	0.01	0.13	0.15	0.16	0.13	0.10	0.23	0.10	0.18	0.14	0.22	0.14	0.07	0.15
HR 7061	−0.11				−0.05	−0.01	−0.04		−0.08	−0.10			0.04		−0.02
HR 7126	0.21		0.08	0.14	0.20	0.18	0.21	0.03	0.10	0.34	0.21		0.32		0.14
HR 7232	0.03	−0.05	0.13	0.09	0.09	0.06	0.06	0.03	0.00	0.02	−0.13	−0.01	−0.05	0.05	0.06
HR 7322	−0.28		−0.21	−0.09	−0.20	−0.25	−0.25	−0.04	−0.18	−0.19	−0.06	0.00	−0.18		−0.16
HR 7534	−0.13		−0.17	0.04	−0.01	−0.05	0.00	0.08	−0.11	−0.03	0.02	0.14	0.04		0.01
HR 7560	0.09		0.12	0.18	0.15	0.08	0.10	0.12	−0.04	0.12	−0.04	0.20	−0.05		0.12
HR 7766	−0.36	−0.26	−0.36	−0.27	−0.29	−0.29	−0.30	−0.26	−0.30	−0.36	−0.40	−0.42	−0.43	0.12	−0.28
HR 7875	−0.44	−0.30	−0.37	−0.32	−0.37	−0.37	−0.41	−0.36	−0.38	−0.43	−0.42	−0.48	−0.36	−0.31	−0.36
HR 7955	0.12		0.16	0.24	0.20	0.14	0.04	0.30	0.14	0.19	0.29		0.13		0.18
HR 8027	−0.37	−0.31	−0.32	−0.37	−0.38	−0.32	−0.26	−0.32	−0.38	−0.37		−0.26	−0.34		−0.32
HR 8041	0.11		0.26	0.23	0.24	0.21	0.11	0.17	0.19	0.26	−0.05		−0.04		0.18
HR 8077	−0.07		0.00	0.01	0.02	−0.04	−0.11	−0.06	−0.06	0.08			−0.22		−0.05
HR 8181	−0.67	−0.57	−0.53	−0.53	−0.65	−0.60	−0.62	−0.58	−0.70	−0.67	−0.76		−0.70		−0.58
HR 8354	−0.66		−0.31	−0.40	−0.52	−0.52	−0.54	−0.59	−0.57	−0.61	−0.68		−0.63		−0.51
HR 8472	0.06		0.15	0.27	0.16	0.09	0.00	0.19	0.01	0.09			−0.04		0.14
HR 8665	−0.32		−0.25	−0.17	−0.17	−0.20	−0.26	−0.20	−0.21	−0.17	−0.36		−0.27		−0.21
HR 8697	−0.25		−0.22	−0.12	−0.12	−0.19	−0.23	−0.17	−0.31	−0.20	−0.21	−0.18	−0.27		−0.18
HR 8729	0.06		0.22	0.26	0.28	0.13	0.11	0.08	0.04	0.16	−0.07		−0.05		0.14
HR 8805	−0.13		−0.12	0.01	−0.07	−0.06	−0.07		−0.11	−0.08	−0.10	0.02	−0.01		−0.04

For stars more metal-rich than [Fe/H] $\simeq -0.2$, the ratios [X/Fe] are independent of [Fe/H] or almost so except for X = O, Na and possibly Mg and Al. These stars of near-solar metallicity are not exclusively young stars, see Fig. 14. The young stars, say $\log \tau_9 < 0.3$, are metal-rich. But there are very old stars of a similar metallicity: two outstanding examples are HR 5019 with [Fe/H] = −0.03 and τ = 14 Gyr and HR 7232 with [Fe/H] = 0.03 and τ = 12 Gyr. Most of the metal-rich

Table 12. (continued)

ID	Fe I	O I	Na I	Mg I	Al I	Si I	Ca I	Ti I	Fe II	Ni I	Y II	Zr II	Ba II	Nd II	α
HR 8853	0.00		0.01	0.09	0.09	0.04	0.02	0.11	−0.01	0.04	0.00	0.10	−0.12		0.06
HR 8885	0.02		0.08	0.19	0.06	0.05	0.04	0.09	0.09	0.12			0.25		0.09
HR 8969	−0.17		−0.07	0.00	−0.09	−0.08	−0.11	−0.11	−0.23	−0.12	−0.19	−0.06	−0.12		−0.07
HD 2615	−0.58	−0.40	−0.50	−0.46	−0.48	−0.47	−0.47	−0.46	−0.59	−0.60	−0.67	−0.58	−0.58	−0.46	−0.47
HD 6434	−0.54	−0.34	−0.45	−0.22	−0.33	−0.37	−0.36	−0.28	−0.59	−0.52	−0.26	−0.20	−0.20	−0.38	−0.31
HD 14938	−0.37	−0.17	−0.23	−0.21	−0.35	−0.30	−0.17	−0.28	−0.31	−0.37	−0.24		−0.36		−0.24
HD 17548	−0.59	−0.48	−0.56	−0.44	−0.52	−0.47	−0.51	−0.47	−0.62	−0.59	−0.68		−0.69	−0.42	−0.47
HD 18768	−0.62		−0.52	−0.45	−0.50	−0.46	−0.57	−0.53	−0.55	−0.58	−0.73		−0.68		−0.50
HD 22879	−0.84	−0.57	−0.81	−0.40	−0.55	−0.65	−0.65	−0.65	−0.87	−0.83	−0.80		−0.93		−0.59
HD 25704	−0.85	−0.57	−0.75	−0.50	−0.55	−0.70	−0.61	−0.58	−0.79	−0.87	−0.85		−0.88		−0.60
HD 30649	−0.51		−0.45	−0.24	−0.23	−0.38	−0.42	−0.36	−0.54	−0.53			−0.72		−0.35
HD 38007	−0.35		−0.28	−0.25	−0.25	−0.25	−0.31	−0.22	−0.33	−0.34	−0.49		−0.46		−0.25
HD 43947	−0.30		−0.25	−0.19	−0.20	−0.24	−0.31	−0.26	−0.38	−0.30			−0.38		−0.25
HD 51929	−0.64	−0.43	−0.57	−0.32	−0.43	−0.48	−0.50	−0.37	−0.68	−0.61	−0.69	−0.54	−0.75	−0.68	−0.42
HD 62301	−0.69	−0.43	−0.66	−0.39	−0.49	−0.51	−0.62	−0.46	−0.61	−0.61	−0.77		−0.78		−0.50
HD 66573	−0.58		−0.48	−0.23	−0.26	−0.39	−0.38	−0.25	−0.57	−0.49			−0.72		−0.31
HD 68284	−0.59	−0.43	−0.50	−0.40	−0.45	−0.48	−0.49	−0.51	−0.58	−0.59	−0.69	−0.59	−0.64	−0.76	−0.47
HD 69611	−0.58	−0.28	−0.49	−0.19	−0.30	−0.39	−0.37	−0.30	−0.63	−0.56	−0.57	−0.41	−0.72		−0.31
HD 74011	−0.65		−0.49	−0.31	−0.35	−0.47	−0.42	−0.37	−0.60	−0.51			−0.80		−0.39
HD 78558	−0.40	−0.16	−0.31	−0.14	−0.16	−0.25	−0.23	−0.14	−0.45	−0.38	−0.52	−0.36	−0.52	−0.57	−0.19
HD 78747	−0.64	−0.38	−0.52	−0.30	−0.39	−0.45	−0.44	−0.34	−0.67	−0.61	−0.57	−0.40	−0.64	−0.43	−0.38
HD 89707	−0.42	−0.36	−0.34	−0.31	−0.36	−0.37	−0.40	−0.37	−0.48	−0.44	−0.51		−0.44		−0.36
HD 91347	−0.48		−0.47	−0.34	−0.35	−0.38	−0.42	−0.46	−0.50	−0.46			−0.69		−0.40
HD 98553	−0.43	−0.45	−0.40	−0.34	−0.38	−0.40	−0.40	−0.36	−0.50	−0.45	−0.57	−0.45	−0.45	−0.52	−0.37
HD 114762	−0.74		−0.52	−0.45	−0.58	−0.44	−0.58	−0.59	−0.64	−0.63			−0.90		−0.52
HD 126512	−0.63		−0.53	−0.26	−0.40	−0.40	−0.44	−0.38	−0.50	−0.52			−0.86		−0.37
HD 130551	−0.62	−0.46	−0.45	−0.44	−0.53	−0.52	−0.52	−0.42	−0.58	−0.61	−0.63		−0.60		−0.47
HD 134169	−0.83	−0.51	−0.68	−0.52	−0.57	−0.65	−0.68	−0.54	−0.83	−0.79	−0.90		−0.97	−0.67	−0.60
HD 144172	−0.44		−0.33	−0.36	−0.48	−0.38	−0.43	−0.38	−0.44	−0.39			−0.45		−0.39
HD 148211	−0.65	−0.45	−0.60	−0.35	−0.48	−0.50	−0.50	−0.44	−0.69	−0.63	−0.75	−0.67	−0.79	−0.50	−0.45
HD 148816	−0.74	−0.46	−0.61	−0.42	−0.50	−0.56	−0.59	−0.47	−0.73	−0.72	−0.77		−0.89	−0.54	−0.51
HD 155358	−0.67		−0.57	−0.39	−0.46	−0.51	−0.56	−0.52	−0.59	−0.53			−0.84		−0.50
HD 157089	−0.59	−0.41	−0.55	−0.37	−0.36	−0.39	−0.41	−0.32	−0.61	−0.59	−0.57	−0.65	−0.68	−0.53	−0.37
HD 159307	−0.71	−0.49	−0.54	−0.47	−0.58	−0.57	−0.59	−0.62	−0.69	−0.68	−0.71	−0.63	−0.74		−0.56
HD 165401	−0.46		−0.37	−0.10	−0.22	−0.30	−0.32	−0.25	−0.50	−0.41			−0.72		−0.24
HD 174912	−0.54		−0.42	−0.34	−0.38	−0.46	−0.47	−0.41	−0.44	−0.48	−0.58		−0.62		−0.42
HD 184499	−0.61		−0.43	−0.24	−0.30	−0.36	−0.43	−0.34	−0.51	−0.47			−0.86		−0.34
HD 188815	−0.58	−0.42	−0.50	−0.38	−0.50	−0.50	−0.54	−0.47	−0.55	−0.59	−0.61		−0.57		−0.47
HD 198044	−0.31	−0.13	−0.23	−0.22	−0.20	−0.22	−0.27	−0.40	−0.26	−0.33	−0.39	−0.43	−0.23		−0.28
HD 199289	−1.03	−0.72	−0.93	−0.63	−0.73	−0.81	−0.80	−0.75	−1.08	−0.98	−1.02		−1.09		−0.75
HD 200973	−0.52	−0.27	−0.37	−0.17	−0.28	−0.33	−0.37	−0.24	−0.58	−0.52	−0.63	−0.47	−0.63		−0.28
HD 201099	−0.50	−0.33	−0.48	−0.28	−0.37	−0.44	−0.43	−0.44	−0.56	−0.53	−0.71	−0.70	−0.70	−0.54	−0.40
HD 201891	−1.06		−0.91	−0.71	−0.86	−0.82	−0.91	−0.74	−1.09	−0.97	−0.94		−1.14		−0.79
HD 205294	−0.36	−0.28	−0.28	−0.26	−0.34	−0.29	−0.29	−0.26	−0.38	−0.40	−0.37	−0.38	−0.33		−0.28
HD 208906	−0.72		−0.59	−0.64	−0.57	−0.60	−0.63	−0.45	−0.66	−0.69	−0.83		−0.78		−0.58
HD 210752	−0.64	−0.56	−0.61	−0.48	−0.49	−0.60	−0.57	−0.58	−0.73	−0.67	−0.83		−0.78		−0.56
HD 215257	−0.65	−0.52	−0.56	−0.55	−0.60	−0.63	−0.55	−0.48	−0.64	−0.67	−0.71		−0.70		−0.55
HD 218504	−0.62	−0.43	−0.58	−0.33	−0.39	−0.48	−0.49	−0.45	−0.64	−0.60	−0.70	−0.54	−0.72	−0.57	−0.44
HD 221830	−0.52	−0.29	−0.38	−0.05	−0.18	−0.26	−0.28	−0.27	−0.47	−0.37	−0.55	−0.34	−0.61		−0.22

stars appear to have originated from an annulus with a radius similar to that of the Sun ($R_{m\odot}$ = 8.4 kpc in the adopted dynamical model). By contrast, stars with [Fe/H] < -0.2 have come from a wide range of galactocentric radii: R_m = 4 to 11 kpc with 6 to 10 kpc for the majority.

Stars of the thin disk have metallicities spanning about 0.5 dex from [Fe/H] about −0.2 to +0.3, but the scatter in [X/Fe] is remarkably small for most of the sampled elements, e.g., X = Si, Ca and Ni. In Fig. 17 we show [Si/Fe] and [Ni/Fe] vs [Ca/Fe] for the ESO and McDonald observations. Since the for-

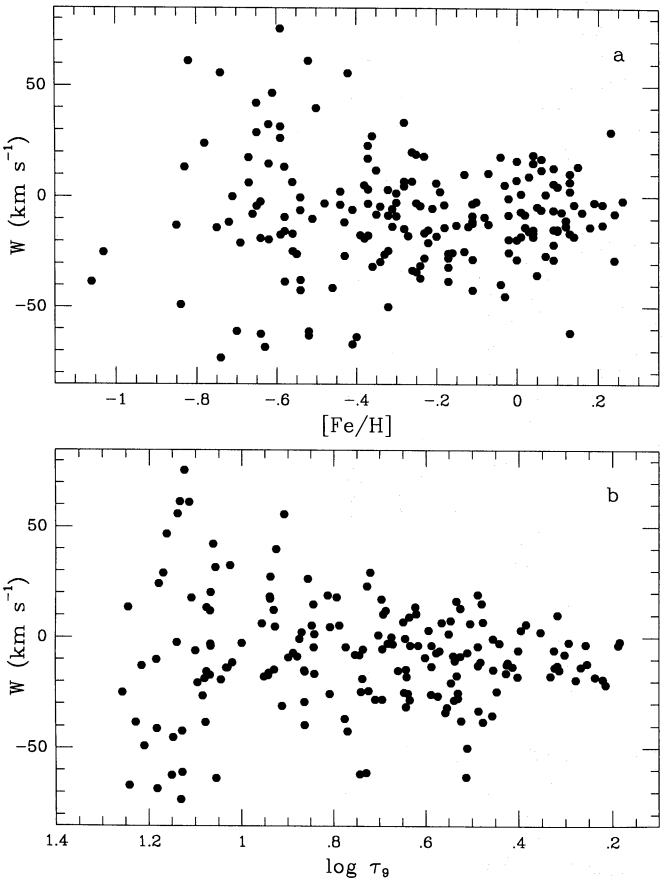

Fig. 16a and b. Stellar velocities perpendicular to the galactic plane, W, vs iron abundance **a** and age **b**, τ_9 is the age in 10^9 years

mer are of higher spectral resolution and, therefore, give, in general, slightly more accurate abundances, they provide the better estimate of the "galactic" scatter in the [X/Fe] values.

For Si and Ca, the mean abundances for 35 stars observed at ESO are [Si/Fe] = 0.046 ± 0.035 and [Ca/Fe] = 0.009 ± 0.031. The numbers given after the "±" here and throughout Sect. 6 are standard deviations, meaning the scatter around the mean, and not the formal errors of the mean. To within a standard deviation (σ about 0.02 to 0.04) there is no trend of either ratio from [Fe/H] = −0.2 to +0.2. There is a suspicion (see Fig. 17) that [Si/Fe] is about 0.04 dex on average smaller in the younger stars ($\log \tau < 0.5$). Several of the stars with the highest [Si/Fe] values have distinctive Na, Mg, and Al abundances (see below) and two others are Barium dwarfs. If these peculiar stars are removed from the sample, the mean [Si/Fe] becomes 0.033 ± 0.024. Since σ = 0.03 for both Si and Ca corresponds to that expected from the errors of measurement of the equivalent widths and the errors of analysis using model atmospheres (see Table 9), the galactic scatter in [Si/Fe] and [Ca/Fe] seems less than 0.03 dex or 7%. The scatter in [Ni/Fe] is also approximately consistent with that expected from the errors of measurement: the mean value is [Ni/Fe] = 0.021 ± 0.047.

However, the increased scatter in some [X/Fe] plots reveals a group of stars with a novel pattern of abundances. For example magnesium provides an interesting contrast to Si and Ca. There is a larger spread in [Mg/Fe] than in [Ca/Fe] (Fig. 18) or [Si/Fe] (Fig. 17). Since we have used only 2 Mg I lines and up to 6 Si I (and 4 Ca I) lines, the Mg abundance is more susceptible to errors in the equivalent widths; this is reflected in the larger dispersion of the abundance differences computed for the 16 stars in common to the ESO and McDonald samples (Table 10). The sensitivities of the Mg I and Si I lines to the model atmospheric structure are almost identical. The effect of the errors from the measurements and, for Mg I relative to Ca I, of a larger error from inappropriate model atmospheres is to distribute the points over a quasi-elliptical region in Fig. 18; such a distribution is seen for the ESO abundances but is not so obvious for the McDonald abundances, presumably because the errors of the equivalent widths for Mg I and Ca I are roughly comparable for the McDonald spectra. From the ESO measurements, we obtain a mean [Mg/Fe] = +0.05 ± 0.06 from 31 stars when 2 Mg-rich stars and two Barium dwarfs (also Mg-rich) are omitted. The dispersion of 0.06 dex is probably not due entirely to the errors of measurement and analysis. Certainly, the galactic scatter in [Mg/Fe] at a given [Fe/H] can not exceed 0.06 dex.

There is a suspicion of a correlation between Mg and O abundances: [Mg/Fe] ≈ 0.15 + 1.5[O/Fe]. The few exceptions to this correlation include two O-rich Ba dwarfs and a few stars unusually rich in Mg (see below for the NaMgAl stars). There is a hint that [O/Fe] declines with stellar age. These tantalising results for O deserve further exploration. Recall that O abundances are available here only for stars observed from ESO and, in most cases, the permitted 7774 Å triplet lines and the 6158 Å line were observed and scaled to the 6300 Å [O I] line.

An outstanding feature of Fig. 18 is the group of Mg-rich stars: HR 448 and 1536 in Fig. 18a and HR 3951, 4688, 5235, 5338, 5423, 8472, and 8729 in Fig. 18b. Apart from HR 5338, which is a Barium dwarf, these stars are also Na and Al rich, slightly enriched in Si but not in Ca, and all are metal-rich ([Fe/H] > 0.05). The mean excess abundance relative to the other metal-rich stars is Δ[X/Fe] = 0.12, 0.14, 0.10, and 0.04 for Na, Mg, Al, and Si respectively with Δ[Ca/Fe] = 0.01. These stars ("NaMgAl stars") are unusually deficient in the heavy elements: the 8 identified examples of the NaMgAl stars have a mean [Ba/Fe] = −0.18 ± 0.07 but other metal-rich ([Fe/H] > 0.0) stars have mean ratios [Ba/Fe] = −0.02 ± 0.11 (ESO) and −0.05 ± 0.12 (McD). The low Ba/Fe ratios of the NaMgAl stars are exemplified by the following statistics. Three of the NaMgAl stars have [Ba/Fe] < −0.2. Such low Ba/Fe ratios are rare; for example, 130 stars have [Fe/H] > −0.40 but only 6 have [Ba/Fe] < −0.20. Three of the 6 are NaMgAl stars and one of the remaining 3 has yet to be investigated for Mg and Al. The comparable statistics for [Ba/Fe] < −0.15 and [Fe/H] > −0.40 are a total of 18 stars of which 6 are NaMgAl stars, 3 have unknown Mg and Al abundances and 9 have "normal" Na, Mg and Al abundances. The NaMgAl stars span a wide range of ages ($\log \tau$ = 0.32 to 0.93) and birth sites (R_m = 6.0 to 8.3 kpc).

We have been unable to identify simple errors in the abundance analysis that would produce the abundance patterns of

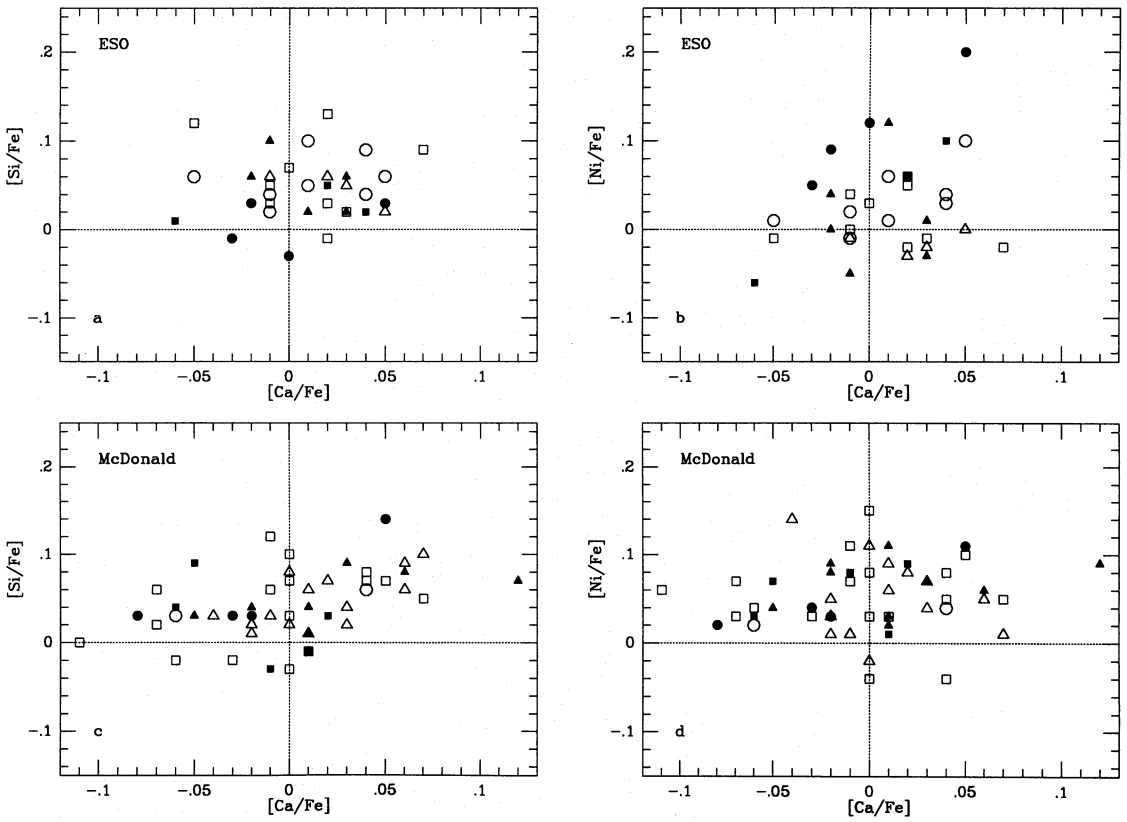

Fig. 17. Scatter diagrams of relative abundances for ESO and McDonald thin disk stars. The symbols mark different metallicity ranges and ages: triangles $-0.20 \leq$ [Fe/H] < 0.00, squares $0.00 \leq$ [Fe/H] < 0.13 and circles [Fe/H] ≥ 0.13. Filled and open symbols denote stars with $\log \tau < 0.5$ and > 0.5, respectively. The Sun is by definition at the origin

the NaMgAl stars. An error in the placement of the continuum of the 8740 Å spectrum would introduce similar errors in the Mg and Al abundances but the Na abundances are derived from a different wavelength region. Errors in the adopted model atmospheres could produce similar errors in Na and Al but would also result in very similar errors in Ca and different errors for Mg and Si. Departures from LTE ionization equilibria are expected to also affect Ca. A contrived pattern of errors in equivalent widths and model atmosphere parameters might be found but other tests do not support this explanation; i.e., the small differences of the abundances for the 16 stars in common to the ESO and McDonald observations. It is difficult to tell whether the NaMgAl stars form a distinct class or are to be considered as part of a larger quasi-continuous galactic scatter in certain of the relative abundances.

The origin of the NaMgAl stars is unclear. One may speculate that the stars have been affected by mass-transfer from a now "dead" companion. For originally relatively old and metal-poor stars transfer of hydrogen-poor material might affect our analysis, based on a normal He/H ratio, to return a high metallicity but approximately the original ratio X/Fe. Just possibly, ejecta from ONeMg novae may account for the anomalies. Alternatively, one may suppose that the NaMgAl excesses were in the interstellar clouds that gave birth to these stars. A deficiency of the heavy elements like Ba suggests an underrepresentation of s-process products from low-mass AGB stars. Further investigations of NaMgAl stars are clearly warranted.

6.2.3. Is the Sun a typical [Fe/H] = 0.0 star?

Inspection of Fig. 15 shows the mean [X/Fe] at the solar metallicity ([Fe/H] = 0) to be non-zero; i.e., the Sun appears to be slightly atypical for its metallicity. Since there is a hint that [X/Fe] for some elements varies with age of the stars, we give the mean stellar abundances for stars within a range ($\log \tau = 0.5$ to 0.7) bracketing the Sun's age. The sample of 14 ESO stars with [Fe/H] > -0.2 gives mean values [X/Fe] $= -0.03 \pm 0.03$(O), $+0.08 \pm 0.05$(Na), $+0.10 \pm 0.06$(Mg), $+0.10 \pm 0.06$(Al), $+0.06 \pm 0.04$(Si), $+0.01 \pm 0.03$(Ca), $+0.02 \pm 0.03$(Ti), $+0.02 \pm 0.04$(Ni) and -0.06 ± 0.11(Ba). For all elements, the Sun ([X/Fe] = 0.0) is within 2 σ of these mean abundances. (The comparable values for the McDonald results are within 1 σ of the ESO values.) The largest anomalies are for Na, Mg and Al but, as discussed above, the sample contains a class of NaMgAl-rich stars. If the probable members of this class are excluded, [X/Fe] is, of course, reduced for Na, Mg and Al: e.g., [Mg/Fe] is lowered to $+0.06 \pm 0.05$. Obviously, the Sun would be representative within the observed dispersion of the mean [X/Fe] values. If these dispersions are not "galactic", however, but mainly caused by observational errors, the Sun would depart marginally, since the errors in the mean [X/Fe] are only about 0.02 dex (note, the *scatter* is given

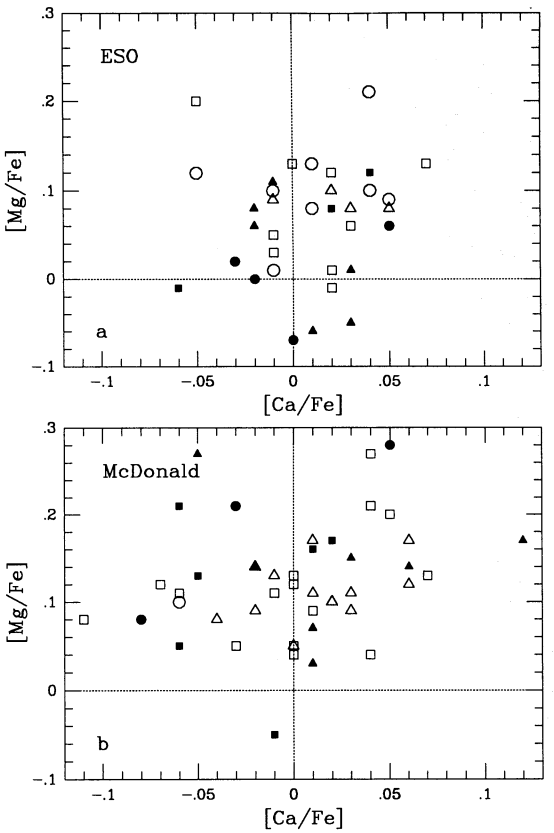

Fig. 18. Comparison between magnesium and calcium abundances for ESO and McDonald, stars with [Fe/H] > -0.2. Symbols as in Fig. 17

above) and the errors in the solar abundances relative to this mean should not be much greater.

If we select stars that have the metallicity and the galactocentric radius of the Sun, say R_m = 8.2 to 8.7 kpc and [Fe/H] = -0.03 to 0.02, the picture changes somewhat. The 5 stars that satisfy these criteria give [X/Fe] = +0.01 $\pm$ 0.08(Na), +0.04 $\pm$ 0.06(Mg), +0.02$\pm$0.04(Al), +0.03$\pm$0.02(Si), +0.01$\pm$0.03(Ca), +0.01 $\pm$ 0.03(Ti), +0.03 $\pm$ 0.06(Ni) and +0.04 $\pm$ 0.09(Ba). One Barium dwarf (HR 2047) was omitted in computing the mean [Ba/Fe]. Oxygen is available for 4 of the 5 stars: [O/Fe] = -0.04. This sample of 5 stars covers a range in effective temperature but, as the small sigma's indicate, the relative abundances are independent of $T_{\rm eff}$. The closest equivalent to the Sun (HR 4277 with $T_{\rm eff}$ = 5880 K, log g = 4.34, [Fe/H] = 0.01, and age of 7.0 Gyr) has $|$[X/Fe]$|$ < 0.05 for all elements with the exception that [Ni/Fe] = 0.08.

These comparisons suggests that the Sun is a quite typical star for its metallicity, age, *and* galactic orbit.

6.2.4. Oxygen and α-elements in the disk at [Fe/H] < -0.2

At a metallicity [Fe/H] around -0.2 to -0.3 both a chemical and a kinematical transition occurs for the galactic disk: the gradients of [α/Fe] vs [Fe/H] seem to get steeper and the scatter of [α/Fe] at a given [Fe/H] is larger for [Fe/H] < -0.3 (Fig. 15), and the vertical velocities W (Fig. 16) have a much larger range for [Fe/H] < -0.2 than for the more metal-rich stars. The [Fe/H] < -0.2 and [Fe/H] > -0.2 samples cover different ranges in age (Fig. 14a): there are no young stars (log $\tau_9 < 0.3$) with [Fe/H] < -0.2 but all except three of the old stars (log $\tau_9 > 1.0$) are more metal-poor than [Fe/H] < -0.2. Note, however, that old metal-rich stars may be too red to be included in our sample due to the selection criteria. We detail now the relative abundances [X/Fe] for O and the α elements for these more metal poor stars.

The increased scatter in [X/Fe] at a given [Fe/H] below [Fe/H] = -0.4 is especially obvious for Mg and Ca. It is hardly due to [Fe/H]-dependent errors in the analysis but most probably has astrophysical origins. These origins may be presumed to blend issues of stellar nucleosynthesis (e.g. the mix of Type II and Ia SNe) and galactic structure (e.g., the history of star formation is likely to depend on the galactocentric radius). Examination of the metal-poor stars shows that the ratios [X/Fe] for X = O, Mg, Si, Ca and Ti are dependent on the R_m of the stars. In Fig. 19, we show a composite relative abundance [α'/Fe] vs [Fe/H]; [α'/Fe] is a straight mean of the [Si/Fe] and [Ca/Fe] values. Si and Ca were chosen because these abundances are the most accurate of the α elements (including O). In Fig. 20 the data is shown for four intervals of R_m. Two novel features of Figs. 19 and 20 stand out. First, stars with [Fe/H] $\simeq -0.6$ show [α'/Fe] to decrease with increasing R_m. Second, the run of [α'/Fe] with [Fe/H] for [Fe/H] ≥ -0.6 may be of a different character for the inner ($R_m < 7$ kpc) and outer ($R_m > 7$ kpc) stars.

It seems reasonable to ascribe the change with R_m of [α'/Fe] at a given [Fe/H] to a more rapid formation of the α elements in the interior parts of the galactic disk, e.g., due to a more rapid star formation there, and thus a greater enrichment by SNe II of the interstellar medium with α elements at a given [Fe/H]. The greater star formation rate may be due to a more rapid collapse of the galactic disk. This is consistent with the strong dependence found in model calculations of the formation timescale of galactic disks on the surface density by Burkert et al. (1992), implying that the disk formed from inside out and that star formation progressed outwards. Similarly, a differential abundance gradient, due to differences in star formation rate, were found in the galactic models of Matteucci & François (1989). The enrichment of iron is determined by a second time constant, namely the time it takes for progenitors of SNe Type I to evolve. As the disk ages and [Fe/H] rises, the gradient of [α/Fe] with R_m levels out, which with the interpretation sketched above indicates that the star formation in the outer parts of the disk becomes relatively more rapid.

At the Sun's galactocentric radius, [α'/Fe] appears to increase smoothly with decreasing [Fe/H] and the scatter about the mean relation is independent of [Fe/H]. The relation for R_m = 7 to 8 kpc is similar to that for 8 to 9 kpc. Here, stars of a given [α'/Fe] come from a portion of the full [Fe/H] range (see Fig. 19) but a very wide range of ages reflecting the poorly defined age-metallicity relation (Fig. 14).

In the outer Galaxy, $R_m > 9$ kpc, the [α'/Fe] vs [Fe/H] relation in the interval -0.7 < [Fe/H] < -0.2 falls slightly

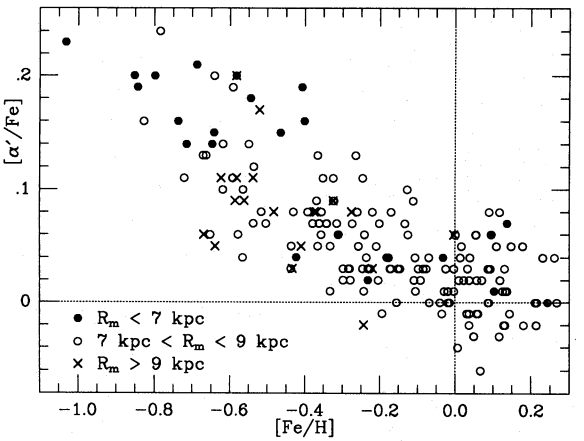

Fig. 19. The run of [α'/Fe] vs iron abundance for all programme stars, separated in three R_m intervals

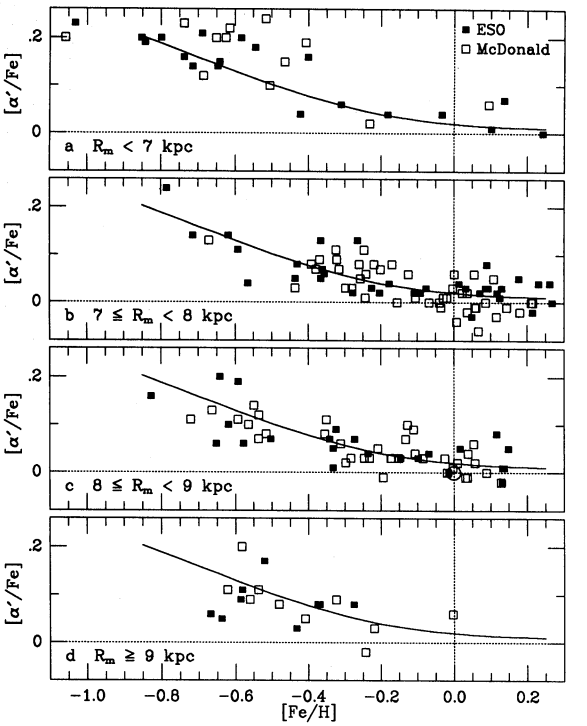

Fig. 20a–d. The run of [α'/Fe] vs iron abundance for four ranges of R_m. The filled squares represent ESO stars and the open squares show stars observed from McDonald. The solid lines show a mean relation for all the stars. In the inner Galaxy (R_m < 7 kpc) [α'/Fe] = 0.2 for [Fe/H] < −0.4 and [α'/Fe] = 0.03 for [Fe/H] > −0.4. At larger distances from the galactic center there is no sign of this step in [α'/Fe]. As a result, at metallicities less than [Fe/H] = −0.4 the inner Galaxy is characterized by a larger [α'/Fe] than it is further out

below that of the R_m = 8 to 9 kpc stars. Two stars (HD 66573, HD 200973) from the outer Galaxy have the high [α'/Fe] characteristic of stars at R_m < 7 kpc. It is possible that this pair belongs to a population of high [α'/Fe] stars spanning a wide range of galactocentric radii but concentrated in the inner Galaxy. It is, of course, also possible that the birth sites of the pair are not given correctly by their R_m; the present orbits place perigalacticon at 7.2 and 7.7 kpc for the pair.

For R_m < 7 kpc, the [α'/Fe] values tend to fall into two groups: [α'/Fe] = 0.2 for [Fe/H] < −0.4 and [α'/Fe] = 0.03 for [Fe/H] > −0.4 with just one star (HD 30649) having an intermediate value. The high [α'/Fe] stars dominate the sample for R_m < 7 kpc which probably just reflects the tendency for the oldest stars (with low [Fe/H]) to have the most eccentric orbits. Although a larger sample is desirable, there is a suggestion that [α'/Fe] for [Fe/H] < −0.5 is almost age-independent for R_m < 7 kpc; these stars are predominantly old, see Fig. 21.

The immediate impression from Fig. 19 is that [α'/Fe] increases smoothly with decreasing [Fe/H]. The evidence for a continuous change of [α'/Fe] at [Fe/H] $\lesssim$ −0.3 is, however, weak, partly in view of the lack of stars with [Fe/H] $\simeq$ −0.5 and $R_m \simeq$ 7 to 9 kpc. The data could be as well represented by two distinct populations of constant [α'/Fe] but with a smaller difference of [α/Fe] than the two possible populations at R_m < 7 kpc. In addition, the lack of stars with R_m > 7 kpc and [Fe/H] $\lesssim$ −0.7 hampers our delineation of the [α'/Fe] vs [Fe/H] trend. We note in passing that the lack of stars around [Fe/H] = −0.5 may not be accidental. A gap in the distribution of [Fe/H] was in fact reported by Suchkov (1981, and references therein). This phenomenon is worth further investigation with larger well defined statistical samples.

One could entertain the view that the R_m < 7 kpc sample may not be a single representative population for which the chemical composition evolved smoothly with metallicity. Figures 19 to 21 may suggest rather either that the stars of R_m < 7 kpc are drawn from two distinct populations (a merger of two stellar systems: an old system (τ > 10 Gyr) of high [α'/Fe] and a younger system of solar abundances?); or the compositions changed abruptly at [Fe/H] $\simeq$ −0.4 from a condition of high [α'/Fe] to low [α'/Fe] (a burst of SNe led to rapid Fe-enrichment? The relatively long-lived precursors of Type Ia SNe are unlikely suppliers of Fe in a burst.). Another possibility might be that the dynamical evolution of the galactic disk introduces a complex bias into our stellar sample, such that for R_m < 7 kpc only stars from discrete age intervals occur.

Oxygen shows a steeper variation with increasing [Fe/H] than the α elements (Fig. 15a). As noted above, [O/Fe] is available only for the ESO stars, and additional stars with [Fe/H] > −0.4 are needed to establish more firmly the run of [O/Fe] vs [Fe/H] for R_m < 7 kpc seen in Fig. 22.

It is generally assumed that oxygen together with Mg, Si and Ca is produced in SNe II. The present results confirm a connection between the production of O and that of Mg, Si, Ca and Ti, but such that the yield of oxygen is relatively larger for the most massive, or initially most metal-poor, stars. We note that there is some variation with initial mass in the ratio of the yield of oxygen relative to that of the α-elements in the recent pre-SN models by Weaver & Woosley (1992). It is not clear, however, whether this variation, possibly coupled to a variation in the IMF, is great enough to explain the steeper slope found for oxygen. Alternatively, our results might suggest an additional source of oxygen in the early (pre)-Galaxy.

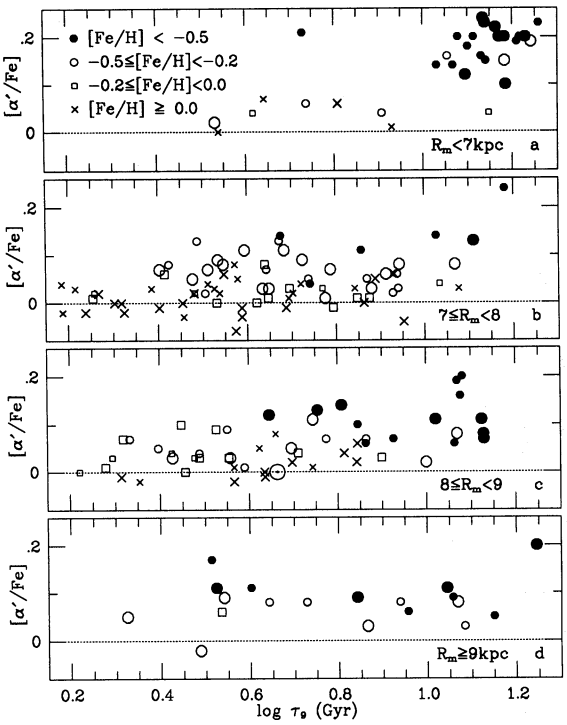

Fig. 21a–d. [α'/Fe] vs logarithmic age for different R_m ranges. The symbols indicate different iron abundance ranges, and small and large symbols show ESO and McDonald stars, respectively

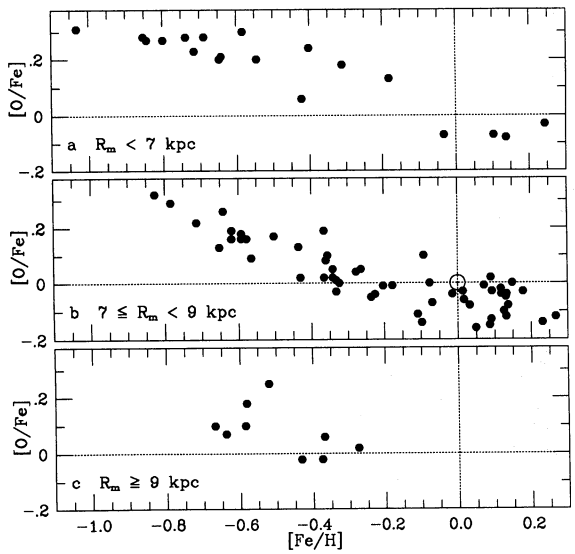

Fig. 22a–c. Oxygen to iron ratios as a function of iron abundance for different ranges of R_m

The discontinuity in compositions of the $R_m < 7$ kpc stars at [Fe/H] $\simeq -0.4$ arises because the abundance ratios of the oxygen and the α-elements to Fe (and Ni) change – *not* because of abrupt changes in the ratios of oxygen to the α-elements or of one α-element to another. The assertion that oxygen and the α-elements have a continuous variation is supported by Fig. 23.

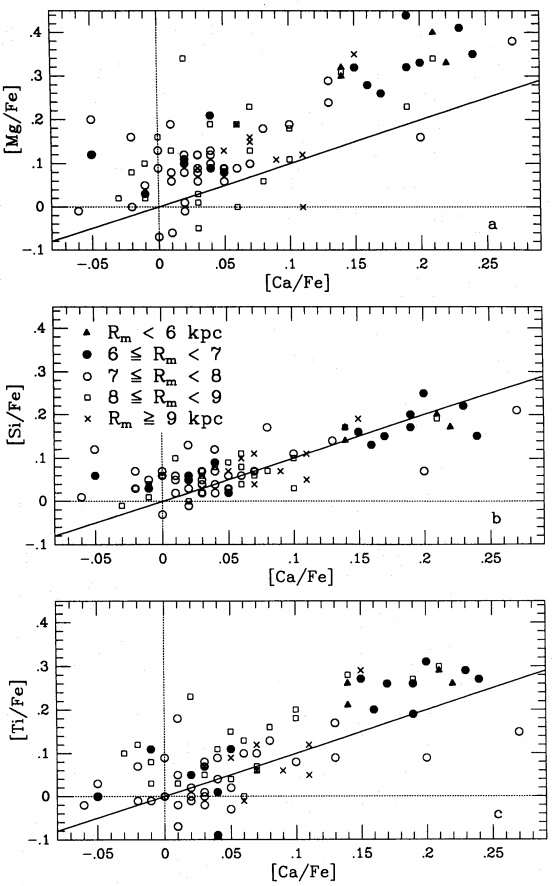

Fig. 23a–c. Magnesium, silicon and titanium abundances compared to the calcium abundances for the ESO stars. The symbols denote different ranges in R_m and the solid lines indicate unity slopes, i.e. [X/Fe] = [Ca/Fe]

This shows that Mg, Si, Ca, and Ti vary in similar but not identical ways from [α/Fe] $\simeq$ 0 at [Fe/H] = 0 to their maximum values in the metal poor stars from (mostly) $R_m < 7$ kpc. On the assumption that [α/Fe] = a + b[Ca/Fe], we find a = 0.05, 0.04 and 0.00 and b = 1.5, 0.7 and 1.4 for Mg, Si and Ti respectively. In other words Mg and Ti show greater excesses relative to iron than Si and Ca. We note in passing that our observed difference between Mg and Si is significantly greater than that calculated for galactic models by Matteucci (1992).

It is of interest to compare the results for the most metal-poor stars in our sample with published values for halo stars. At [Fe/H] = −0.8 and $R_m < 7$ kpc we find [α/Fe] = 0.40(Mg), 0.20(Si), 0.25(Ca) and 0.35(Ti) for our sample. Numerous investigations of α-elements in halo stars have reported abundances with respect to iron. In general, these analyses show that Mg, Si, Ca and Ti have identical overabundances to within the errors of measurement, for example, Gratton & Sneden (1991) report [Si/Fe] = 0.30 ± 0.08, [Ca/Fe] = 0.29 ± 0.06 and [Ti/Fe] = 0.28 ± 0.10. These values are consistent with the small α to α abundance differences from our study. Unfortunately, Gratton & Sneden do not report Mg abundances. There are indications that our disk stars have higher Mg/Si and Mg/Ca

ratios than the halo stars: see, for example, François (1986) who gives [Mg/Si] = 0.0 ± 0.11 from 7 stars with [Fe/H] < −1, and Magain (1989) who found [Mg/Ca] = 0.01 ± 0.08 with an uncertainty of about ±0.02. It is difficult at present to be certain that these apparent differences between our old disk stars and halo stars are reflecting real abundance differences. We note that differences between the results obtained by different investigators and even by the same investigators in different papers can exceed the halo-disk differences: for example, Gratton & Sneden (1991) gave [Ca/Fe] = 0.29 ± 0.06 but Magain (1989) obtains 0.47 ± 0.02 (mean error). It is also possible that the [α/Fe] values in the halo are dependent on [Fe/H] in the probable sense that the values increase with decreasing metallicity. Then, mean values are dependent on the spread in [Fe/H] of the samples and the halo-disk difference should be assessed at a common [Fe/H]. Note that the resulting slopes in Figs. 15a-e and 23 for Si and Ca and the other elements, as compared to iron, seem to rule out the proposals that Si (cf. Matteucci & Greggio 1986) or Ca (cf. Trimble 1991, Table 6 and references cited therein) has been produced extensively in Type Ia Supernovae. Concerning the fractions of different α elements produced in different types of supernovae, see Sect. 6.2.6, below.

6.2.5. Nickel

Nickel, in sharp but expected contrast to the α-elements, varies in lockstep with Fe – see Fig. 15h). Nickel is well represented in our spectra by Ni I lines. Our assessment of the galactic scatter is based on the ESO results that give a slightly smaller star-to-star scatter than the McDonald results. If the sample is divided into eight subgroups by R_m (< 7, 7-8, 8-9, > 9 kpc) and by [Fe/H] (< −0.4 and 0 to −0.4), [Ni/Fe] is equal to zero to within a standard deviation of typically 0.02 to 0.03 for all subgroups. In particular, the metal-poor stars at R_m < 7 kpc that have the striking [α/Fe] values are not distinguishable by their [Ni/Fe] values: the 12 stars at R_m < 7 kpc give a mean [Ni/Fe] = 0.01±0.03 and the metal-poor stars at R_m > 7 kpc have [Ni/Fe] = 0.00±0.02. The only possibly significant deviation from [Ni/Fe] = 0.0 is found for the metal-rich stars for which [Ni/Fe] seems to increase with increasing [Fe/H]; for example, 5 stars with [Fe/H] > 0.15 give a mean [Ni/Fe] = 0.08 ± 0.03. Since these are on average the youngest stars in our sample, this possible trend of [Ni/Fe] with [Fe/H] is also interpretable as an age dependence. Systematic errors affecting the most metal-rich stars may also contribute to this small increase of [Ni/Fe]. With the exception of the very metal-rich stars, the standard deviation of [Ni/Fe] for the subgroups (σ = 0.03) shows that the galactic scatter is very small, certainly σ_g < 0.03.

6.2.6. Sodium and aluminium

The odd-Z elements Na and Al, each represented by a lone stable isotope, are generally discussed apart from the even-Z light or α-elements (Mg, Si, Ca, Ti). In some discussions, Na and Al are considered with respect to Mg, i.e., [Na/Mg] vs [Mg/H] is preferred to [Na/Fe] vs [Fe/H] as a diagnostic. There would appear to be sound theoretical arguments for this preference because Na, Mg, and Al have all been identified as products of Ne and C-burning in massive stars. Especially for those massive stars in the disk that synthesized the bulk of the Mg observed in our sample of disk stars the yield of Mg, a product of α-captures, is not expected to be very sensitive to a massive star's metallicity. Synthesis of Na and Al that accompanies Mg is controlled by the neutron flux during Ne and C burning. The neutron flux is dependent on the initial metallicity and primarily on the initial O abundance; the oxygen (^{16}O) is converted to ^{22}Ne (via ^{14}N) in Helium burning and the "excess" neutrons in ^{22}Ne (Z = 10, N = 12) are, when liberated, essential to the synthesis of Na and Al. In this picture, one expects production of Na (and Al) to be higher in the more metal-rich stars, say [Na/Mg] = a·[Mg/H] where $a > 0$. Synthesis of other α-elements also occurs through α-captures but principally during the burning stages following Ne and C burning, with yields that are relatively insensitive to the initial metallicity of the massive stars. These qualitative arguments are backed by calculations of massive stars (Woosley & Weaver 1982a) that suggest the chemical evolution of Na and Al in the disk is likely to be most clearly revealed by the variation of Na and Al with Mg. Calculations of nucleosynthesis by SNe Ia show that they should make only very small amounts of Na and Al (Nomoto et al. 1984).

There is, of course, another reason why Fe is a less appropriate reference element than Mg. Iron is synthesised through explosive Si-burning in Type Ia and II supernovae. In the disk, Type Ia SNe are thought to be the leading contributor of iron. Type II SNe contribute little iron but are probably the major source of the α-elements and Na and Al. Thus, reference of the odd-Z elements Na and Al to an α-element couples elements synthesised in a single type of SNe whereas comparison of the odd-Z elements and Fe involves elements synthesised in different types of SNe. Note that some synthesis of Na (and, perhaps, Al too) can occur in hydrogen-burning shells during ON-cycling (Denisenkov 1989). Massive yellow supergiants are Na-rich (Boyarchuk & Lyubimkov 1985) and loss of their envelopes

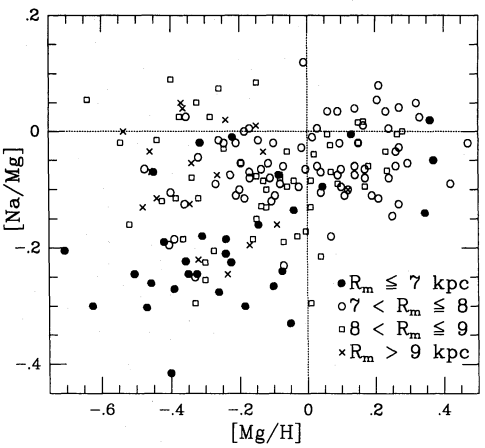

Fig. 24. Sodium and magnesium abundances compared at different R_m ranges

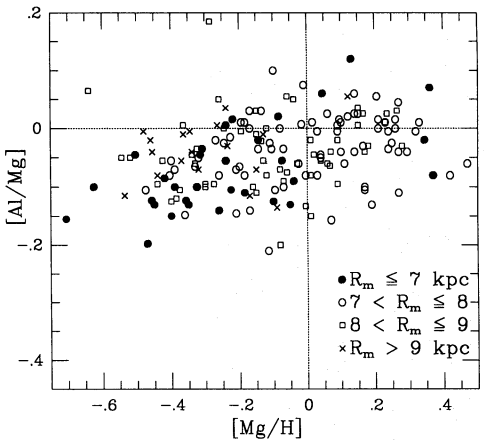

Fig. 25. Aluminium and magnesium abundances compared at different R_m ranges

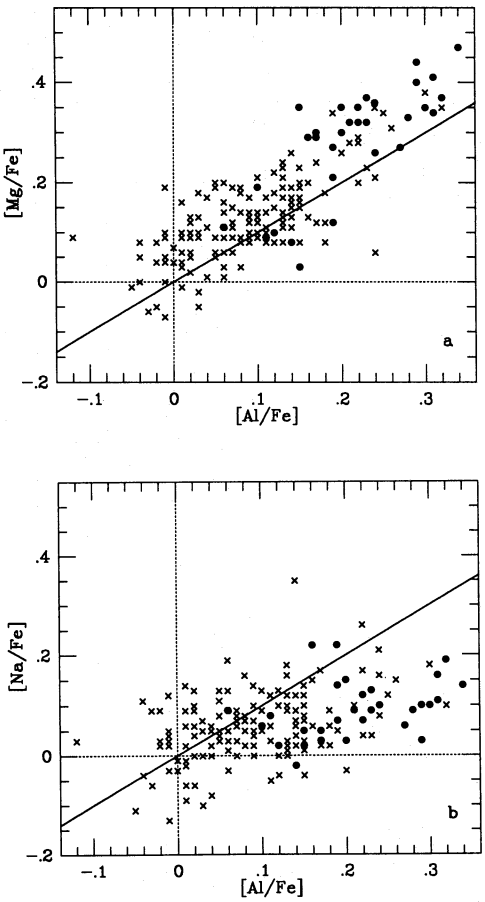

Fig. 26a and b. Magnesium and sodium abundances vs aluminium. Stars with $R_m < 7$ kpc are shown as filled circles. Loci for [X/Fe] = [Al/Fe] are indicated by the solid lines

will lead to some Na enrichment of the interstellar medium. Later, additional Na will be contributed as these stars explode as Type II SNe. A fraction of the low mass giants of globular clusters are enriched in Na (and Al) and deficient in O (Drake et al. 1992; Sneden et al. 1991, 1992; Kraft et al 1992) as a result, perhaps, of ON-cycling in a H-burning shell (Denisenkov & Denisenkova 1990). If these Na-rich O-poor stars have counterparts among stars of the old disk, mass shed by these stars would lead to Na enrichment of the disk on a long time scale. Such a time scale is suggested by the analysis discussed at the end of this section.

The Na/Fe ratio varies very little with metallicity (cf. Fig. 15f). In fact, for [Na/Fe] it is questionable whether there is any increase at all with decreasing [Fe/H]. Certainly, [Na/Fe] does not follow [Mg/Fe]'s with decreasing [Fe/H]. Aluminium, on the other hand, in its run of [Al/Fe] with [Fe/H] mimics more closely the run of [Mg/Fe] with [Fe/H].

An underabundance of Na and Al relative to Mg and Si (the odd-even effect) was predicted by Arnett (1971) and found for Pop. II stars by Peterson (1981, cf. also François 1986). The observed effect among our stars is significantly greater for Na than for Al, from which we conclude that the C burning processes, which produce Na, are relatively less efficient than the Ne burning that produces Al, in the most massive stars. One should look for verification of this effect in SN II models.

Our results show that Na is poorly correlated with Mg. This is well shown by Fig. 24 where [Na/Mg] for $R_m > 7$ kpc is almost independent of [Mg/H]. The more striking result is that [Na/Mg] is much smaller for [Mg/H] < -0.2 and $R_m < 7$ kpc than at greater R_m. This result reflects the fact that [Na/Fe] is approximately independent of metallicity for the $R_m < 7$ kpc stars while [Mg/Fe] is much larger in the old and metal-poor stars. The pattern of Na abundances persists when Si, Ca, or Ti is substituted for Mg. This pattern is barely perceptible for Al vs Mg or the other α-elements – see Fig. 25 which shows [Al/Mg] to decline slightly with decreasing [Mg/H] with only the merest hint of a dependence on R_m. The contrasting behaviour of Na and Al is clearly seen in Fig. 26 where Al and Mg are found to be well correlated for the metal-poor stars. On the other hand, Na and Al are almost uncorrelated except that [Na/Fe] is marginally larger in the Al-rich stars, which are predominantly metal-poor stars from $R_m < 7$ kpc.

We have attempted to determine empirically what the yields are from supernovae of different types for the different elements observed. Essentially this can be done from the slopes in Fig. 15, by using a suitable model of the chemical evolution of the disk. Such a model, with infall of gas and allowance for a time delay between the prompt production of α elements by Type II SNe and the slower production of iron etc. from Type I SNe, has been described by Clayton (1988) and modified by Pagel (1989). This one-zone model has the virtues of being simple and analytical but still reproduces essential properties of the Disk population such as the metallicity distribution for G dwarfs.

Using this model, relations between the abundance ratio, [X/II], of an element X relative to an element II, assumed to be only produced in SNe II, and [II/H] can be calculated, cf. Fig. 27. These relations are dependent on the true yields of X from SN Ia and II, respectively. We denote the true yield of SNe II, relative to the sum of Type I and II yields, by R_{II}. By

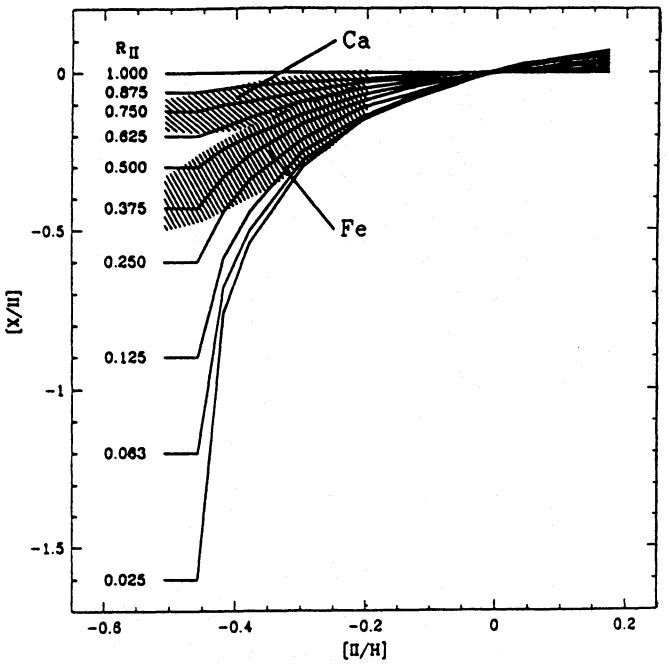

Fig. 27. The abundance [X/II] of an element X, relative to that of another element (II), as a function of [II/H]. Element II is supposed to be formed entirely in SNe Type II. The curves correspond to calculations, made using the model for the galactic disk by Pagel (1989), for different values of the fraction of the true yield of X from SNe Type II, relative to the sum of the yields from SNe Type Ia and II. Observed abundances in disk stars for X=Ca and Fe, respectively, and II=O and Mg are shown by the hatched areas

plotting the observed abundances in Fig. 27 we can thus estimate R_{II} for different elements.

In doing this in practice we have adopted the parameters of the model of Pagel (1989). In particular this means a normalised time delay parameter $\omega\Delta$ of 0.5, which with a value of ω of 0.3 Gyr^{-1} (Clayton 1988) corresponds to a delay between Type II and Type Ia SNe of 1.7 Gyr. The particular choice of model parameters is, however, not very important for the results below. As type II elements we have chosen oxygen *and* magnesium (i.e. performed the analysis with both alternatives and then averaged the results). Both elements are, according to the SN models by Thielemann et al. (1991) almost entirely formed in SNe Type II. This choice was due to the fact that oxygen observations only exist for less than half the number of stars and moreover the oxygen abundances were scaled to results for the oxygen line judged to be most reliable, namely the forbidden 6300 Å line, which was observed for even fewer stars. The Mg abundances also suffer from uncertainties, in particular due to the small number of lines observed.

The resulting empirical R_{II} values are given in Table 13 and compared with theoretical values, estimated from supernovae models by Thielemann et al. (1991).

The agreement for most elements between yields estimated from the observed stellar abundances and those derived from SN models is quite satisfactory, in view of the fact that the theoretical SN yields have been derived from just two models at particular masses. Thus, no integrations across the mass spectrum have been performed, neither has the gradual increase of the initial abundance of elements been considered. The two elements that depart seriously, Na and Al, are both quite uncertain in the nucleosynthesis calculations for SNe. They are assumed to be formed in explosive carbon and neon burning, respectively, and their yields are dependent on the neutron excess and thus on the Ne abundance which, through helium burning, is dependent on the initial oxygen abundance of the pre-SN star. The calculations of the synthesis of Na and Al by Woosley & Weaver (1982b) in SN II models, giving results for two different overall metal abundances that differ by a factor of 100, suggest that the discrepancy for Al may well be due to this dependence on initial abundances while their calculated difference in Na production between initially metal rich and metal poor Type II SNe seems far too small to account for the low R_{II} value observed. Other known sources of Na, such as the NeNa cycle probably operating in the main sequence for massive stars and leading to detectable enrichment of Na in supergiant atmospheres (Boyarchuk et al. 1988), should not contribute enough Na to significantly affect galactic abundances (cf. Denisenkov & Ivanov 1987). The Na production, possibly occurring in the dying deflagration wave of carbon burning in SN Ia, is "practically unknown" (Nomoto 1992). Nomoto et al. (1992) derive a solar Na/O abundance ratio from SN II models, when integrating over the proper mass distribution. This indicates that Type II SNe are the main contributors of Na. If so, the dependence of the Na yield on the initial overall metal abundance has to be very significant. Alternatively, Fig. 27 and Table 13 suggest a considerable contribution from "delayed sources", such as Type Ia SNe, in fact, there is independent evidence for that. We thus find a tendency for the Mg abundance to be greater relative to Na in the inner part of the Galaxy, as compared with the outer part, at a given [Mg/H]. This is shown in Fig. 24. The corresponding tendency for the α elements relative to Fe was interpreted above as a result of differences in star formation rate and evolution time for SNe of different types.

Table 13. The fraction of the true yields of SN II relative to SN I + SN II, estimated from the abundance results and compared to estimates from supernova models

Element	R_{II}(abundances)	R_{II}(SN models)
O	1.00	0.98
Na	0.49	1.00[1]
Mg	0.87	0.96
Al	0.62	0.97
Si	0.65	0.69
Ca	0.74	0.56
Ti	0.76	0.71
Fe	0.29	0.25
Ni	0.33	0.19

[1] Not given for SN Ia by Thielemann et al. (1991)

Obviously, the synthesis of Na in the Galaxy needs further studies.

6.2.7. The heavy elements

The four elements heavier than iron in our sample are traditionally identified with synthesis by the neutron capture s-process. Resolution of solar system abundances into s- and r-process components shows that the major fraction of each element is synthesised by the s-process: 0.73(Y), 0.79(Zr), 0.88(Ba), and 0.68(Nd) according to Cameron (1982). The small r-process contributions probably originate in Type II SNe of moderate mass (Mathews & Cowan 1990). The s-process contribution is primarily from what is termed the "main" s-process component; the "weak" component makes the dominant contribution to elements between the iron group and krypton. The "main" component is ascribed to asymptotic giant branch stars of intermediate and low mass. (The "weak" component comes from He burning in massive stars that subsequently become Type II SNe.) Relative abundances of "main" s-process nuclides are set primarily by the severity of the exposure to neutrons. Severe exposure enhances the heavier elements (here, Ba and Nd) relative to the lighter elements (here, Y and Zr). Clearly, comparison, as in Fig. 15, of the heavy elements to iron involves a mix of sites of nucleosynthesis: the heavy element comes primarily from AGB stars with a minor contribution via the r-process from Type II SNe, the iron in these disk stars is principally a product of Type Ia SNe with a non-negligible contribution from Type II SNe.

In halo stars ([Fe/H] < -1.5) the relative abundances of the heavy elements show that the r-process and not the s-process makes the dominant contribution. This important result was established by Sneden & Parthasarathy (1983) and Gilroy et al. (1988) following a prediction by Truran (1981). It appears that the relative abundances of heavy elements in halo stars are described by a solar r-process distribution. To the extent that the compositions of our old metal-poor disk stars are expected to merge smoothly with those of halo stars, we expect a gradual decrease of the contribution of the s-process and hence minor changes in the relative abundances of the four elements with decreasing metallicity. At [Fe/H] $= -1$, however, the s-process continues to dominate the heavy element abundances.

Our Y, Zr, Ba and Nd abundances greatly strengthen previously reported conclusions about the evolution of the s-process abundances in the disk. First as Fig. 15 shows, [Ba/Fe] and the other ratios are close to zero over the entire sample; we comment below on the scatter in [Ba/Fe] at a given [Fe/H]. Second the relative abundances of the heavy elements are solar to within the errors of measurement. These two observational results set constraints on the sources of the s-process elements.

Examination of the abundances shows, as may be inferred from Fig. 14, that the principal factor behind the marked scatter in Fig. 15 is a clear variation of [Ba/Fe] with age (τ). If the metal-rich stars ([Fe/H] > 0.06) and those with $R_m < 7$ kpc are omitted, [Ba/Fe] and age are seen to be approximately linearly

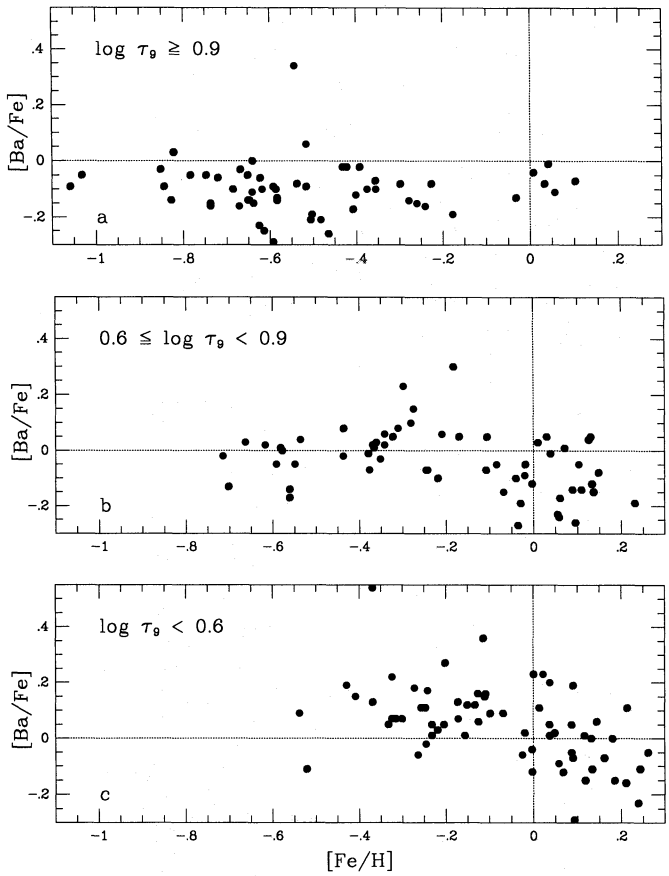

Fig. 28. Barium and iron abundances compared for different stellar ages

related - see Fig. 28. The metal-rich stars are principally young stars ($\log \tau_9 < 0.5$) but, contrary to the linear trend, include several stars with very low [Ba/Fe] ratios, e.g., HR 4533 with [Ba/Fe] $= -0.22$ and $\log \tau_9 = 0.30$, and HR 448, a NaMgAl star, with [Ba/Fe] $= -0.29$ and $\log \tau_9 = 0.53$. The stars with $R_m <$ 7 kpc appear to define a shallower relation between [Ba/Fe] and τ with the oldest stars fitting the relation well but the youngest ones ($\log \tau_9 = 0.5$ to 0.8) falling 0.1 to 0.2 dex below the linear trend. With these two exceptions, [Ba/Fe] is a fair chronometer. At present the modest scatter around the linear trend receives a significant contribution from the errors of measurement. It would be of interest to determine heavy element abundances with greater precision in order to test [Ba/Fe] or equivalent ratios as a chronometer. A gradient in Ba/Fe at a given [Fe/H] relative to R_m may also be present.

Continuing evolution of the [s/Fe] ratio with increasing [Fe/H] means that the stars primarily responsible for s-process synthesis are longer-lived than those responsible for the Fe. If Fe is produced mainly by SNe Type Ia, the s-process elements must have been produced in red giants with lower masses than the primary masses of the binaries yielding SNe Ia. Adopting a mass range for the latter of 5–7 $M_\odot$ (Matteucci & Tornambè 1987) we find that a major fraction of s-process elements were produced in low mass red giants (say $M \lesssim 3M_\odot$). This identification is consistent with the spectroscopic signatures that sug-

gest that the neutron source $^{13}C(\alpha,n)$ and not $^{22}Ne(\alpha,n)$ drove the s-process (Lambert 1991).

In the language of chemical evolution, the result [Ba/Fe] = 0 implies that Ba (and other s-process elements) is a primary element with a yield proportional to that of Fe. However, the simplest concept of the s-process envisages the s-process yields to be proportional to the supply of seed (Fe) nuclei and, hence, [Ba/Fe] $\approx$ [Fe/H] is anticipated and Ba is designated a secondary element. Obviously, the observations clearly show Ba to be a primary and not a secondary element. This conflict between observation and expectation has long been considered a key puzzle - see Tinsley (1980). Clayton (1988) uncovered a key component in the solution to the puzzle.

As we have shown, the major contributors to the s-process enrichment of the disk are low-mass AGB stars ($M < 2M_\odot$). In such stars, the neutron source in their He-burning shells must be the reaction $^{13}C(\alpha,n)$. Clayton notes that if, as is quite likely, the ^{13}C supply is independent of a star's metallicity, the neutron density varies inversely as the metallicity because it is the latter that controls the neutron poisons. Then the yield of Ba, which depends on a convolution of the neutron density and the seed abundance (i.e. metallicity), is likely to vary only weakly with the metallicity. It remains, of course, to incorporate this intriguing suggestion into models of the s-process and dredge-up of AGB stars of different metallicities. At present, the stumbling block is the lack of *ab initio* predictions of the ^{13}C supply in a He-burning shell and the dredge-up from the shell to the envelope. Even without *ab initio* predictions, it would be of interest to see if parametrized models can reproduce the run of [Ba/Fe] with [Fe/H] and the remarkable invariance of the s-process relative abundances with [Fe/H].

For the sampled stars, the relative abundances of Y, Zr, Ba, and Nd have solar values to within the errors of measurement. Figure 29 shows the abundances of Y, Zr and Nd vs Ba, which is the best observed of the s-elements. The light s-element yttrium appears to follow the heavy s-element barium very closely, (Y = $-0.01 + 0.94$Ba, $\sigma = 0.10$) while (light) Zr and, possibly, (heavy) Nd may deviate slightly from proportionality: (Zr = $0.03 + 0.80$Ba, $\sigma = 0.11$ and Nd = $-0.02 + 0.72$Ba, $\sigma = 0.14$). We do not believe that these deviations are significant, however, since both Zr and Nd are here represented by very weak lines, and the deviations may therefore be due to systematic overestimates of their equivalent widths in the metal poor stars, i.e., a very weak line is more likely to be measured if it is made too strong by noise, and likely not to be measured if it is weakened by noise. As a measure of the neutron exposure, we constructed the quantity [hs/ls] = $\langle$[Ba/Fe] + [Nd/Fe]$\rangle$/$\langle$[Y/Fe] + [Zr/Fe]$\rangle$ where hs and ls denote "heavy" and "light" s-process elements respectively. The quantity [hs/ls] is strikingly close to the solar value (i.e., zero) for all the ESO stars in which the four heavy elements were measured:

$$
\begin{aligned}
[\text{hs/ls}] &= +0.01 \pm 0.07 \quad ([\text{Fe/H}] < -0.4,\ 11 \text{ stars}) \\
&= -0.01 \pm 0.05 \quad (-0.4 \le [\text{Fe/H}] < -0.2,\ 6 \text{ stars}) \\
&= -0.01 \pm 0.07 \quad (-0.2 \le [\text{Fe/H}] < -0.0,\ 6 \text{ stars}) \\
&= -0.02 \pm 0.09 \quad ([\text{Fe/H}] \ge 0.0,\ 18 \text{ stars.})
\end{aligned}
$$

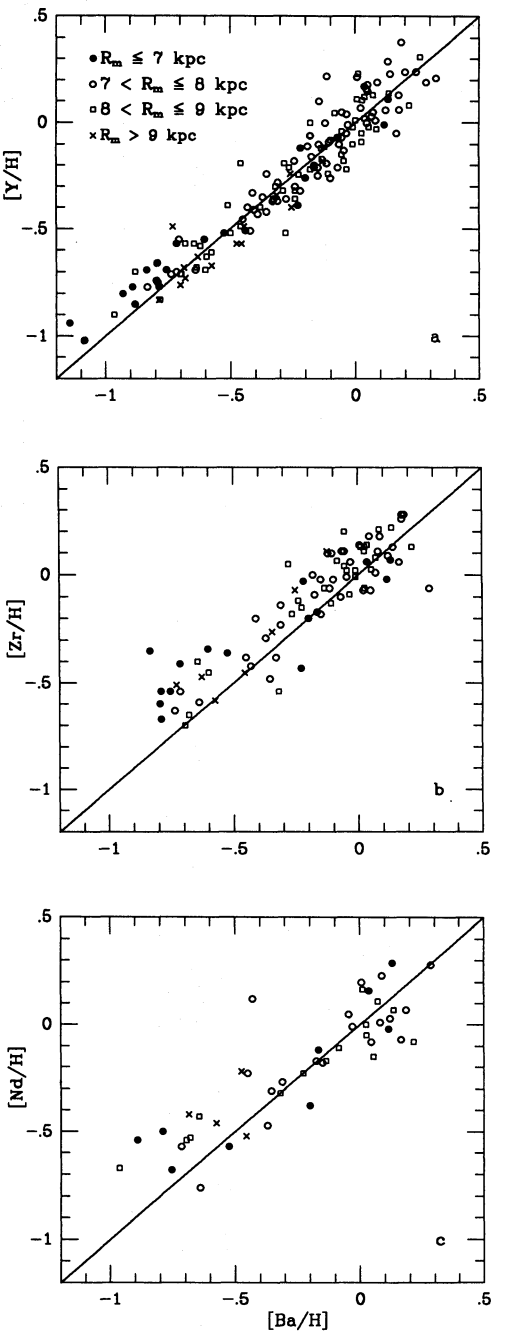

Fig. 29. Comparisons of s-element abundances for different ranges of R_m. The lines shows loci for direct proportionality between the abundances

The standard deviations are consistent with those expected from the errors of measurement. A similar conclusion holds for [Ba/Y] which is available for a larger sample of stars. Even the $R_m < 7$ kpc metal-poor stars do not have distinctive ratios of the heavy elements. The constancy of [hs/ls] shows that the neutron exposure varies very little as [Fe/H] increases in the disk: At the s-process site a change in the parameter $\tau_0(\text{mb}^{-1})$ (see Käppeler et al. 1989) from 0.31 to 0.5 increases [hs/ls] by 0.3.

A detailed abundance analysis for many heavy elements should be undertaken to set limits on the neutron exposure differences.

6.2.8. Barium dwarfs

By inspection of Fig. 28, it is possible to pick out stars that are unusually rich in Ba (and Y, Zr, and Nd) for their age. We identify these stars as low luminosity or dwarf counterparts of the classical Barium giants. Earlier, we discussed in detail one of these Barium dwarfs (HR 107, see Tomkin et al. 1989). Six stars may now be classified as Barium dwarfs: HR 107, 2906, 4285, 4395, 5338 and HD 6434. Relative to the expected [Ba/Fe] for the stars' ages, barium is overabundant such that the [Ba/Fe] excess is 0.2 to 0.5 dex. The Barium overabundance is confirmed, when measurements are available, by Y, Zr and Nd. Four additional stars may be less extreme Barium dwarfs: HR 646, 1780, 3775, and 8885.

Barium stars, both giants and dwarfs, are spectroscopic binaries (McClure 1989; North & Duquennoy 1992). The provenance of our Ba dwarfs will be assured if it is shown that they are spectroscopic binaries.

HR 2047, χ^1 Ori, appears enriched in s elements when compared to stars of similar iron abundance ([Fe/H] = -0.03, [Y/H] = +0.31, [Ba/H] = 0.26). It lacks an isochronic age determination due to its proximity to the ZAMS, but other evidence suggests that it is a young star: Soderblom & Mayor (1993) label the star as a "probable spectroscopic member" of the Ursa Major kinematics group, with an age of 0.3–0.4 Gyr. Stimets & Giles (1980) determined a rotational period of 5.10 days. Irwin et al. (1992) conclude that it has a 0.15 $M_\odot$ companion, probably an M dwarf. Assuming that HR 2047 is a young star and extrapolating the Ba vs age relation (Fig. 14c) to a young age indicates that the star has normal s-element abundances.

The six Barium dwarfs represent 3% of our entire sample. It appears that the six are metal-poor ($-0.5 <$ [Fe/H] < -0.1), as are the classical Barium giants. Of the stars with [Fe/H] < -0.1, the six dwarfs are 5% of our sample. This frequency of occurrence is similar to but possibly slightly higher than estimated for Barium giants. Although there may be corrections for selection effects, we note that a 5% mix of Barium dwarfs is consistent with Frantsman's (1992) prediction for the mass transfer scenario. Our Barium dwarfs do not include stars as enriched in heavy elements as some of the classical Barium giants for which [Ba/Fe] = +1.0 has been reported. Dwarfs and subgiants with [Ba/Fe] $\simeq 1$ are known, see, for example Luck & Bond (1991) who list several F-type stars. Perhaps, the lack of these stars in our sample is due to their lower frequency of occurrence.

It should be noted that the surface layers of the hotter F stars (such as HR 107 and HR 4395) may be polluted by rather small amounts of mass transfer since their convection zones are relatively shallow. As the star later evolves up the subgiant branch the convection zone deepens and the pollution is considerably diluted. Therefore it is uncertain whether the Barium dwarfs will show any detectable Ba star characteristics when they eventually reach the giant branch.

The Ba dwarfs in Fig. 28 are located at the upper edge of the [Ba/H] vs age relation (Fig. 14c). This location is consistent with production of Ba stars by means of mass transfer: an s-process enriched AGB star transfers mass to a less evolved companion converting it to a Ba star. Transfer enhances the Ba abundance of the mass-accreting star, and the addition of large amounts of mass rejuvenates the star and creates a star that is apparently younger than other stars of its metallicity. The net effect is to place Ba dwarfs above the mean [Ba/H] vs age relation. It would then be by chance that the Ba dwarfs are near the upper envelope and not distinctly above it. Mass transfer from stars less evolved than AGB stars (i.e. not s-process enriched) may also contribute to the spread of the age-metallicity relations by placing stars below the intrinsic relations. It seems unlikely, however, that mass transfer effects are primarily responsible for the remarkable spread in the age-metallicity relations.

Finally we point out that the mass transfer hypothesis suggests that radial velocity variations should be searched for among the barium dwarfs.

6.3. Age-Metallicity-Radius relations and scatter in [Fe/H] *and* [α/Fe]

The iron abundance is plotted relative to age for our sample stars in Fig. 14a. For stars of intermediate ages a great scatter is found; only the youngest and oldest stars show the expected and rather well defined high and low iron abundances, respectively. (Note, however, that the sample is biassed *against* high-metal-abundance old stars through the lower effective-temperature limit, i.e., β limit.) The great spread at intermediate ages is no doubt physical, since the mean errors in [Fe/H] and logarithmic age are about 0.1 dex. We note that such a spread has also been found in between young open clusters (Nissen 1988; Boesgaard 1989; Garcia Lopez et al. 1989) as well as old open clusters (Friel & Janes 1991).

It is of great interest to explore the scatter in diagrams of abundances vs age (Fig. 14) to see whether there is further structure depending on the properties of the stellar orbits. Figure 14 with its different symbols according to galactocentric distance directly suggests such a dependence. In order to study this further we have divided the $R_m - \log \tau_9$ plane by lines separated by 1 kpc in R_m and 0.2 dex in $\log \tau_9$. Next, the mean abundances were calculated for the stars in each rectangle, defined by the dividing lines. These mean values of [Fe/H] are given in Table 14.

In this table both an age dependence and a radial dependence of [Fe/H] may be traced. For the oldest stars there is, however, no indication of any radial gradient. For the 138 stars with $\log \tau_9 <$ 1.0, we find tentatively [Fe/H] $\approx 0.85 - 0.39 \log \tau_9 - 0.10 R_m$, $\sigma = \pm 0.21$, but this relation has limited value since the stellar sample is rather small and biassed (again we recall that no stars with $\log \tau_9 < 0.15$ are included, nor any very old metal-rich stars). We note that the age variation found is consistent with the age-metallicity relation derived by Twarog (1980) and Meusinger et al. (1991) for a great number of F dwarfs as well

Table 14. Mean [Fe/H] for different R_m and logarithmic Age groups. Two lines are given for each age group; the first gives the abundance means for our sample as it is and the second (in italics) gives the volume corrected results, as obtained from the procedure described below. Numbers within parenthesis refer to groups containing less than 3 stars. All but 7 of the 189 programme stars were included. These 7 lack age determinations

	R_m (kpc)							
log τ_9	4-5	5-6	6-7	7-8	8-9	9-10	10-11	4-11
1.4-1.2			−.84			(−.58)		−0.80
			−.73			*(−.58)*		*−0.71*
1.2-1.0	(−.68)	−.65	−.54	−.41	−.57	−.53	(−.62)	−0.55
	(−.69)	*−.68*	*−.41*	*−.29*	*−.56*	*−.50*	*(−.62)*	*−0.47*
1.0-0.8			−.07	−.17	−.25	−.38	(−.67)	−0.22
			−.11	*−.14*	*−.16*	*−.35*	*(−.67)*	*−0.16*
0.8-0.6			−.26	−.20	−.14	(−.37)	(−.43)	−0.20
			−.22	*−.17*	*−.09*	*(−.37)*	*(−.38)*	*−0.17*
0.6-0.4			(0.00)	−.07	−.16	−.28	(−.52)	−0.12
			(0.00)	*−.08*	*−.14*	*−.23*	*(−.52)*	*−0.11*
0.4-0.2				+.07	−.09	(−.41)		−0.03
				+.03	*−.09*	*(−.41)*		*−0.05*
0.2-0.0				(+.23)				(0.23)
				(+.23)				*(0.23)*

Table 15. Scatter (s.d.) in [Fe/H] for different R_m and log Age groups. The first line for each age entry gives the scatter for the sample as it is and the second line (in italics) gives the volume corrected scatter. Numbers are given for groups containing more than 3 stars

	R_m (kpc)							
log τ_9	4-5	5-6	6-7	7-8	8-9	9-10	10-11	4-11
1.4-1.2			.23					0.23
			.23					*0.22*
1.2-1.0		.10	.20	.29	.15	.08		0.19
		.12	*.26*	*.27*	*.18*	*.07*		*0.24*
1.0-0.8			.25	.21	.28	.14		0.25
			.26	*.19*	*.24*	*.13*		*0.22*
0.8-0.6			.30	.23	.27			0.26
			.25	*.20*	*.22*			*0.22*
0.6-0.4				.18	.12	.19		0.19
				.18	*.10*	*.18*		*0.17*
0.4-0.2				.12	.15			0.18
				.12	*.13*			*0.16*

as with recent (but different) theoretical models by Sommer-Larsen & Yoshii (1990) and Tosi (1988). The radial abundance gradient agrees well with those found by Grenon (1987, 1989), who, however in his 1989 study does not find any significant age variation. The gentle increase of the mean value of [Fe/H] with time in the disk found by other authors is ascribed by Grenon to mixing of sub-populations born at different R_m and to selection bias against metal-rich stars. This latter criticism may well apply to our study. The finding by Grenon (1987) that the radial gradient in the thin disk is independent of age is also consistent with our results but disagrees with that of Lewis & Freeman (1988).

A most interesting property is that a considerable scatter remains around our tentative relation between [Fe/H], log τ_9 and R_m. In order to investigate this further we have calculated the scatter or standard deviation in [Fe/H], σ([Fe/H]), for each region in the R_m-log τ_9-plane. The results are given in Table 15. It is noteworthy that the scatter in [Fe/H] stays significantly higher than that expected from observations and analysis ($\sigma <$ 0.10 dex). Admittedly, systematic errors in the analysis might introduce errors into the [Fe/H] values by more than 0.10 dex, but such possible errors should be similar for most stars (i.e., a zero-point shift and possibly a scale error) and hardly affect the intrinsic scatter in the R_m-log τ_9-regions significantly.

However, the scatter is partly generated by our selection procedure for the programme stars, requiring a roughly equal number of stars in each δm_1 (i.e., approximately [Fe/H]) interval. In order to compensate for this bias we have calculated volume corrections by using the extensive *uvby-β* catalogue of Erik Heyn Olsen (1988), kindly put at our disposal by him in computer-readable form. The extracted catalogue contains 4725 F and early G-type stars in a number of zones in the sky. The sky coverage is complete down to V = 6.5. For fainter stars (V between 6.5 and 8.3), however, only about half the southern sky (right ascensions between 8 to 22 hours) is complete. We do not expect this partial incompleteness of the catalogue to introduce any appreciable bias in the volume correction procedure presented below since we only use stars close to the Sun:

Following the procedure used for the programme stars, we calculated the δc_1 and δm_1 indices for these stars, applied the selection criteria (1) and (2), and grouped the selected stars into the metallicity groups of Table 1. The sample of all remaining 446 stars with a distance less than 40 pc (a distance chosen to ascertain completeness within the observed regions), was next used for calculating volume corrections for each metallicity group of our sample of programme stars. The metallicities of the 446 stars were derived from an empirical relation between [Fe/H], $b-y$ and δm_1 found from our programme stars, which has a dispersion of only 0.072 dex in [Fe/H]. The "raw" metallicity distribution of the 446 stars is compared to that of the programme stars in Fig. 30a and b. The photometric observational errors of the correction sample (the 446 stars) are judged to be similar to those of the programme stars. We then deconvolved the photometric metallicity distribution in Fig. 30a for a Gaussian error distribution with σ = 0.072 dex in [Fe/H] to obtain the "true" distribution which was then used to correct the programme star distribution. In Fig. 30c the resulting volume corrections are presented.

Next, these volume corrections were applied to the metallicity distributions. In further subdivision of the sample we adopted the same corrections independently of stellar age and stellar orbital parameters. We judge the errors due to this to be of minor importance.

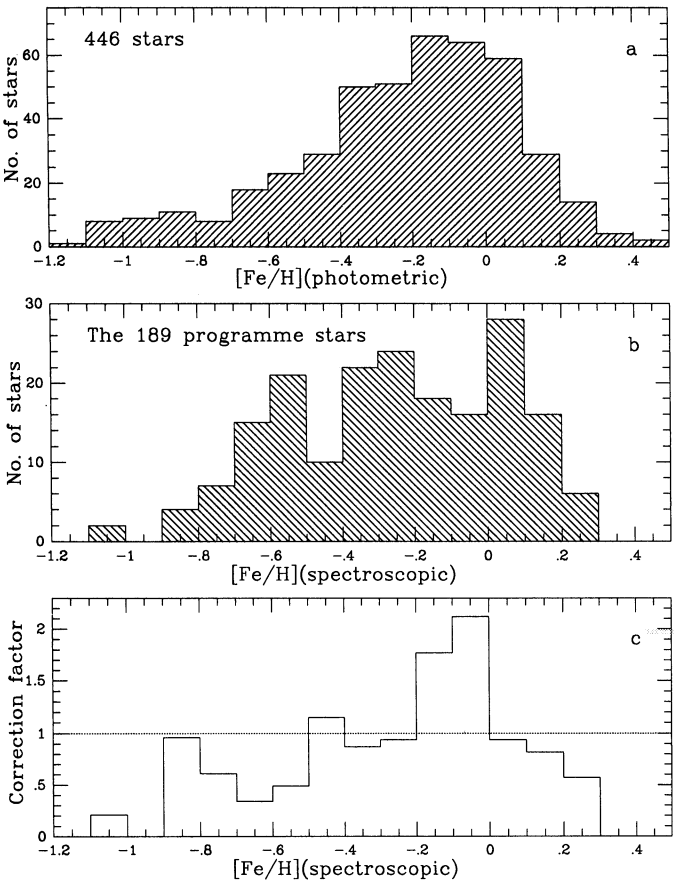

Fig. 30a–c. Demonstration of the volume corrections applied to our metallicity-biassed selection of stars: **a** shows the distribution of [Fe/H] = $f(b-y, \delta m_1)$ values for 446 disk stars within 40 pc of the Sun and selected by the same criteria as the programme stars. **b** shows the distribution of spectroscopic [Fe/H] values of our 189 programme stars. **c** shows the volume corrections (weights) applied our stars; before division with the data in **b** the data in **a** were deconvolved by the 0.072 dex scatter introduced by the derivation of [Fe/H] values from photometric data

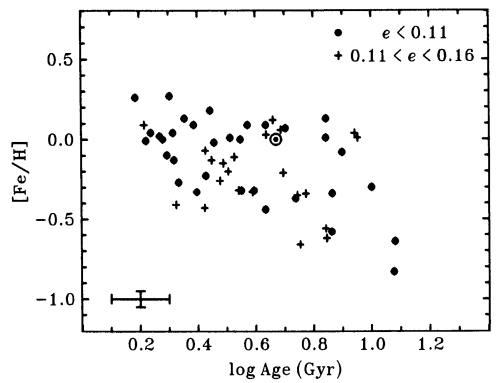

Fig. 31. The age-metallicity relation in for stars in the solar circle

The results from this volume correction of the scatter in [Fe/H] are shown in italics on separate lines in Table 15. It is seen that the effects are small – most of the scatter still remains after the corrections.

We note from Table 15 that there may be some increase of σ([Fe/H]) with stellar age, as one would expect if dynamic diffusion of orbits has mixed stars from different Galactocentric distances into our sample. An estimate based on Wielen's (1977) study of kinematic properties of K and M dwarfs with estimated ages and on our observed metallicity gradient (∂[Fe/H]/$\partial R_m \simeq -0.1$) shows that a scatter of about 0.1, 0.2 and 0.3 dex in [Fe/H] is in fact to be expected for stars in the solar neighbourhood with $\log \tau_9 = 0.0$, 0.7 and 1.0, respectively. Adding an observational error of 0.1 dex in the [Fe/H] determinations to this would lead to σ([Fe/H]) values on the order of those given in Table 15 (cf. the rightmost column, which gives the scatter in [Fe/H] for all R_m in a given age interval). From this one might be tempted to conclude that the observed scatter in [Fe/H] at a given age is merely reflecting the diffusion of stars from other regions in the galactic disk into the solar neighbourhood.

In order to study an age-metallicity relation free from the influence of stars from other galactocentric distances, we have defined subsamples of stars with $7.7 < R_m < 9.3$ kpc, $|Z_{max}| < 0.26$ kpc, and near-circular orbits ($e < 0.11$ or $e < 0.16$). The results are shown in Fig. 31. In the age range 2-10 Gyr, where selection effects near the colour cutoffs of our sample should be unimportant, the scatter of the most restricted sample ($e < 0.11$) is only 10% smaller (0.22 dex) than that of the full sample (0.24 dex). Thus, even for stars restricted to the solar circle does the age-metallicity relation show large and significant scatter.

The scatter remains when the stellar sample is divided into different R_m-log τ_9 groups. Since R_m is rather well conserved during the history of the disk (Grenon 1987, 1989), and the stars were presumably formed in relatively circular initial orbits, one would expect the metallicity scatter in each R_m-log τ_9 region to be significantly smaller if diffusion were the main contributor to the scatter. Thus, the explanation for the scatter as a result of orbital diffusion proposed by François & Matteucci (1992), does not seem viable. We also note that Strömgren (1987) on the basis of $uvby$-β photometry for A5-G0 Pop I dwarfs found significantly smaller velocity dispersions and age variations than Wielen predicted; a fact that also casts doubts upon the diffusion as the origin of the scatter. Additional strong arguments for smaller velocity dispersions at intermediate stellar ages in the disk have been given by Sommer-Larsen & Antonuccio-Delogū (1993). Taking the diffusion effects on R_m schematically into consideration, following Grenon (1987) and Wielen (1977), and adding the expected observational errors, we find that a residual scatter of at least 0.10 dex and probably 0.15 dex remains to be explained by other mechanisms.

A mechanism which could cause the scatter in [Fe/H] is infall of relatively unprocessed gas. If this infall occurs and star formation takes place before efficient mixing evens out the chemical inhomogeneities, a local scatter in [Fe/H] will result. We note that a scatter of about 0.2 dex may be consistent with a total infall to the disk of about 1 solar mass of metal-poor gas per year, as is estimated from the high-velocity clouds (Oort 1967; Hulsbosch 1975; cf. also Mirabel 1982), provided that mixing

with galactic gas occurs in an annulus with a width of about 1 kpc on a time scale of about 1 Gyr or longer. Since the total mass of the gas disk is about $8 \cdot 10^9$ $M_\odot$ (Baker & Burton 1975), this requires a correlation in time and space between the infall and star formation, so that a considerable fraction of the stars is formed out of the infalling material. Roughly the chance has to be about ten times greater for an infalling atom to become stellar than for an atom of the normal interstellar gas in the disk. If mixing occurs on shorter time scales than a few galactic years[1] the infall hypothesis may still be viable, provided that infall of gas triggers star formation as was suggested already by Larson (1972), which has then to take place on a time scale shorter than the characteristic mixing time. The latter can hardly be shorter than the order of 10^8 years.

The distribution of [α/Fe] across the R_m-log τ_9 plane is given in Table 16. (Here and below [α/Fe] = $\frac{1}{4}$([Mg/Fe] + [Si/Fe] + [Ca/Fe] + [Ti/Fe].) We note a possible small age gradient for log $\tau_9 < 1.0$ and a significant gradient ∂[α/Fe]/$\partial R_m < 0$ for the oldest stars - this phenomenon was discussed in Sect. 6.2.4.

Table 16. Mean [α/Fe] for different R_m and log Age groups. The table gives the volume corrected data. The observed values are very similar. Numbers within parentheses refer to less than 3 stars

	R_m (kpc)						
log τ_9	4-5	5-6	6-7	7-8	8-9	9-10	10-11
1.4-1.2			+.26			(+.27)	
1.2-1.0	(+.24)	+.25	+.17	+.10	+.15	+.08	(+.12)
1.0-0.8			+.07	+.06	+.08	+.08	(+.08)
0.8-0.6			+.10	+.06	+.06	(+.05)	(+.09)
0.6-0.4			(+.06)	+.06	+.08	+.08	(+.24)
0.4-0.2				+.03	+.05	(+.04)	
0.2-0.0				(−.02)			

Table 17. Scatter (s.d.) in [α/Fe] for different R_m and log Age groups with more than 2 stars. The table gives the volume corrected data. The observed values are very similar

	R_m (kpc)						
log τ_9	4-5	5-6	6-7	7-8	8-9	9-10	10-11
1.4-1.2			.01				
1.2-1.0		.04	.07	.08	.06	.02	
1.0-0.8			.03	.02	.04	.05	
0.8-0.6			.08	.04	.05		
0.6-0.4				.05	.05	.03	
0.4-0.2				.04	.04		

[1] One galactic year is the time for one revolution of the Galaxy at the R_m in question.

The scatter σ([α/Fe]) across the R_m-log τ_9 plane is, in contrast to σ([Fe/H]), astonishingly small as is seen in Table 17. Apart from a possible increase in σ([α/Fe]) for log $\tau_9 \geq 1.0$ there is *hardly any significant scatter in* [α/Fe] *at a given age and galactocentric distance.* The number of NaMgAl stars (8), discussed in Sect. 6.2.2, is so small that they do not increase the scatter in any [α/Fe] value of Table 16 by more than 0.02 dex. This indicates that the products of the synthesis of supernovae of different types are generally well mixed locally in the interstellar gas. It excludes local bursts of star formation as an explanation of σ([Fe/H]), because such bursts would be expected to produce an even larger scatter in [α/Fe], cf. Gilmore & Wyse (1991). Only minor gradients are present in [α/Fe] and, hence, the contribution from dynamic diffusion to σ([α/Fe]) is expected to be small. If a significant fraction of the scatter in [Fe/H] is ascribed to infall of metal-poor gas, the small scatter in [α/Fe] indicates that the characteristic mixing time of this infalling gas is much longer than that of the gas from supernovae of different types.

An alternative way to explain the remarkably small scatter in [α/Fe] would be to invoke the production of both α elements and iron in similar or identical sites; the relative yields then being dependent on initial stellar mass or metal abundance in order to account for the variation of [α/Fe] with [Fe/H] and R_m (cf., e.g., Edmunds et al. 1991, who, however, predict a steepening slope in the [α/Fe] vs [Fe/H] relation as [Fe/H] increases, which is contrary to our result in Figs. 19 and 20.).

Still another idea to explain the large scatter in [Fe/H] as compared with [α/Fe] would be that the galactic disk could contain two different stellar populations, with distinctly different metallicities (Δ[Fe/H] $\approx$ 0.15 dex) at similar stellar ages, presumably as the result of a major merger event. We have not, however, been able to trace any systematic dynamic differences between these postulated populations. Thus we do not find support for an idea similar to that suggested by Strobel (1991) for explaining the scatter in the age-metallicity relation for clusters invoking two independent but almost simultaneous processes, occurring for thick and thin disk objects, respectively. Finally, local fractionation processes, that separate hydrogen from heavier elements when stars are formed may also be thought of as an explanation. There is, however, no independent empirical support for the presence of such processes. On the contrary, accurate studies of metal abundances in open galactic clusters suggest very small "cosmic scatter". Here, we take the rather conservative view that the pattern seen in Tables 14-17 is most naturally explained by star-formation proceeding outwards in the Galaxy, infall and relatively slow mixing of relatively metal-poor gas, and excellent mixing between products of SNe Type II and Type I. We note that the infall of unprocessed (or only slightly processed) gas is also a main candidate for solving the so-called G-dwarf problem (cf., e.g., Pagel 1992, and references quoted therein).

6.4. Possible groups of stars

When inspecting the abundance results and combining them with the orbital data we found tendencies for stars to cluster

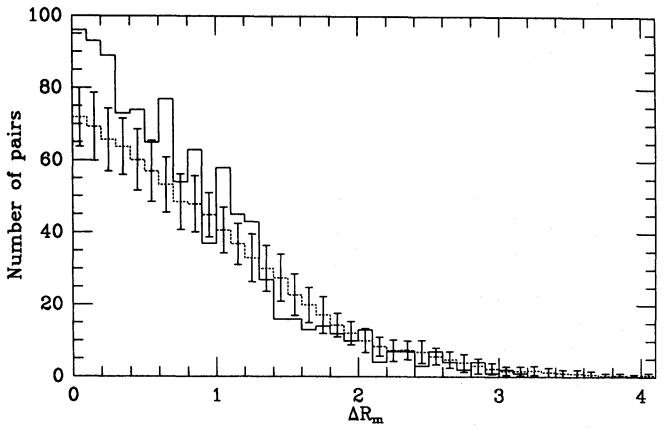

Fig. 32. Histogram of the number of pairs of stars, selected by their similarity in chemical abundances as described in the text, as a function of the difference in R_m between the two components, (solid line). The dotted line and the error bars show the corresponding distribution for 60 calculated synthetic samples of stars derived from the model described in the text. There appears to be a 15% over-representation of pairs in the observed sample (relative to the model), especially for pairs with similar values of R_m. This is probably caused by physical grouping of stars which were born together

at certain abundances and orbital elements. We decided to test the significance of such observations by making a model of the distribution of our stellar sample in the space of abundances, orbital elements and ages, draw model samples from that and compare them with the real stellar sample with respect to clustering tendencies. In practice this was done in the following way:

We calculated a quantity for all pairs of stars i and j,

$$S_{ij} = 2\left(\frac{[\mathrm{Fe/H}]_i - [\mathrm{Fe/H}]_j}{0.05}\right)^2 + 2\left(\frac{[\alpha/\mathrm{H}]_i - [\alpha/\mathrm{H}]_j}{0.06}\right)^2 + \\ + 1\left(\frac{[\text{“odd”}/\mathrm{H}]_i - [\text{“odd”}/\mathrm{H}]_j}{0.07}\right)^2, \quad (16)$$

where

$$[\text{“odd”}/\mathrm{H}]_i = \frac{1}{2}([\mathrm{Na/H}]_i + [\mathrm{Al/H}]_i).$$

We next defined a suspected pair (i, j) by $S_{ij} \leq 5.0$.

The denominators in Eq. (16) were chosen to represent typical mean errors in the corresponding quantities. The weights were doubled for [Fe/H] and [α/H] since these are based on a significantly greater number of accurate equivalent widths than are the values of ["odd"/H]. We then plotted the number of suspected pairs in our sample relative to their difference in R_m, $\Delta R_{m,ij} \equiv |R_{m,i} - R_{m,j}|$.

The resulting histogram is illustrated in Fig. 32. In order to test whether there is an excess of real pairs in this diagram at small ΔR_m we used a model of the stellar sample designed in the following way:

We divided the plane of [Fe/H] and R_m, quantities that are supposed to be well determined and relatively time independent, into a number of areas ("boxes"), 0.1 dex and 1.0 kpc wide, respectively. A number of model stars in each such box, equal to the corresponding number of the true distribution, were given random [Fe/H] and R_m values within the box limits. From these model stars we calculated values of [α/Fe], ["odd"/Fe] and $\log \tau_9$, using the following relations derived from the true sample:

$$[\alpha/\mathrm{Fe}] = 0.048 - 0.07\,[\mathrm{Fe/H}] + 0.14\,[\mathrm{Fe/H}]^2, \quad \sigma = 0.041 \quad (17)$$

$$[\text{“odd”}/\mathrm{Fe}] = 0.062 + 0.11\,[\mathrm{Fe/H}] + 0.35\,[\mathrm{Fe/H}]^2, \sigma = 0.054 \quad (18)$$

$$\log \tau_9 = 0.872 - 0.303\,[\mathrm{Fe/H}] - 0.038\,R_m, \quad \sigma = 0.19, \quad (19)$$

and a random Gaussian scatter with the relevant σ was added. The analysis and the relations, Eqs. (17)-(19), were based only on the 138 sample stars with $\log \tau_9 < 1.0$ since the relations will be more complex if the oldest stars are to be included. The full analysis was performed with 60 different model samples. The total number of synthetic pairs found was 906 ± 35, while the number of suspected pairs found in the analysis of the observed sample was 1030. As is seen in Fig. 32 this excess occurs at rather small ΔR_m values which is to be expected for a real physical clustering. We thus conclude that the clustering in our sample is real. We estimate that it may include only 12 stars altogether, assuming, in the extreme, that all real pairs belong to one large group of stars with similar properties. Alternatively, and more probably it involves many more than 12 stars in multiple smaller groups of which, e.g., a group of 5 stars with [Fe/H] and R_m close to the solar values might be one. (Note, however, that the ages we derive for the "solar group" members scatter between 2 and 7 Gyr.)

7. Conclusions

"Chemical evolution of the Galaxy" has been the subject of numerous models that attempt to describe the evolution of the galactic gas and stars from earliest times to the present. Measurements of the chemical compositions of young and old stars and the present gas are but one observational constraint on the models. To varying degrees, models also attempt to account for observed relations between stellar ages, metallicities, kinematics and galactic locations, as well as quantities such as the mass fraction of gas, the presence of dark matter and so on. At the outset of this study and even at its conclusion, it was clear to us that more successful and compelling models were unlikely to be constructed without a considerable expansion of the reliable data on the chemical compositions of galactic stars. In this study we elected to concentrate on the galactic disk. To the interested bystander, galactic chemical evolution implies some simple predictions about the chemical composition of the disk, such as that the metallicity of the disk should increase with time and depend on galactocentric radius; there should be an age-metallicity relation (young stars are more metal-rich than old

stars); and the chemical composition should evolve with time but fluctuations in the relative abundances would be likely as different stellar sources contribute different elements in different locations (SNe II in the spiral arms, SNe Ia out of the arms, etc). *None of these simple predictions is realised by our Galaxy!* Yet, one outcome of our survey is that the basic observational facts related to these predictions are quite simple but remarkably complex models are required to account for these facts!

Our goal here is not to reiterate the many points made in the preceding discussion but rather to highlight the observational facts that any convincing theory of chemical evolution must reproduce. We restrict comment here to the principal facts derived from our survey.

Age-metallicity relation. It has become customary to adopt the age-metallicity relation derived by Twarog (1980, or as revised by Carlberg et al. 1985) from Strömgren photometry of F stars as a challenge to be met by a model of galactic chemical evolution. Our results show clearly that the concept of a well defined tight age-metallicity relation is unfounded: the slope of [Fe/H] vs age ($\tau_\star$) over the lifetime of the disk (say 15 Gyr) is very flat with a large scatter in metallicity at all ages – see Fig. 14. The relation is particularly flat for the α-elements and slightly steeper for Ba and the other elements which sample the s-process. The lack of a striking slope and the scatter was evident from work on young open clusters – see Nissen (1988), Boesgaard (1989) and Strobel (1991). Also Gies & Lambert (1992) and Kilian (1992) have recently found young nearby B main sequence stars to have CNO abundances about a factor of two lower than those of the Sun. In this context, the oft-cited "disparity" between the composition of the local H II regions and the Sun is not unusual: briefly, the Orion and other local H II regions are deficient in oxygen and other elements relative to the Sun. The observer would note that Orion is an extension to $\tau = 0$ of the scatter so evident in Fig. 14. The observed age-metallicity relation is "simple" in the sense that for the disk the average metallicity has increased by very little over the disk's lifetime and the scatter at all times has been almost as large as the difference between the average metallicity then and now. Our results define the relation only for stars born at about the Sun's galactocentric radius. The relation may be different in the outer and innermost parts of the galactic disk. It must be borne in mind too that our stellar sample is not an unbiassed census of the stars at all ages but we probably do not overestimate the spread in metallicity at a given age. (Our procedure for selecting stars prevents us from attempting a discussion of the frequency distribution of the metallicities – the G dwarf problem.)

The considerable scatter in [Fe/H] at a given τ and R_m seems to imply that the chemical enrichment in the Galaxy is fairly inhomogeneous. This departs from expectation of simple models but, on the other hand, the simplifying assumption of instantaneous mixing in these models was never well founded. The observed great scatter in [Fe/H] is to be contrasted with the observed small scatter in abundance ratios relative to iron.

Relative abundances vs metallicity. Three sites for stellar nucleosynthesis are thought to contribute to the chemical evolution – SNe II/massive stars, SNe Ia/exploding white dwarfs, and AGB stars. These sources are distributed differently across the local regions of the Galaxy: SNe II are restricted to star-forming regions, SNe Ia may be more widely distributed having migrated from their birthplaces, and similarly for AGB stars, especially those of low mass and long lifetimes. Also, the AGB stars return their processed material to the interstellar medium at low velocity but the supernovae do so at high velocity. This difference surely affects the redistribution of processed material across the Galaxy. With these differences between the principal sites of nucleosynthesis, it seems surprising that an abundance ratio of elements supplied from different sites should show remarkably little scatter. We showed that in the thin disk, say [Fe/H] > -0.2, almost all abundance ratios show a scatter not significantly greater than our small errors of measurement which are typically put at 10% or less. We recall that both the ratio Si/Fe, which presumably measures a mix of SNe II and SNe Ia products, and the ratio Ni/Fe, which is primarily controlled by SNe Ia products, show a very small scatter. A similar result applies to ratios of the heavy elements indicating that the AGB stars have maintained a near-uniform s-process exposure as the SNe Ia supplemented by SNe II have driven the metallicity up by a factor of 3 from [Fe/H] = -0.2 to +0.3. There is a noticeable scatter in the ratio of the heavy element to iron ratios (e.g., [Ba/Fe]) but this is seen to depend on age and once the age dependence is removed [Ba/Fe] has a scatter that is compatible with the small errors of measurement. The age dependence is presumed to reflect the fact the s-process donating AGB stars are longer lived than the SNe Ia (and the SNe II). For the thick disk, say [Fe/H] < -0.3, certain abundance ratios were shown for the first time by our survey to be dependent on the galactocentric radius (R_m) of a star's birthplace: this is most clearly demonstrated by the ratio of α-elements to Fe. Once this is recognized, the scatter at a given R_m in all element ratios assumes the small values seen in the thin disk. At first sight – an observer's view – this lack of galactic scatter seems very surprising and hence a carrier of information about the Galaxy's chemical evolution.

The explanations for the small scatter in, e.g., [α/Fe] relative to that in [Fe/H], discussed above, enroll various more or less non-classical phenomena, such as considerable infall into the disk of metal-poor gas, possibly triggering star formation, or merging events of major subsystems with different [Fe/H] but similar [α/Fe] at a given τ, or local fractionation of elements in the star forming process with differences in the degree to which hydrogen is separated from heavier elements, or a closer correlation in time and space than is generally expected between the sites of nucleosynthesis for different elements like Si and Fe. Each of these possible explanations has considerable unresolved problems and interesting implications that need further detailed study.

We should finally note that the relative abundances [X/Fe] obtained for X=O, Mg, Si, Ca, Ti and Na and Al as a function of [Fe/H] are different for different elements and certainly not always as expected from the, admittedly as yet preliminary, supernovae models. E.g., Na follows Fe astonishingly closely, suggesting an origin in intermediate mass objects rather than SNe II, or, possibly, that the yield from the latter is severly de-

pendent on the initial metal abundance. Further comparison with detailed SN models is desirable.

Galactic Abundance Gradients. Traditionally, galactic abundance gradients refer to the radial gradient of an elemental abundance ratio. Published estimates based primarily on analyses of emission lines of H II regions and analyses of the absorption line spectra of luminous stars show a weak gradient not exceeding 0.1 dex kpc^{-1} in the sense that the outer Galaxy is more metal-poor. Our results support this conclusion (Table 14). However, our finding of significant abundance variations even for a fixed age and galactocentric radius advices caution in the choice of objects from which to investigate radial gradients. A striking result appeared here for the first time. Examination of the customary plots of [X/Fe] vs [Fe/H] showed real scatter in [α/Fe] at a given [Fe/H] for the metal-poor stars. This was traced to the fact that [α/Fe] at [Fe/H] < -0.4 is dependent on R_{m}: [α/Fe] is greater at a given [Fe/H] for the stars from the inner Galaxy. This result has a simple explanation that was independently anticipated by different models of galactic chemical evolution (cf. Larson 1976; Burkert et al. 1992). It implies that star formation and associated SNe II continued at a faster rate in the inner Galaxy.

Fluctuations in relative abundances. In spite of the overall and astonishing uniformity in heavy element abundance ratios we have been able to identify two new chemically unusual types of stars: the Ba dwarfs and the NaMgAl stars. Although none of these groups is very extreme in its abundances (departures by typically 0.3 dex and 0.1 dex, respectively, occur) their existence seems fairly well established, at least in the first case. The question whether the peculiarities were primordial or acquired during the stellar evolution (presumably as a result of mass transfer from a companion in later evolutionary stages) is not resolved here and needs further study. It should, however, be noted that the average chemical composition of local stars with solar [Fe/H] are slightly non-solar and, in fact, like the abundances of a mild NaMgAl star. This may be an argument for the NaMgAl phenomenon to reflect primordial abundances of the interstellar clouds.

As an exercise in quantitative statistical stellar spectroscopy, this survey has rewarded us with several major new observational results on how the local disk evolved chemically. But issues remain for additional surveys to address further. To conclude the paper, we shall comment on several projects worthy of attention.

An obvious omission is the lack of data on several elements that sample in different ways the principal sites of stellar nucleosynthesis. For example, comparable data on C and N and direct measurement of all stars for O using the [O I] lines would be of interest. A search should be undertaken for the source of Na: is Na synthesised in low mass red giants? The r-process is not directly sampled by our group of elements; Eu is an accessible monitor of the r-process.

A new survey of the moderately metal-poor stars should be undertaken to map out, as a function of R_{m}, the run of [X/Fe] vs [Fe/H] from [Fe/H] < -0.3 to the "halo" transition at [Fe/H] $\simeq -1$. It is not obvious that this relation should in fact merge smoothly with the halo results. One can conceive of situations in which the transition occurs smoothly at certain R_{m} but not at others.

The large scatter in the age-metallicity plane remains unexplained in part. Possible contributing factors need to be explored observationally. For example, it would be of interest to examine a large sample of H II regions or B stars to obtain a measure of the present Galaxy's uniformity of composition with respect to R_{m} and to galactic longitude. Also a broad (photometric) survey for determining [Fe/H] and age for a large unbiassed sample of stars is underway but remains to be completed.

Finally, we should not forget that small but important effects of galactic chemical evolution may be masked by random and systematic effects in the abundance analyses. And conversely, effects attributed to galactic chemical evolution may arise from systematic effects in the analyses. With the advances in instrumentation that have occurred since we initiated the survey, one can envisage that a larger survey could be undertaken more efficiently with a modest improvement in accuracy, as far as the random errors are concerned. The systematic errors remain a challenge: notably, the effects of convection and stellar granulation and of non-LTE. We suspect that these will be conquered only in the long term and that the short term solution will be to devise tests of chemical evolution that use samples of similar stars such that the random errors may largely cancel. Many of our results are, in effect, firmly based on such differential analyses.

Acknowledgements. E.H. Olsen is thanked for letting us use his large data base of *uvby-β* photometry for the selection of programme stars and for statistical corrections to our limited sample of stars.. V.V. Smith is thanked for conducting part of the observations at the McDonald 2.7 m telescope. R. Kurucz is thanked for making available the enormous amounts of line data which proved to have such an important impact on our analysis. We are much indebted to M. Grenon and J. Sommer-Larsen for computing the galactic orbital parameters given in Sect. 5.2.2 and permitting us to use them in this study. We thank W.F. van Altena and M. Mayor on behalf of several CORAVEL observers, and the CAMC group, for access to data in advance of publication. Information from the SIMBAD data base at the CDS, Strasbourg, was very useful in compiling the published kinematic data. We are thankful to R.A. Bell for supplying data on molecular opacities. K. Eriksson, K. Freeman, K. Nomoto, E.H. Olsen, B. Pagel, J. Silk and S. Woosley are thanked for valuable discussions and suggestions. JA thanks the Danish Natural Science Research Council, the Carlsberg Foundation, the Danish Board for Astronomical Research, and the Smithsonian Institution for financial support of this research. BE and BG acknowledge support in the form of several grants from the Swedish Natural Science Research Council. DLL and JT acknowledge support from the US National Science Foundation and the Robert A. Welch Foundation. PEN acknowledges support from the Danish Natural Science Research Council.

References

Abt H.A. 1983, ARA&A 21, 343
Abt H.A. 1987, ApJ 317, 353
Abt H.A., Levy S.G. 1976, ApJS 30, 273

Allen C.W. 1973, Astrophysical Quantities, Athlone Press, University of London, 197
Aller L.H., Greenstein J.L. 1960, ApJS 5, 139
van Altena W.F., Lee J.T., Hoffleit E.D. 1993, General Catalogue of Trigonometric Parallaxes, Ed. of 1993, Yale University Observatory, New Haven
Anders E., Grevesse N. 1989, Geochimica et Cosmochimica Acta 53, 197
Andersen J. 1991, A&AR 3, 91
Andersen J., Clausen J.V., Gustafsson B., Nordström B., VandenBerg D.A. 1988a, A&A 196, 128
Andersen J., Clausen J.V., Magain P. 1989, A&A 211, 346
Andersen J., Clausen J.V., Nordström B. 1984, A&A 137, 281
Andersen J., Clausen J.V., Nordström B., Tomkin J., Mayor M. 1991, A&A 246, 99
Andersen J., Edvardsson B., Gustafsson B., Nissen P.E. 1988b, in: IAU Symp. No. 132, The impact of very high S/N spectroscoy on stellar physics, eds. G. Cayrel de Strobel and M. Spite, Reidel, Dordrecht, 441
Andersen J., Gjerløff H., Imbert M. 1975, A&A 44, 349
Andersen J., Garcia J.M., Giménez A., Nordström B. 1987, A&A 174, 107
Andersen J., Nordström B., Ardeberg A., Benz W., Imbert M., Lindgren H., Martin N., Maurice E., Mayor M., Prévot L. 1985, A&AS 59, 15
Ardeberg A., Lindgren H., Nissen P.E. 1983, A&A 128, 194
Arnett W.D. 1971, ApJ 166, 153
Arvesen J.C., Griffin R.N., Pearson B.D. 1969, Applied Optics 8, 2215
Baker P.L., Burton W.B. 1975, ApJ 198, 281
Bell R.A. 1993, private communication
Bell R.A., Eriksson K., Gustafsson B., Nordlund Å. 1976, A&AS 23, 37
Bergbusch P.A., VandenBerg D.A. 1992, ApJS 81, 163
Bertelli G., Bressan A., Chiosi C. 1992, ApJ 392, 522
Biémont E., Baudoux M., Kurucz R.L., Ansbacher W., Pinnington E.H. 1991, A&A 249, 539
Blackwell D.E., Shallis M.J. 1977, MNRAS 180, 177
Boesgaard A.M. 1989, ApJ 336, 798
Boyarchuk A.A, Lyubimkov L.S. 1985, Bull. Crimean Astrophys. Obs. 66, 119
Boyarchuk A.A, Gubeney I., Kubad I., Lyubimkov L.S., Sakhibullin N.A. 1988, Sov. Astrophys. 28, 202
Broadfoot A.L. 1972, ApJ 173, 681
Burkert A, Truran J.W., Hensler G. 1992, ApJ 391, 651
Cameron A.G.W. 1982, Ap&SS 82, 123
Carlberg R.G., Dawson P.C., Hsu T., VandenBerg D.A. 1985, ApJ 294, 674
Carlsberg Meridian Catalogue 1989, Vol. 4, Copenhagen Univ. Obs., Royal Greenwich Obs., Real Instituto y Obs. de la Armada, San Fernando, Spain
Carlsberg Meridian Catalogue 1991, Vol. 5, Copenhagen Univ. Obs., Royal Greenwich Obs., Real Instituto y Obs. de la Armada, San Fernando, Spain
Cayrel de Strobel G. 1990, in: XI IAU EAM, New Windows on the Universe, eds. F. Sanches and M. Vazquez, 195
Cayrel R., Cayrel de Strobel G., Campbell B. 1985, A&A 146, 249
Chamberlain J.W., Aller L.H. 1951, ApJ 114, 52
Chmielewski Y., Friel E., Cayrel de Strobel G., Bentolila C. 1992, A&A 263, 219
Clayton D.D. 1988, MNRAS 234, 1
Crawford D.L. 1975, AJ 80, 955
Crawford D.L., Barnes J.V. 1969, AJ 74, 407
Crawford D.L., Barnes J.V. 1970, AJ 75, 978
Crawford D.L., Barnes J.V., Faure B.Q., Golson J.C., Perry C.L. 1966, AJ 71, 709
Crawford D.L., Barnes J.V., Golson J.C. 1970, AJ 75, 624
Delbouille L., Roland G., Neven L. 1973, Photometric Atlas of the Solar Spectrum from λ 3000 to λ 10000, Institut d'Astrophysique de Liège
Denisenkov P.A. 1989, Sov. Astron. Lett. 14(6), 435
Denisenkov P.A., Denisenkova S.N. 1990, Sov. Astr. Letters 16, 275
Denisenkov P.A., Ivanov V.V. 1987, Pis'ma Astron. Zh. 13, 52
Drake J., Smith V.V., Suntzeff N.B. 1992, ApJ 395, L95
Edmunds M.G., Greenhow R.M., Johnson D., Klückers V., Vila M.B. 1991, MNRAS 251, 33p
Edvardsson B., Bell R.A. 1989, MNRAS 238, 1121
Edvardsson B., Gustafsson B., Nissen P.E. 1984, ESO Messenger 38, 33
Edvardsson B., Nissen P.E., Gustafsson B., Andersen J. 1985, in: IAU Symp. No. 111, Calibration of Fundamental Stellar Quantities, eds. D.S. Hayes, L.E. Pasinetti and A.G. Davis Philip, Reidel, Dordrecht, 575
Edvardsson B., Gustafsson B., Andersen J., Nissen P.E., Lambert D.L., Tomkin, J. 1990, in: Proc. Nordic-Baltic Astronomy Meeting, eds. C.-I. Lagerkvist, D. Kiselman and M. Lindgren, Uppsala, 93
Edvardsson B., Andersen J., Gustafsson B., Lambert D.L., Nissen P.E., Tomkin J. 1993, A&AS in press (Paper II)
Eggen O.J., Lynden-Bell D., Sandage A.R. 1962, ApJ 136, 748
Eriksson K., Toft S.C. 1979, A&A 71, 178
Flannery B.P., Ayres T.R. 1978, ApJ 221, 175
François P. 1986, A&A 160, 264
François P., Matteucci F. 1992, ESO preprint no. 893
Frantsman Yu.L. 1992, Sov. Astron. J. 36, 155
Freeman K. 1991, in: Dynamics of Disc Galaxies, ed. B. Sundelius, Dept. of Astronomy and Astrophysics, Gothenburg University, 15
Fricke W., Schwan H., Lederle T. et al. 1988, Veröff. Astron. Rechen-Inst. Heidelberg, No. 32, Braun, Karlsruhe
Friel E.D. Janes K.A. 1991, in: The Formation and Evolution of Star Clusters, ASP Conf Ser. 13, ed. K. Janes, 569
Furenlid I., Meylan T. 1990, ApJ 350, 827
Garcia Lopez R.J., Rebolo R., Beckman J.E. 1988, PASP 100, 1489
Gehren T. 1988, Rev. Mod. Astr. 1, 52 (Springer-Verlag, Berlin)
Gehren T., Reile C., Steenbock W. 1991, in: Stellar Atmospheres: Beyond Classical Models, eds L. Crivellari, I. Hubeny and D.G. Hummer, Kluwer, Dordrecht, 387
Gies D.R., Lambert D.L. 1992, ApJ 387, 673
Gigas D. 1986, A&A 165, 170
Gilmore G., Wyse R.F.G. 1991, ApJ 367, L55
Gilroy K.K., Sneden C., Pilachowski C.A., Cowan J.J. 1988, ApJ 327, 298
Gratton L. 1953, Liege Conference, p.419
Gratton R.G., Sneden C. 1991, A&A 241, 501
Gratton R.G., Gustafsson B., Eriksson K. 1993, in preparation
Gray D.F. 1992, PASP 104, 1035
Grenon M. 1987, JA&A 8, 123
Grenon M. 1989, Ap&SS 156, 29
Grønbech B., Olsen E.H. 1976, A&AS 25, 213
Grønbech B., Olsen E.H. 1977, A&AS 27, 443
Gustafsson B. 1992, in: Inside the Stars, IAU Coll. 137, ed. W. Weiss, PASP, special issue, in press
Gustafsson B., Bell R.A. 1979, A&A 74, 313

Gustafsson B., Bell R.A., Eriksson K., Nordlund Å. 1975, A&A 42, 407
Gustafsson B., Edvardsson B., Nissen P.E., Lambert D.L., Tomkin J., Andersen J. 1992, in: IAU Symp. No. 149, The Stellar Populations of Galaxies, eds. B. Barbuy and A. Renzini, Kluwer, Dordrecht, 75
Hoffleit D., Jaschek C. 1982, The Bright Star Catalogue, Yale University Observatory, New Haven
Holweger H. 1970, A&A 4, 11
Holweger H. 1971, A&A 10, 128
Holweger H. 1973, A&A 26, 275
Holweger H., Müller E.A. 1974, Solar Phys. 39, 19
Holweger H., Bard A., Kock A., Kock M. 1991, A&A 249, 545
Holweger H., Heise C., Kock M. 1990, A&A 232, 510
Hulsbosch A.N.M. 1975, A&A 40, 1
Irwin A.W., Yang S., Walker G.A.H. 1992, PASP 104, 101
Jørgensen H.E., Gyldenkerne K. 1975, A&A 44, 343
Käppeler F., Beer H., Wisshak K. 1989, Rep. Prog. Phys. 52, 945
Kilian J. 1992, A&A 262, 171
Kiselman D. 1991, A&A 245, L9
Kiselman D. 1993, submitted to A&A
Kraft R.P., Sneden C., Langer G.E., Prosser C.F. 1992, AJ 104, 645
Kurucz R.L. 1989, Magnetic tapes with atomic line data for Ca through Ni, private communication
Kurucz R.L., Furenlid I., Brault J., Testerman L. 1984, Solar Flux Atlas from 296 to 1300 nm, National Solar Observatory, Sunspot, New Mexico
Kurucz R.L., van Dishoeck E.F., Tarafdar S.P. 1987, ApJ 322, 992
Lambert D.L. 1989, in: American Inst. of Physics Conf. Proc. 183, Cosmic Abundances of Matter, ed. C.J. Waddington, American Inst. of Physics, New York, 168
Lambert D.L. 1991, in: Evolution of Stars - The Abundance Connection, eds. G. Michaud and A.V. Tutukov, Kluwer, Dordrecht, 299 ed. C.J. Waddington, American Inst. of Physics, New York, 168
Larson R.B. 1972, Nat 236, 21
Larson R.B. 1976, MNRAS 176, 31
Lemke M. 1992, preprint
Lewis J.R., Freeman K.C. 1988, AJ 97, 139
Luck R.E., Bond H.E. 1991, ApJS 77, 515
Mäckle R., Holweger H., Griffin R., Griffin R. 1975, A&A 38, 239
Magain P. 1984, A&A 134, 189
Magain P. 1987, A&A 181, 323
Magain P. 1988, in: IAU Symp. No. 132, The Impact of Very High S/N Spectroscopy on Stellar Physics, eds. G. Cayrel de Strobel and M. Spite, Kluwer, Dordrecht, 485
Magain P. 1989, A&A 209, 211
Magain P., Zhao G. 1992, preprint
Mathews G.J., Cowan J.J. 1990, Nat 345, 6275
Mathisen R. 1984a, unpublished report, Univ. of Oslo
Mathisen R. 1984b, Publ. Ser. Inst. Theor. Astroph., Oslo, No. 1
Matteucci F. 1992, in: New Results on Standard Candles, ed. F. Caputo et al., Mem. Soc. Astr. It., in press
Matteucci F., François P. 1989, MNRAS 239, 885
Matteucci F., Greggio L. 1986, in: Proc. NATO Adv. Study Inst., Nucleosynthesis and its implications on nuclear and particle physics, eds. J. Audouze and N. Mathieu, 315
Matteucci F., Tornambè A. 1987, A&A 185, 51 and A&A 196, 341
Mayor M. 1985, in: IAU Coll. No. 88, Stellar Radial Velocities, eds. A.G.D. Philip and D.W. Latham, Davis Press, Schenectady N.Y., 35
McClure R.D. 1989, in: IAU Coll. 106, Evolution of Peculiar Red Giant Stars, eds. H. Johnson and B. Zuckerman, Cambridge University Press, 196
McWilliam A. 1988, Ph.D. thesis, University of Texas, Austin
Meusinger H., Reimann H.-G., Stecklum B. 1991, A&A 245, 57
Mirabel I.F. 1982, ApJ 256, 112
Moore C.E., Minnaert M.G.J., Houtgast J. 1966, The Solar Spectrum 2935 Å to 8770 Å, National Bureau of Standards, Monograph 61
Morbey C.L., Griffin R.F. 1987, ApJ 317, 343
Neckel H., Labs D. 1964, Solar Physics 90, 205
Nissen P.E. 1981, A&A 97, 145
Nissen P.E. 1988, A&A 199, 146
Nissen P.E., Edvardsson B. 1992, A&A 261, 255
Nissen P.E., Edvardsson B., Gustafsson B. 1985, in: Proc. ESO Workshop, Production and Distribution of C,N,O Elements, eds. I.J. Danziger, F. Matteucci, and K. Kjär, ESO, Garching, 131
Nissen P.E., Twarog B.A., Crawford D.L. 1987, AJ 93, 634
Nomoto K., Thielemann F-K., Yokoi K. 1984, ApJ 286, 644
Nomoto K. 1992, private communication
Nomoto K. et al. 1992, in: Nuclei in Cosmos, ed. F. Käppeler, J. Phys. G., in press
Nordlund Å., Dravins D. 1990, A&A 228, 155
Nordström B., Andersen J. 1989, in: The Gravitational Force Perpendicular to the Galactic Plane, eds. A.G.D. Philip and P.K.Lu L., Davis Press, Schenectady N.Y., 153
North P, Duquennoy A. 1992, in: Binaries as Tracers of Stellar Formation, eds. A. Duquennoy and M. Mayor, Cambridge University Press, 202
Olsen E.H. 1983, A&AS 54, 55
Olsen E.H. 1988, A&A 189, 173
Olsen E.H. 1989, private communication
Olsen E.H., Perry C.L. 1984, A&AS 56, 229
O'Neill J.A., Smith G. 1980, A&A 81, 100
Oort J.H. 1967, in: Radio Astronomy and the Galactic System, IAU Symp. 31, ed. H. van Woerden, Academ. Press, 279
Pagel B.E.J. 1970, QJRAS 11, 172
Pagel B.E.J. 1989, Rev. Mex. Astron. Astrofis. 18, 161
Pagel B.E.J. 1992, in: The stellar Populations of Galaxies, IAU Symp. 149, eds. B. Barbuy and A. Renzini, Kluwer, Dordrecht, 133
Paresce F. 1984, AJ 89, 1022
Peterson R.C. 1981, ApJ 244, 989
Plez B., Brett J.M., Nordlund Å. 1992, A&A 256, 551
Popper D.M., Ulrich R.K. 1986, ApJ 307, L61
Roman N.G. 1954, AJ 59, 307
Roman N.G. 1955, ApJS 2, 195
Samain D. 1979, A&A 74, 225
Sanders W.L. 1977, A&AS 27, 89
Saxner M. 1984, Ph. D. Thesis, Uppsala University
Saxner M., Hammarbäck G. 1985, A&A 151, 372
Schaller G., Schaerer D., Meynet G., Maeder A. 1992, A&AS 96, 269
Schuster W.J., Nissen P.E. 1988, A&AS 73, 225
Schwarzschild M., Schwarzschild B., Searle L., Meltzer A. 1957, ApJ 125, 123
Simmons G.J., Blackwell D.E. 1982, A&A 112, 209
Sneden C., Parthasarathy M. 1983, ApJ 267, 757
Sneden C., Kraft R.P., Prosser C.F., Langer G.E. 1991, AJ 102, 2001
Sneden C., Kraft R.P., Prosser C.F., Langer G.E. 1993, AJ in press
Soderblom D.R., Mayor M. 1993, AJ 105, 226
Sommer-Larsen J., Antonuccio-Delogū V. 1993, MNRAS in press
Sommer-Larsen J., Yoshii Y. 1990, MNRAS 243, 468

Spite F. 1990, in: Lecture Notes in Physics Vol. 356, Accuracy of Element Abundances for Stellar Atmospheres, ed. R. Wehrse, Springer-Verlag, 69
Steffen M. 1985, A&AS 59, 403
Steffen M., Ludwig H.-G., Krüss A. 1989, A&A 213, 371
Stimets R.W., Giles R.H 1980, ApJ 242, L37
Strobel A. 1991, A&A 247, 35
Strömgren B. 1987, in: Proc. NATO Adv. Study Inst., The Galaxy, eds. G. Gilmore and R. Carswell, Reidel, Dordrecht, 229
Strömgren B., Perry C.. 1965, Photoelectric *uvby* Photometry for 1217 Stars Brighter than V=6.5, Institute for Advanced Study, Princeton
Strömgren B., Olsen E.H., Gustafsson B. 1982, PASP 94, 5
Suchkov A.A. 1981, Ap&SS 77, 4
Thielemann F-K., Nomoto K., Hashimoto M. 1991, Supernovae, Les Houches, Session LIV, eds. J. Audouze, S. Bludman, R. Mochkovitch and J. Zinn-Justin, Elsevier Science Publ.
Tinsley B.M. 1979, ApJ 229, 1046
Tinsley B.M. 1980, Fundamentals of Cosmic Physics 5, 287
Tomkin J., Lambert D.L., Edvardsson B., Gustafsson B., Nissen P.E. 1989, A&A 219, L15
Trimble V. 1991, A&AR 3,1
Tosi M. 1988, A&A 197, 33 and A&A 197, 47
Truran J.W. 1981, A&A 97, 391
Twarog B.A. 1980, ApJ 242, 242
VandenBerg D.A. 1983, ApJS 51, 29
VandenBerg D.A. 1985, ApJS 58, 711
VandenBerg D.A. 1992, ApJ 391, 685
VandenBerg D.A., Bell R.A. 1985, ApJS 58, 561
VandenBerg D.A., Poll H.E. 1989, AJ 98, 1451
Vernazza J.E., Avrett E.H., Loeser R. 1976, ApJS 30, 1
Vogt S.S., Tull R.G., Kelton P. 1978, Applied Optics 17, 574
Wallerstein G. 1962, ApJS 6, 407
Wamsteker W., Driessen C., Munoz J.R., Hassall B.J.M., Pasian F., Barylak M., Russo G., Egret D., Murray J., Talavera A., Heck A. 1989, A&AS 79, 1
Weaver T.A., Woosley S.E. 1992, ApJ and Rev. Mod. Phys., submitted
Wheeler J., Sneden C., Truran, J.W. 1989, ARA&A 27, 279
Wielen R. 1977, A&A 60, 263
Wiese W.L., Smith M W., Miles B.M. 1969, National Stand. Ref. Data Ser., Nat. Bur. Stand. 22
Wilson R.E. 1953, General Catalog of Stellar Radial Velocities, Carnegie Inst. of Washington, Washington, D.C.
Woosley S.E., Weaver T.A. 1982a, in: Essays in Nuclear Astrophysics, eds. C.A. Barnes, D.D. Clayton and D.N. Schramm, 377
Woosley S.E., Weaver T.A. 1982b, in: Supernovae: A Survey of Current Research,d eds M. Rees and R.J. Stoneham, D. Reidel Publ. Co., 79

Note added in proof: Kiselman (1993, A&AS, in press) has made an empirical investigation of the effects of granulation on equivalent widths in the solar photosphere. The investigation considers 13 lines of different elements, ionization stages, excitation energies and equivalent widths, 5 of which are used in this work. Kiselman supports the results of Holweger et al. (1990), and he finds no clear non-linearities in the relation between continuum intensity and line strength. He concludes that no effects have been found that could signal significant problems for abundance analysis using homogeneous model atmospheres. There is one notable qualification to this statement: the combination of non-LTE effects and inhomogeneities may introduce non-linear behaviour of equivalent widths, seriously falsifying plane-parallel LTE analyses. In our case we may expect the oxygen abundances derived from high-excitation O I lines to be affected; however, our results have been empirically scaled to oxygen abundances derived from the 6300 A [O I] line which is probably formed close to LTE (cf. Sect. 3.2.2).